UNIVERSIDADE ESTADUAL PAULISTA
"JÚLIO DE MESQUITA FILHO"
Campus de Ilha Solteira

VINÍCIUS GERMANOS CLEANTE

Effects of Railway Track Vibration Induced by Passing Trains on an Energy Harvesting Device

Ilha Solteira
2015

Effects of Railway Track Vibration Induced by Passing Trains on an Energy Harvesting Device

Vinícius Germanos Cleante

Dissertation presented to the Faculdade de Engenharia - UNESP - campus of Ilha Solteira, in order to obtain the title of Master in Mechanical Engineering.
Knowledge area: Solid Mechanics.

Prof. Dr. Michael John Brennan
Adviser

Ilha Solteira
2015

**UNIVERSIDADE ESTADUAL PAULISTA
"JÚLIO DE MESQUITA FILHO"**
Campus de Ilha Solteira

Efeitos da Vibração em Linha Férrea Induzida pela Passagem de Trens em um Dispositivo de Captação de Energia

Vinícius Germanos Cleante

Dissertação apresentada à Faculdade de Engenharia – UNESP – Campus de Ilha Solteira, para obtenção do título de Mestre em Engenharia Mecânica.
Área de Conhecimento: Mecânica dos Sólidos.
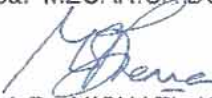
Prof. Dr. Michael John Brennan
Orientador

Ilha Solteira
2015

unesp

UNIVERSIDADE ESTADUAL PAULISTA
CAMPUS DE ILHA SOLTEIRA
FACULDADE DE ENGENHARIA DE ILHA SOLTEIRA

CERTIFICADO DE APROVAÇÃO

TÍTULO: Effects of Railway Track Vibration Induced by Passing Trains on an Energy Harvesting Device

AUTOR: VINÍCIUS GERMANOS CLEANTE

ORIENTADOR: Prof. Dr. MICHAEL JOHN BRENNAN

Aprovado como parte das exigências para obtenção do Título de Mestre em Engenharia Mecânica, Área: MECANICA DOS SÓLIDOS, pela Comissão Examinadora:

Prof. Dr. MICHAEL JOHN BRENNAN
Departamento de Engenharia Mecânica / Faculdade de Engenharia de Ilha Solteira

Prof. Dr. FABRICIO CÉSAR LOBATO DE ALMEIDA
Departamento de Engenharia Mecânica / Faculdade de Engenharia de Ilha Solteira

Prof. Dr. GIANLUCA GATTI
Departamento de Engenharia Mecanica, Energia e Gestão / University of Calabria

Data da realização: 24 de julho de 2015.

ACKNOWLEDGMENT

First, I would like to thank God for giving me wisdom and especially perseverance. Without this, I believe I would not be able to learn from my mistakes and difficulty and become a better person.

I would like to thank Professor Mike for believing in me and accept to be my advisor. I am sure there could be no better person to guide me during the course of this project. Certainly, I will not forget his teachings.

To my parents, Cleiton and Maria, there are no words to describe how grateful to you. I want to thank from the bottom of my heart for the words of encouragement to follow the way that I believe to be the best for me.

To my friends from UNESP, I would like to thank for fun times. I am sure that those moments made my days easier. In special, I would like to thank my friends Bruce, Cristian and Oscar, for yours friendship and support since I have arrived in Ilha. Thank you for the academic discussion. Be assured that you were a fundamental part for me to have reached this goal.

"We cannot teach people anything; we can only help them discover it within themselves."

Galileo Galilei

ABSTRACT

With advances in technology, and with the need to seek for solutions to reduce the effects of global warming, makes energy harvesting a popular research topic. The particular interest in this project is the harvesting of energy from ambient vibrations, which has applications in hostile environments or in remote areas. This type of device has the capacity feed microelectromechanical systems that use a low power, for example sensors for structural health monitoring, wireless sensors, radio communications, etc. In this work, an investigation is conducted to determine how much energy can be scavenged from vibrations due the passage of a train. A study is conducted to investigate the optimum parameters design of an energy harvester subject to vibrations induced by trains passing at different speeds. Vibration Data from two sites in the United Kingdom is used for this purpose. An approximate analytical expression for energy harvested from a linear harvester subject to a time-limited periodic excitation is evaluated using the harmonic components of the sleeper vibrations. The results are compared with those obtained through numerical analysis. Also, the behaviour of the linear energy harvester subject to vibrations induced by several passing trains is evaluated for ranges of speeds observed in measurement data sets at Steventon site.

Keywords: Energy harvester. Linear oscillator. Passing train. Sleeper vibrations.

RESUMO

Com avanços em tecnologia, e com a necessidade em buscar soluções para reduzir efeitos do aquecimento global, tornou captação de energia uma área de pesquisa popular. O particular interesse deste projeto é a extração de energia a partir de vibrações em ambientes no qual possui aplicação em ambientes hostis ou em áreas remotas. Este tipo de dispositivo possui a capacidade de alimentar sistemas microeletrônicos que utilizam pouca energia, por exemplo sensores de monitoramento da saúde estrutural, sensores sem fio, radio comunicação, etc. Neste trabalho, uma investigação é conduzida para determinar a quantidade de energia que pode ser extraída a partir de vibrações devido a passagem do trem. Um estudo é conduzido para investigar o design dos parâmetros ótimos para um extrator de energia submetido a vibrações induzidas por trens passando com diferentes velocidades. Dados de vibração de dois locais no Reino Unido é utilizado para este propósito. Uma expressão analítica aproximada para energia extraída por um extrator linear submetido a excitação periódica de tempo limitado é avaliado utilizando os componentes harmônicos das vibrações em um dormente. Os resultados são comparados com os obtidos através da análise numérica. Também, o comportamento de um extrator de energia linear submetido a vibrações induzidas por diversos trens passantes, é avaliado para trens com uma faixa de velocidade observado nos dados mensurados em Steventon.

Palavras-chave: Captação de energia. Osciladores linear. Trem passante. Vibrações no dormente.

LIST OF FIGURES

APPEDIX A:

APPENDIX B:

LIST OF TABLES

CONTENT

1   INTRODUCTION

1.1   Background

Energy harvesters convert any type of energy to electrical energy. Studies in this subject have been carried out for many years, but recent attempts to address issues related to climate change and to increase the performance of these devices, has resulted in this subject receiving a great deal of attention.

Advances in technology has reduced the maintenance cost of these devices and allowed the exploration of different types of energy sources, principally in the environment, where access is difficult. For example, the supply of energy for medical implants has been investigated (MIAO et al., 2006; DAGDEVIREN et al., 2014), especially for pacemakers (AMIN KARAMI; INMAN, 2012), as is the energy supply for wireless sensor networks (SARI; BALKAN; KULAH, 2007; KULAH; NAJAFI, 2008; TAN et al., 2009; WISCHKE et al., 2011; LU et al., 2015).

There are sources of energy that can generate large scale electrical energy. Hydro-electric power plants (POBERING; SCHWESINGER, 2004) and wind power plants (MORAIS et al., 2008) are examples of such sources, where the strength and the flux of water and wind rotate large turbines and generate electrical energy to supply houses, cities and states. However, many other energy sources in the environmental can generate small amounts of electrical energy that would be sufficient to power electronic devices. Photovoltaic sources harvest solar radiation and indoor illumination, providing energy to supply various devices from water boilers (CHOW; HE; JI, 2007) to calculators (HIROKANE et al., 2010). Kinetic energy is a great potential energy source due its presence in almost every type of environment. This mechanical phenomenon is due to movement, and if present in reciprocating form, can be used as a vibrational energy source. This specific subject, that studies the applicability of energy harvesters due human motion (RENAUD et al., 2005; YLLI et al., 2013, YLLI et al., 2015), bridge vibration (ALI; FRISWELL; ADHIKARI, 2011), railway vibration (NELSON et al., 2008; TAN et al., 2009), and others, is seen as an important source of energy.

1.2   Literature review

Many researchers have investigated the scavenging energy from vibrations in the environment for many years, and since the increase in concern of global warming, the demand

for sustainable devices has also increased. Energy harvesters convert vibrational energy, i.e. kinetic energy, into electrical energy through transducers. The most common transducers are electrostatic, piezoelectric and electro-magnetic.

1.2.1   Electrostatic energy harvester

Basically, an electrostatic energy harvester consists of two conductive plates which are electrically separated by a gap, filled with air or a dielectric material. The plates move relative to each other. This device works in two modes; a charge-constrained mode and voltage-constrained mode (TORRES; RINCON-MORA, 2009). In the charge-constrained mode, the charge is kept constant by the use of a capacitor. Due the distance change between the two plates, the voltage also changes. In the voltage-constrained mode, the voltage between the two plates is kept constant while the charge increases with the decrease in distance between the plates (MITCHESON et al., 2004; TORRES; RINCON-MORA, 2009).

The advantages of using energy harvesters with electrostatic transducer are due to the fact that they are compatible with microelectromechanical systems (MEMS), and they are able to generate moderate levels of energy without the use of different materials (HOFFMANN; FOLKMER; MANOLI, 2009). The disadvantage of electrostatic transducers is that for them to work, the capacitor should be pre-charged (LEE et al., 2009).

1.2.2   Piezoelectric energy harvester

Piezoelectric transducers are devices that when stimulated electrically, their structure responds with a physical deformation (indirect piezoelectric effect). Also, when they undergo a mechanical deformation, they generate an electrical charge. Common piezoelectric materials are made from ceramics or polymers (ANTON; SODANO, 2007). Polymer transducers have a low cost and are highly flexible, however, it is the ceramic materials, like lead-zicornate-titanate (PZT), that have higher piezoelectric coefficients.

A cantilever beam is the most commonly used structure for an energy harvesting application using a piezoelectric transducer. A small layer of piezoelectric material is applied to one of the beam surfaces This model is known as a unimorph piezoelectric harvester (COONDOO et al., 2015). If the same material is applied to two surfaces, this is known as a bimorph piezoelectric harvester (DWIVEDY; REDDY; GARG, 2015).

Piezoelectric transducers are devices able to generate a voltage, between 3 to 10 V (SODANO; INMAN; PARK, 2005), without requiring a pre-charge to work (SHU; LIEN, 2006). Piezoelectric materials are, however, very sensitive to temperature, and therefore need to be applied in environment with limited temperature variability (ANTON; SODANO, 2007). If piezoelectric materials are subject to high temperatures, they can become de-polarized and inoperative.

1.2.3   Electromagnetic energy harvester

Electromagnetic transducers are mechanical devices that follow the principle of Faraday's law (STEPHEN, 2006), where the relative motion between a coil and a magnet generates a voltage. The structure of an electromagnetic energy harvester consists, basically, of a coil, a magnet and a spring.

One of the first studies of energy harvesting using this technology was by Williams and Yates (1996). Amirtharajah et al. (1998) later enhanced the efficiency of an electromagnet transducer. The advantage of use electromagnetic transducers is the fact that they do not require an external energy supply to make them work. Moreover, these devices can be designed so that there is no direct mechanical contact between the components parts. However, in comparison with electrostatic and piezoelectric transducers, the power obtained by the electromagnetic energy harvester is of order of μW to several mW (SAHA et al., 2008).

1.3   Energy harvesting in a railway environment

Vibration due to the passage of trains is one of the largest environmental problems with railways. Researchers have spent much time investigating and improving the performance of both railway structures and trains. This has allowed the development of trains with increasingly faster speeds. Nowadays, the vibration generated by a train is seen as a potential energy source to power wireless sensors for structural health monitoring or temperature monitoring purposes, for example.

Nelson et al. (2008) investigated the use of a piezoelectric transducer and a voice-coil attached to the bottom of the rail to harvest energy from the vertical vibration due to the passage of loaded and unloaded freight trains. Experimental results showed that the average power scavenged was approximately 1 mW for both techniques.

Hansen et al. (2010) designed a power harvesting device and embedded it into a rail sleeper. The vertical vibration of the sleeper due the passage of a train was converted into rotational motion and amplified through a gearbox. In field tests, the mechanical device was able to harvest 0.22 W due the passage of a loaded freight train and 0.01 W from an unloaded freight train.

Tehrani et al. (2013) investigated the amount of mechanical energy that a linear energy harvester could scavenge due the passage of an Inter-city 125 high speed train composed of 2 power cars and 8 passenger cars with a velocity of 195 km/h. They showed that a harvester with a natural frequency of 16.6 Hz and damping ratio of 0.02 could scavenge 0.15 J for a device that had a 1 kg inertial mass. Gatti et al. (2014) developed a linear mathematical model of such a device, considering a time-limited periodic excitation to evaluate the amount of mechanical energy that could be harvested.

1.4   Objectives

The main objective of this dissertation is to investigate the amount of energy that can be scavenged from railway vibration due the passage of a high-speed train using a linear energy harvester. The effects of the mechanical parameters on the robustness of such an energy harvesting device, considering the passage of many trains with different speeds, is also investigated.

1.5   Outline of dissertation

- Chapter 1: Introduction, literature review and dissertation objectives
- Chapter 2: Presentation of the theoretical fundamentals and a model for a linear harvester considering time-limited periodic excitation.
- Chapter 3: Description of the structure of a railway track and the effects of the railway parameters on its vibration. Outline of the main source of vibration at low frequency from a train and the description of models to describe the trainload excitation and the track deflection due to the quasi-static excitation of the track by the train.
- Chapter 4: A numerical simulation of a railway application and evaluation of the parameters of a linear resonator to scavenge energy from trains with different speeds.

- Chapter 5: Evaluation of the parameters of an energy harvesting device through numerical simulations using the model of an energy harvester for time-limited periodic excitations to scavenge energy from passing train with different speeds.
- Chapter 6: Final remarks and suggestions for future work.

2   ENERGY HARVESTING FROM HARMONIC EXCITATION

2.1   Introduction

With the increase in energy demand, studies in ways to extract renewable or non-renewable energy has become one of the most important topics in Engineering. After years of development and discovery, energy harvesting from ambient vibration has become a challenging topic for researchers.

Researchers have studied many types of oscillators for energy harvesting, but the most common is the linear resonator. It is a simple system in which the undamped natural frequency is tuned to the excitation frequency (STEPHEN, 2006). Considering harmonic excitation, where there is excitation at one frequency or multiple harmonics of this frequency, the principle of superposition can be applied as the system is considered to be linear. Thus, once a single harmonic has been studied, it is easy to extend the analysis for all harmonics.

This chapter investigates the base excitation of a single-degree-of-freedom (SDOF) mass-spring-damper oscillator. Assuming that the power harvested is the same as the power absorbed by the damper (WILLIAMS; YATES, 1996), a mathematical model for an energy harvesting device considering steady-state excitation is developed with the aim to identify the optimum operational condition for the harvester to scavenge the maximum amount of energy. An approximate expression is then derived for an energy harvesting device for both the transient and steady-state response. Again, the aim is to identify the optimum operational condition.

The intention here is not show the differences in technologies to convert mechanical energy into electrical energy, but to demonstrate how generators work to extract energy from environmental vibrating sources.

2.2   Base excitation

The base-excited single degree-of-freedom (SDOF) system shown in Fig. 1 is considered in this chapter. The vibrating base transmits vibration to the seismic mass through the spring and damper. Depending on the system configuration, the vibration of the mass can be greater or lower than the amplitude of the base vibration.

Figure 1– SDOF mass-spring-damper base-excited system.
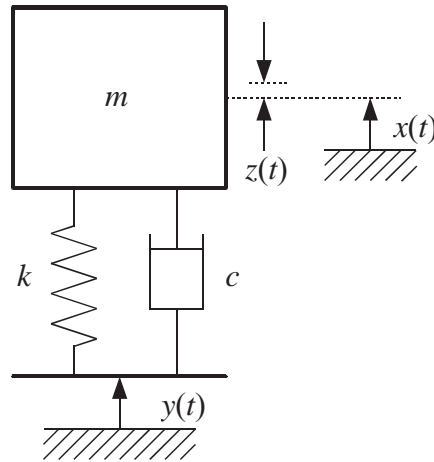
Source: Author.

The equation of motion for the system in Fig. 1 is (RAO, 2008):

$$m\ddot{x}(t)+c\dot{x}(t)+kx(t)=c\dot{y}(t)+ky(t). \tag{1}$$

where m is the seismic mass, k the spring stiffness, c the viscous damping, $y(t)$ the base displacement and $x(t)$ is displacement of the mass and t is time. The overdots represent differentiation with respect to time. Letting $z(t)=x(t)-y(t)$, the equation of motion can be rewritten in terms of the relative motion between the seismic mass and base displacement as

$$m\ddot{z}(t)+c\dot{z}(t)+kz(t)=-m\ddot{y}(t). \tag{2}$$

Considering the base excitation is given by $y(t)=Y\cos(\omega t)$, the relative motion is given by $z(t)=Z\cos(\omega t-\varphi)$, where Y and Z are the base and the relative displacement amplitudes, respectively, ω is the excitation frequency and φ is the phase angle. Equation (2) can be rearranged to give the modulus of the relative transmissibility T of the system, which is given by

$$T=\left|\frac{Z}{Y}\right|=\frac{m\omega^2}{\sqrt{\left(k^2-m\omega^2\right)^2+\left(c\omega\right)^2}}. \tag{3}$$

To gain more insight into the effects of the system parameters, both numerator and denominator are divided by $m\omega_n^2$, so that Eq. (3) can be rewritten in non-dimensional form as

$$T = \left|\frac{Z}{Y}\right| = \frac{\Omega^2}{\sqrt{\left(1-\Omega^2\right)^2 + 4\zeta^2\Omega^2}}, \tag{4}$$

where $\zeta = c/2m\omega_n$ and $\Omega = \omega/\omega_n$ in which $\omega_n = \sqrt{k/m}$ is the undamped natural frequency of the system. Equation (4) is plotted in Fig. 2 for different values of damping ratio.

Figure 2 – Relative displacement transmissibility as a function of frequency ratio for different values of damping ratio: $\zeta = 0.01$, ($\cdot\cdot\cdot$) green dotted line; $\zeta = 0.05$, (——) black solid line; $\zeta = 0.1$, (— · —) blue dashed dotted line; $\zeta = 0.25$,(— —) red dashed line.
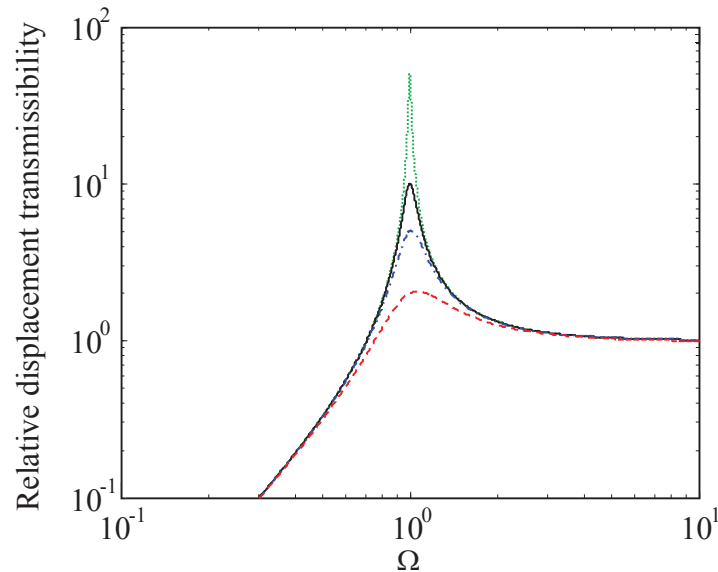
Source: Author.

As can be seen in Fig. 2, for an excitation frequency much lower than the undamped natural frequency $(\Omega \ll 1)$, the relative displacement amplitude is less than the base displacement amplitude. As the excitation frequency increases so that it is close to the undamped natural frequency of the system, the system acts as a displacement amplifier. For frequencies much higher than this $(\Omega \gg 1)$, the relative displacement amplitude is equal to the base displacement amplitude. When the system is operating at its resonance frequency, that is, the excitation frequency is equal to the undamped natural frequency $(\Omega = 1)$, the relative displacement amplitude is very large compared to the base displacement. In this condition, the

damping controls the system behaviour. Varying the damping changes the shape of the transmissibility curve, making it a very important property in the harvesting of energy from low levels of vibration.

To increase the amplitude of vibration of the seismic mass, the damping ratio must be decreased. However, for a small amount of damping the harvesting device should be large enough to accommodate a large motion of the seismic mass compared to the transducer housing.

2.3   Energy harvesting from time-unlimited periodic vibration

As discussed in the previous section, a SDOF mass-spring-damper is used to model an oscillator which can convert mechanical energy from vibrating energy into electrical energy. This was first proposed by Williams and Yates (1996). Since then many researchers, for example (STEPHEN, 2006; GUYOMAR et al., 2007; SERRE, 2009; CASSIDY et al., 2011), have used this model, mostly to study electromagnetic, piezoelectric and electrostatic generators.

Since the early studies on energy harvesting from vibration, most researchers have conducted their analysis based on harmonic base excitation for an unlimited time, i.e., steady-state vibration. For a SDOF system subjected to harmonic base excitation, the maximum energy harvested is obtained when the frequency of excitation coincides with the undamped natural frequency of the device.

In this dissertation , the conversion of mechanical energy to electrical energy is not considered. Rather, the optimum mechanical parameters of the device are sought by assuming that the electrical energy harvested is equal to the mechanical energy dissipated.

2.3.1   Existing model

The base-excited SDOF system shown in Fig. 1 is considered, whose equation of motion is given by Eq. (2). Assuming that the vibrating source induces the mechanical base of the system to oscillate as $y(t) = Y \cos(\omega t)$, the steady-state solution of the differential equation is given by (RAO, 2008) as

$$z(t) = Z \cos(\omega t - \varphi), \tag{5}$$

where φ is the phase angle and is given by

$$\varphi = \arctan\left(\frac{c\omega}{k - m\omega^2}\right). \tag{6}$$

The energy harvested for one cycle $(2\pi/\omega)$ is given by (STEPHEN, 2006)

$$E = \int_0^{\frac{2\pi}{\omega}} c\dot{z}(t)^2 \, dt. \tag{7}$$

Substituting for $z(t)$ from Eq. (5) gives

$$E_{cycle} = c\omega^2 Z^2 \int_0^{2\pi/\omega} \sin^2(\omega t - \varphi) \, dt = \pi c \omega^2 Z^2. \tag{8}$$

The average power flow is given by $P_{avg} = \omega E_{cycle}/2\pi$, which results in (STEPHEN, 2006)

$$P_{avg} = \frac{1}{2} c \omega^2 Z^2. \tag{9}$$

Equation (9) shows that the power tends to infinity ($P_{avg} \to \infty$) as $c \to \infty$ or $Z \to \infty$. However, in the first case, if the damping is very large, there is no relative motion and the base displacement amplitude needs to be infinite ($Y \to \infty$), which is not a plausible situation.

Substituting for Z from Eq. (3) into Eq. (9), the average power results in

$$P_{avg} = \frac{c m \omega^6 Y^2}{2\left(\left(k^2 - m\omega^2\right)^2 + (c\omega)^2\right)}. \tag{10}$$

Setting $V = \omega Y$, where V is the amplitude of the base velocity, and $c = 2m\zeta\omega_n$, Eq. (10) can be rewritten as

$$P_{avg} = m\omega V^2 \frac{\Omega^6 \zeta}{\left(1-\Omega^2\right)^2 + 4\zeta^2\Omega^2}. \tag{11}$$

2.3.2   Maximum Power Harvested for a Linear Device

As well as the mass, the excitation frequency and the amplitude of the base velocity play an important role. The performance of a linear energy harvesting device is influenced principally by two parameters, frequency and damping ratio. As seen in the previous section, a higher transmissibility of motion occurs when the oscillator is operating at resonance and a lower damping ratio result in a higher relative motion. From this, assuming $\Omega = 1$ in Eq. (11), the maximum power harvested is given by

$$P_{max} = \frac{m\omega V^2}{4\zeta} \tag{12}$$

If $\zeta \to 0$, the average power tends to infinity and appears to achieve its highest performance. However, setting the damping ratio to zero ($\zeta = 0$) implies that the device is not harvesting any energy at all. Also, it means that the amplitude of the relative displacement is very large. This is not a plausible operating condition, because this will require that size of the oscillator to be very large.

Because of the restriction in housing size, the damping ratio should be defined as function of maximum relative displacement amplitude. From Eq. (4), for a mechanical system at resonance, the minimum damping ratio is related to the maximum relative displacement by

$$\zeta_{min} = \frac{Y}{2Z_{max}}. \tag{13}$$

Substituting Eq. (13) into Eq. (12), the average power can be expressed by

$$P_{avg} = \frac{m\omega^3 Y Z_{max}}{2} = \frac{m\omega A Z_{max}}{2} \tag{14}$$

where A is the base acceleration amplitude.

Williams et al (2001) and Saba el al (2012) suggested that, for an excitation force composed of multiple harmonics, the power harvested is proportional to the rate of change of acceleration (ωA). The frequency that this occurs is the one that the undamped natural frequency of the oscillator should be tuned to.

2.4   Energy harvester model from time-limited periodic vibration

As seen in the previous section for harmonic excitation from environmental sources, many researchers assume a steady-state response condition. That is, the energy is disregarded in the transient stages. However, depending of the vibrating source, the transient responses could be more dominant than the steady-state response.

Gatti et al. (2014) presented an approximate equation for energy harvest considering both the initial starting transient and the steady-state condition. They compared the situation between time limited and time unlimited periodic vibration showed that the oscillator has better performance for unlimited excitation time, i.e., the starting transient has a detrimental effect. Despite the difficulty of modelling energy harvesters for transient plus steady-state, it is essential to do this for situations where there is a short excitation time (LALLART; INMAN; GUYOMAR, 2010; KREMER; LIU, 2014).

This section presents a discussion on the operating conditions where it will be possible to scavenge the maximum amount of energy for an initial transient plus steady-state response. As before, the analysis presented considers only the mechanical energy, disregarding the transduction mechanism.

2.4.1   Existing model

The base-excited SDOF mass-spring-damper shown in Fig. 1, whose equation of motion is given by Eq. (2) is considered here. Considering, now, that vibrating source excites the base of the device with a periodic harmonic excitation, $y(\tau) = Y \cos(\Omega \tau)$, where $\tau = \omega_n t$ and assuming zero initial conditions, the full solution of the differential equation of motion is given by (RAO, 2008)

$$z(\tau) = \frac{Y\Omega^2}{\sqrt{\left(1-\Omega^2\right)^2 + 4\zeta^2\Omega^2}}\left(\cos\left(\Omega\tau - \varphi\right) - \frac{e^{-\zeta\tau}}{\sqrt{1-\zeta^2}}\cos\left(\sqrt{1-\zeta^2}\,\tau - \alpha\right)\right), \tag{15}$$

where the phase angles are $\varphi = \arctan\left(\dfrac{2\Omega\zeta}{1-\Omega^2}\right)$ and $\alpha = \arctan\left(\dfrac{\left(1+\Omega^2\right)\zeta}{\left(1-\Omega^2\right)\sqrt{1-\zeta^2}}\right)$.

The energy harvested over n excitation cycles is given by (STEPHEN, 2006)

$$E = 2m\zeta\omega_n^2 \int_0^{\frac{2\pi n}{\Omega}} \left(\frac{\partial z(\tau)}{\partial \tau}\right)^2 d\tau. \tag{16}$$

Now, the optimal operational condition for a base-excited SDOF system, as seen in section 2.1, is when the undamped natural frequency of the oscillator coincides with the excitation frequency and there is very light damping. In this case, for $\Omega = 1$ and $\zeta^2 \ll 1$ the relative displacement given by Eq. (15) simplifies to

$$z(\tau) = \frac{Y}{2\zeta}\left(1 - e^{-\zeta\tau}\right)\sin(\tau). \tag{17}$$

Differentiating this and substituting the result into Eq. (16) gives

$$E = 2m\xi\omega_n^2 \int_0^{\frac{2\pi n}{\Omega}} \left(\frac{\partial z(\tau)}{\partial \tau}\right)^2 d\tau = \frac{e^{-4\pi n\zeta}Y^2\left[\left(4+\zeta^2\right)\left(-1+4e^{2\pi n\zeta}-\zeta^2+4\pi n\zeta e^{4\pi n\zeta}\right)\right]}{16\zeta^3\left(4+\zeta^2\right)} + \cdots$$

$$\cdots + \frac{e^{-4\pi n\zeta}Y^2\left[\zeta^2\left(4-4e^{2\pi n\zeta}+\zeta^2\right)\right] - Y^2\left[\left(4+\zeta^2\right)\left(3-\zeta^2\right)+\zeta^4\right]}{16\zeta^3\left(4+\zeta^2\right)}. \tag{18}$$

Assuming a very low damping ratio ($\zeta^2 \ll 1$) and $V = \omega_n Y$, the overall energy harvested Eq. (18) can be rewritten as

$$E = \frac{1}{2}m\omega_n^2 Y^2 \frac{\pi n}{\zeta}\left(1 - \frac{3 + e^{-4\pi n\zeta} - 4e^{-2\pi n\zeta}}{4\pi n\zeta}\right). \tag{19}$$

It can be seen that the expression for the energy harvested for time-limited excitation is proportional to the mass, to the square of the base velocity amplitude and to the number of excitation cycles, and it is inversely proportional to the damping ratio.

2.4.2 Maximum power harvested for a linear device

As discussed in the last section, it is essential to determine the parameters that result in a high performance of the energy harvester. It is noted in Eq. (19) that the optimum operational condition is influenced by the size of the seismic mass, the base velocity amplitude, the number of excitation cycles and the damping ratio. However, it is the expression inside the parenthesis that changes the optimum damping ratio in function of the number of excitation cycles. So, introducing $\sigma = \pi n \zeta$, the energy harvester expression, normalized by the mass, to the base velocity amplitude and number of excitation cycles squared, can be rewritten as

$$\hat{E} = \frac{E}{\frac{mV^2}{2}(\pi n)^2} = \frac{1}{\sigma} - \left(\frac{3 + e^{-4\sigma} - 4e^{-2\sigma}}{4\sigma^2} \right). \qquad (20)$$

Thus, the approximate expression for energy harvested is rewritten as function of only one variable. To identify the optimum value of σ for which the normalized energy is maximum, Eq. (20) is numerically solved and it is graphically represented in Fig. 3 using a log-log scale. Examining Fig. 3, it is clear that the there are two asymptotes for $\sigma << 1$ and $\sigma >> 1$. They are given, respectively by $\hat{E} = 4\sigma/3$ and $\hat{E} = 1/\sigma$, and are also plotted in Fig. 3. It is not possible to determine a simple expression for the maximum of Eq. (20), however, an approximate optimum value for its maximum can be determined by setting the two asymptotes to be equal, which is when $\sigma = \sqrt{3}/2 = 0.866$. The numerical solution of Eq. (20), is given by $\sigma = 0.9463 \approx 1$. Examining Fig. 3, it can be seen that the maximum energy harvested is not very sensitive to σ when it is close to $\sigma = 1$. Thus it suggested that a simple rule to determine the optimum damping is given by

$$\zeta_{opt} \approx \frac{1}{\pi n}. \qquad (21)$$

Figure 3 – Numerical solution to the approximated energy harvested equation as function of σ (—) black solid line. The green solid dashed line is for $\hat{E} = 4\sigma/3$; the magenta solid long dashed line is for $\hat{E} = 1/\sigma$; the blue thin dash dotted line is for $\sigma = 0.866$; and the red thin dash two dotted line is for $\sigma = 0.9463$.
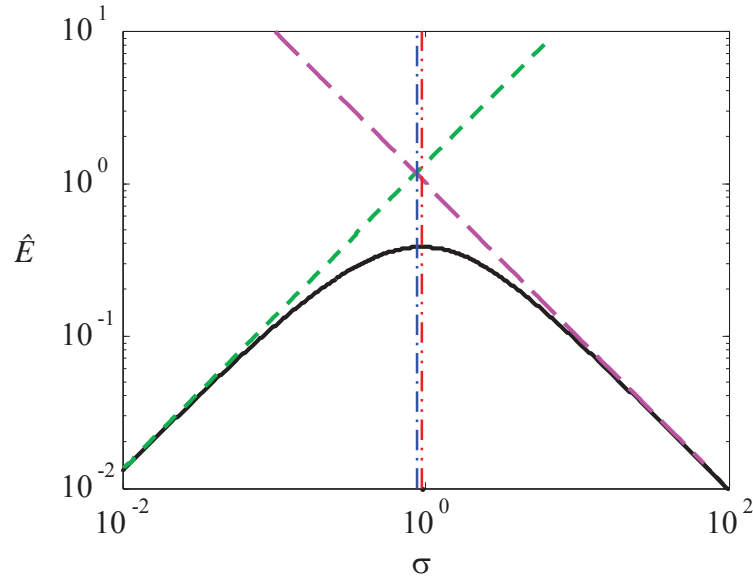
Source: Author.

Substituting this into Eq. (18) and (20), the approximate maximum energy harvested is found to be

$$E_{max} \approx \frac{1}{2}mV^2\left(\frac{\pi n}{2}\right)^2\left(1-e^{-4}+4e^{-2}\right) \tag{22}$$

and the maximum relative displacement amplitude is given by

$$Z_{max} = \frac{Y\pi n}{2}\left(1-e^{-2}\right). \tag{23}$$

To check the approximate model introduced in this section, Eq. (19) is plotted in Fig. 4 (○) blue circles as a function of the damping ratio and for different numbers of excitation cycles and compared with the solution obtained by integrating Eq. (16) (—) red solid line. It can be seen that both solutions are indistinguishable. Thus, it can be concluded that the expression derived for energy harvested considering the initial transient and the steady-state response is

reasonable. The maximum energy at different time cycles calculated using the approximate expression given in Eq. (23), is also plotted in Fig. 4 as a horizontal black dotted lines. It can be seen that the approximate energy harvester expression has good agreement with the numerical results.

Figure 4 – Non-dimensional energy harvested, as a function of the damping ratio for different values of the number of excitation cycles. Energy computed by the approximate relation given in Eq. (19) (○) blue circles, energy computed numerically integrating Eq. (16) (—) red solid lines; maximum energy peaks from Eq. (23) (·· ·) black dotted line.
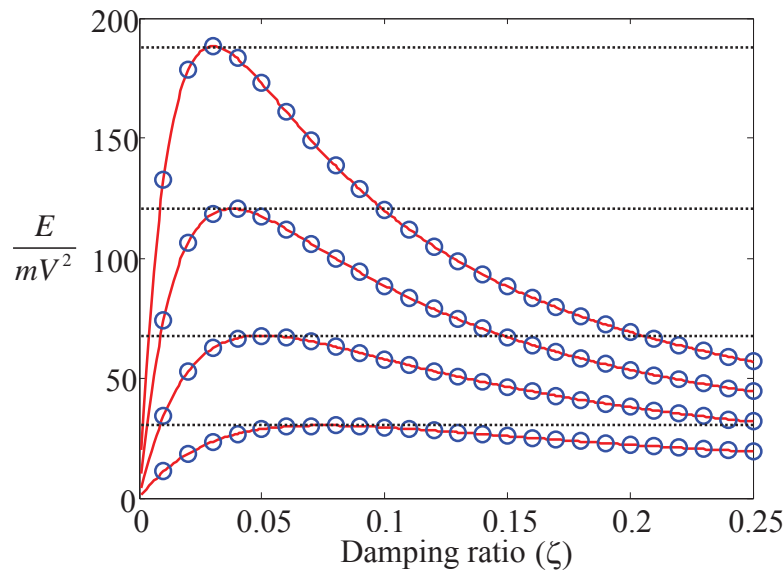
Source: Author.

Analysing the energy harvesting equation as a function of damping ratio for different numbers of excitation cycles, it is clear that the best oscillator performance does not occur when the damping ratio is minimum as it was for the steady-state condition. As the number of excitation cycles increases the design of the energy harvester parameters changes to maintain the optimum performance. As the excitation time increases the optimum damping becomes smaller.

2.5   Conclusions

A SDOF mass-spring-damper mechanical system has been used to characterize an energy harvester device embedded in a vibrating environmental source. When the excitation frequency is close to the undamped natural frequency, the oscillator operates at its best

condition. However, the optimum design for an energy harvester device has its performance limited by the size of the oscillator housing.

The study revealed that analysis about the average power harvested expression may be incorrectly interpreted. If damping is set to be very large, the average power tends to infinity. However, in this case there is no relative motion between the base and the seismic mass. If the damping is set to zero, there is no way to extract energy.

In practise, in many cases, the excitation source acts for a limited time, implying that both transient and steady state response should be considered. In this study, a model of an energy harvester for a time-limited harmonic excitation has been studied. It has been shown that, different to the energy harvester subjected to steady-state periodic excitation, the optimum damping for time-limited excitation is given by $\zeta = 1/\pi n$, where n is the number of excitation cycles. The study showed that the expression for a time-limited excitation has a good agreement with the solution achieved by numerical integration.

3 RAILWAY VIBRATION

3.1 Introduction

One of the most efficient systems for rapidly transporting people from one place to another is by railway. The increase in demand and with higher train speeds brings some undesirable problems, such as noise and vibration (THOMPSON, 2008). Much effort has been applied to increase the performance of high-speed trains. Equally, much effort has been spent reducing vibration to improve passenger comfort inside the train and to avoid discomfort of those who live near to railways lines. These vibrations occur due to the wheel/rail interaction and they can be subcategorized as trainload excitation, also known as quasi-static excitation, roughness excitation, flat wheel and others, known as dynamic excitation (SHENG; JONES; THOMPSON, 2004; LOMBAERT; DEGRANDE, 2009; THOMPSON, 2008).

Thompson (2012) compared the quasi-static and dynamic excitation, and showed that the first one is dominant at low frequencies (between 25 to 50 Hz, depending on the train speed) and generates high levels of vibration on the sleepers. Dynamic excitations, principally due the roughness between the wheel/rail interactions, is dominant at higher frequencies (higher than 25 to 50 Hz depending on the train speed). In a numerical prediction, Auersch (2005) obtained similar results for sleeper vibration and also showed that the quasi-static deflection is only dominant in very low frequencies for ground vibration close to the track.

In this chapter, the infrastructure of a railway track and its components are first described. The results obtained by Triepaischajonsak (2012) in her PHD thesis, concerning the influence of the track parameters and the vehicle parameters are then discussed. An analytical model to predict the dominant frequencies generated by a trainload is introduced as a model for the track deflection due the quasi-static excitation. Finally, using the latter model, the dominant frequencies and the track deflection of two different high speed trains (HST) pass-by train are determined.

3.2 Infrastructure

A typical railway track structure is shown in cross-section in Fig. 5. The rails are fastened to transversal supports, called sleepers, by clips. These supports, that can be of wood, concrete or steel, have the function of keeping a set distance from one rail to another and to keep the rails at a fixed position. In turn, these structures are placed on ballast and subgrade for

the purpose of reducing the propagation of noise and vibration generated by the passage of a train.

Figure 5– Rail track structure.
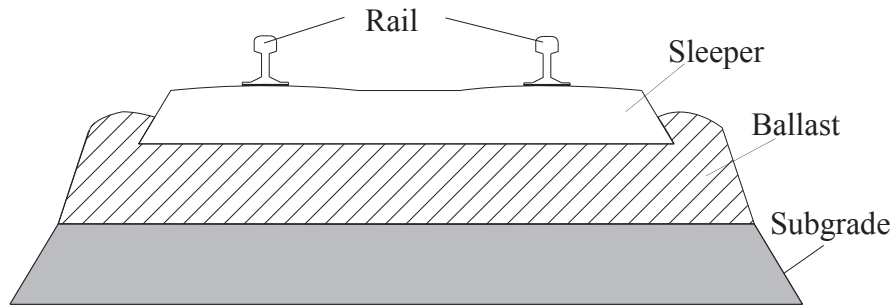
Source: Author.

3.2.1   Rail

Rails are longitudinal steel members placed on the equally spaced sleepers. The rails are the critical component in guiding the rolling stock. Their strength and stiffness must be ample to maintain a steady shape and a smooth track configuration, and to resist various forces exerted by travelling rolling stock (SELIG; WATERS, 1994). A main function of the rails is to accommodate and transfer wheel/axle loads on the track to the supporting sleepers (ESVELD, 2001). The standard form of rail used around the world is the flat bottom rail. It has a wide base that increases its adherence with the sleeper, giving more stability. However, to keep the rails in the correct position, screws or clips fasten them, as shown in Fig. 6, which depicts an example of a flat bottom rail fastened on a sleeper.

Figure 6 – Rail/sleeper assemble: (a) Fastened rail; and (b) expanded view of sleeper/rail assembling.

(a)   (b)
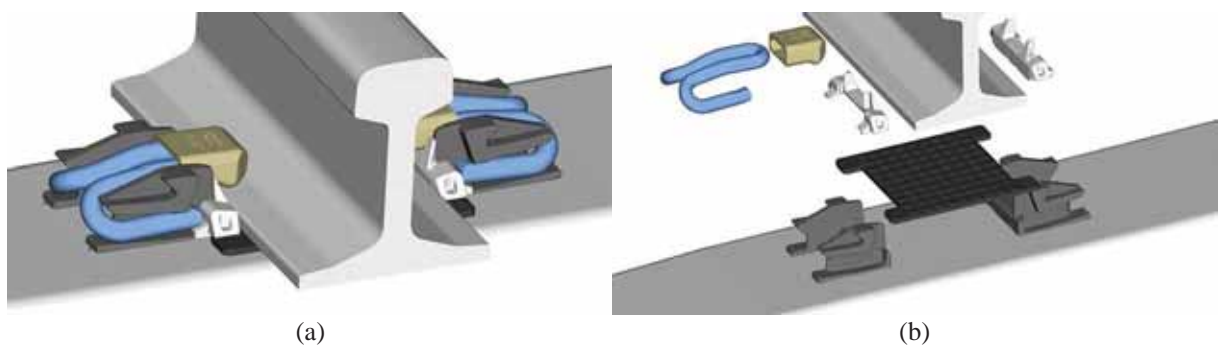
Source: Drawing of Pandrol (http://www.pandrol.com).

3.2.2   Sleeper

The main functions of a sleeper, following Selig and Waters (1994), are to distribute uniformly loads from the rail to the ballast, support the rail and restrain longitudinal, lateral and vertical movement due the passage of a train.

The sleeper is also known as a railroad tie, and was commonly made of either softwood or hardwood. Due to technology many years ago and the ease with which wood could be cut and drilled made it useful as a material for a sleeper (ESVELD, 2001).

The need to increase structural performance of a railway track meant that concrete and steel played an important role in this area. In addition to their capacity of lasting for more than 40 years (HOWE, 1976). Concrete sleepers can be placed 25% further from each other than those made of wood (ESVELD, 2001) and they have good performance under most situations.

There are other types of sleepers, for example the twin-bloc, which are a mix of concrete and steel. They are made of two concrete blocks with each end being connected by a steel bar. This type of structure may be up 30% lighter than a concrete sleeper.

3.2.3   Ballast

Ballast is a layer of free draining coarse aggregate used as a tensionless elastic support for the sleepers. This layer comprises graded crushed stone, gravel, and crushed gravel such as granite and basalt, which depends on local availability. It provides support and transfers the load from the track to the subgrade and the ground. Ballast has the function of providing stability to the sleepers absorbing shock and impact due the train passage (ESVELD, 2001).

3.3   The influence of the vehicle parameters on sleeper vibration

3.3.1   The effect of the axle load

Triepaischajonsak (2012) studied the effects of the axle trainloads. She showed, through the increase of the body mass, that the increase in the trainload value introduces a significant gain in the quasi-static deflection. She also showed that the vibration due the dynamic excitation increases at low frequencies, but the quasi-static deflection is still the main reason for the vibration in rail and the sleeper.

3.3.2   The effects of the train speed

Considering a study on clay soil and with train speeds varying between 10 to 50 m/s, Triepaischajonsak (2012) showed that an increase in train speed results in a significant increase in the amplitude for higher frequency of vibration. This occurs because the frequencies of the quasi-static load are proportional to the ratio of the carriage length to the train speed. So, as the vehicle velocity increases, i.e. the train speed, the dominant excitation frequencies are shifted to higher frequencies.

3.4   The prediction of vibration due to moving loads

A simple model of the passage of a train is just a sequence of travelling loads. Thompson (2008) showed, that the quasi-static excitation occurs when the trainloads apply a force, due the carriage weight, distributed in its wheelsets on a railway track, causing a small deflection of the rail, known as the quasi-static deflection. He also showed that the quasi-static excitation is dominant at low frequencies. For example, a train speed of 100 km/h, quasi-static vibrations dominate up to 25 Hz and for a train speed of 300 km/h, this is up to 100 Hz. At high frequencies, roughness excitation is greater than that due to the quasi-static deflection. For low frequencies, where vibration is dominated by the quasi-static excitation, the dynamics of the train can be disregarded.

3.4.1   Dominant frequencies of a passing train

Disregarding the dynamic excitation and the locomotive cars, Ju et al. (2009) derived an expression to predict the dominant frequencies due to the passage of a train and the influence factor for each frequency based on the characteristics of a train car. The spectrum of the loads due to wheels passing at a point is given by (JU; LIN; HUANG, 2009)

$$P\left(f\right) = \sum_{j=1}^{N_c} \sum_{k=1}^{N_w} P_{axle} e^{-i2\pi f\left(t_k + jt_c\right)} \tag{24}$$

where N_c is the number of train carriages, N_w is the number of pairs of wheels for each carriage and P_{axle} is the load of a pair of wheels, f is frequency and $i = \sqrt{-1}$; $t_k = s_k / S$, in which S is

the train speed (in meters per second) and s_k is the distance between the kth wheel and the beginning of the carriage, is the time taken to kth wheel set to pass and $t_c = L_c/S$, in which L_c is the distance between two carriage centres, is the time taken for the passage of each carriage. Substituting these into Eq. 24, the influence factor R_f can be determined and is given by (JU; LIN; HUANG, 2009)

$$R_f = |P(f)| = \left| \sum_{j=1}^{N_c} \sum_{k=1}^{N_w} P_{axle} e^{-i2\pi f(s_k + jL_c)/S} \right|. \tag{25}$$

The dominant frequencies of a passing train are defined as the largest influence factors and they are found at frequencies where (JU; LIN; HUANG, 2009)

$$f_{dom} = \frac{n}{t_c} = \frac{nS}{L_c} \tag{26}$$

where n is a integer multiple. This means that the dominant frequencies from a passing train are only dependent on the ratio between the train speed and the carriage length. If Eq. (26) is substituted into Eq. (25), the influence factor can be rewritten as

$$R_f = |P(f_{dom})| = \left| \sum_{j=1}^{N_c} \sum_{k=1}^{N_w} P_{axle} e^{-i2\pi n(s_k/L_c + j)} \right|. \tag{27}$$

From Eq. (27), it is shown that for normalized frequencies which correspond to an integer number, i.e. the dominant frequencies, the influence factor from a passing train are only dependent on the ratio between the wheel position and the carriage length, and more importantly, are independent of the train speed.

Two high speed train (HST) types[1] are considered. They are an Inter-city 125 class 43 with two power cars (one at each end), and 8 passenger coaches passing with a speed of 199 km/h, and a diesel multiple unit (DMU) class 220 Voyager with 4 passenger coaches, all driven,

---

[1] Two high speed train (HST) models with different geometry were chosen based on passing trains measured at Steventon and Grazeley Green sites by Triepaischajonsak (2012). A better explanation about them is given in Chapter 4.

passing with a speed of 118 km/h. The carriages are composed of two bogies with a pair of wheelsets on each bogie. The parameters for these train vehicles are given in Table 1. For an Inter-city 125, the distance between each wheelset and the begging of the carriage (s_k) are given by 2.15 m; 4.75 m; 18.15 m; and 20.75 m. For a DMU Voyager, the distances are 2.185 m; 4.435 m; 18.385 m; and 20.635 m. Applying these values for s_k in Eq. (25), Fig. 7 shows the influence factor normalized by the trainload for both trains.

Table 1 – Parameters for vehicles.

Parameters / Types of vehicle	Inter-city 125	DMU
	Mk3 passenger car	Voyager
Bogie centres (L_b) [m]	16	16.2
Bogie wheelbase (L_a) [m]	2.6	2.25
Vehicle length (L_c) [m]	22.86	22.82
Axle load [kN]	108.3*	81.2*

* Assumption value.
Source: Triepaischajonsak (2012).

The harmonic nature of the excitation introduced by the multiple axles is clearly seen in Fig. 7. This confirms that the dominant frequencies of a trainload are an integer multiple of the product of the ratio between the carriage length and the train speed. The vibration due to the passage of the power car was neglected for the purpose of calculating the vibration induced by the passage of a train. A higher train speed shifts the dominant frequencies to higher frequencies but does not affect their amplitudes (LOMBAERT; DEGRANDE, 2009).

Figure 7 – Influence factor of two HST model: (a) Inter-city 125 class 43 with 199 km/h; and (b) Class 220 with 114 km/h.

(a)

(b)
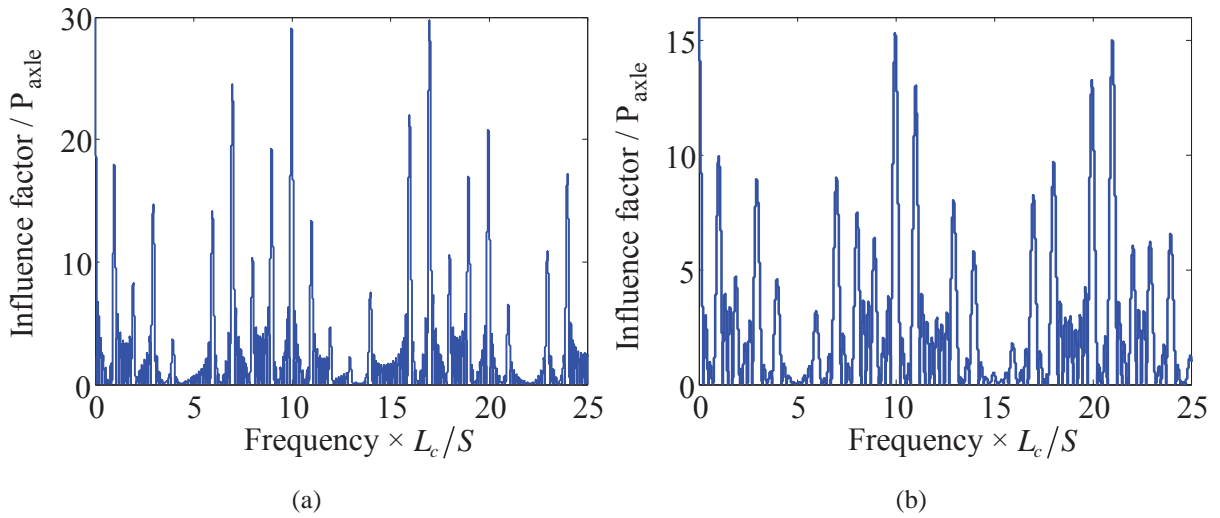
Source: Author.

3.4.2 Track deflection

Understanding the mechanism of excitation is fundamental to determining the behaviour of the vibration induced by the passage of a train. Each wheel exerts a static load on the track, causing a deflection that is localized around the wheel.

Grassie et al. (1982) showed that for low excitation frequencies, up to 100 Hz, a track resting on a simple elastic support is satisfactory for the analyse of track deflection due to the static moving load. Krylov and Ferguson (1994), Sheng et al. (1999) and Thompson (2008) presented an analytical model, assuming that the rail is modelled as a single Euler-Bernoulli beam, which makes it possible to calculate the deflection $w(x,t)$ of the track due the moving load with a constant speed. The track is treated as an elastic beam lying on a Winkler foundation, defined by its support stiffness k_f per unit length. $E_r I_r$ is the rail bending stiffness (Young's modulus E_r, and second moment of area, I_r). The differential equation of motion of the track for a static load P_{axle} acting on a beam is given by (THOMPSON, 2008)

$$E_r I_r \frac{\partial^4 w}{\partial x^4} + k_f w = P_{axle}\delta(x - St) \tag{28}$$

where δ is the Dirac delta and x is the position of each train wheelset in relation to the beginning of the train. The solution of Eq. (28) is given by (THOMPSON, 2008)

$$w(x,t) = \frac{P_{axle}\beta}{2k_f} e^{-\beta|x-St|}\left(\cos\left(\beta|x-St|\right) + \sin\left(\beta|x-St|\right)\right) \qquad (29)$$

where β and k_f are given by

$$\beta = \left(\frac{k_f}{4E_r I_r}\right)^{1/4} \text{ and } k_f = \left(\frac{1}{k_P} + \frac{1}{k_b}\right)^{-1}\Big/L_s$$

and, k_P and k_b are the stiffness of rail pad and the ballast per unit length, respectively and L_s is the sleeper spacing.

3.4.3 Numerical track deflection calculation

The deflections due the static moving loads are calculated for two sites in the UK, Steventon and Grazeley Green. The parameters for the bending-stiffness, rail pad and ballast stiffness are given in Table 2. Measurements on the rail-track structure carried out by Triepaischajonsak (2012) showed that the parameters for both sites are the same. However, as the railway lines are located in different places, they are subjected to the passage of different trains, whose geometry and speed are different for each site. The vehicles parameters are presented in Table 1.

The time history of the track deflection together with the spectrum for the passage of only one passenger coach is first calculated. Following this, the same analysis is carried out to determine the time history and the Fourier coefficients due the passage of an entire Inter-city 125 HST, disregarding the power car, and the DMU class 43 Voyager.

Figure 8 shows the solution of Eq. (29) due the passage of an Inter-city 125 HST with a speed of 199 km/h at Steventon. In particular, in Fig. 8a, the solid line shows the passage of a single wheel set, the solid and dashed line shows the passage of a single bogie and the solid, dashed and dotted lines show the passage of an entire passenger car. From the time history it can be seen that the fast contact of each wheelset with the rail leads to a small deflection in a

very short time. This excitation mechanism, similar to an impulse, is clearly seen in Fig. 8b. The passage of a single wheelset generates a spectrum with energy only at low frequencies, in this case up to 50 Hz. The spectrum due the quasi-static excitation is controlled by two factors, one is the train speed and the other is its dependence on β, or more specifically on the stiffness of the rail track structure since the bending stiffness does not vary along the track.

Table 2 – Parameters for a ballasted railway track (two rails).

Parameters		Values	
		Steventon	Grazeley Green
Rails	Mass per unit track length	120 kg/m	
	Bending stiffness	1.26×10^7 Nm²	
Rail pad	Rail pad stiffness per unit track length	3.5×10^8 N/m²	
Sleeper	Mass per unit length	490 kg/m	
	Sleeper spacing [m]	0.6	
Ballast	Ballast stiffness	3.15×10^8 N/m²	
	Mass per unit length	1200 kg/m	

Source: Triepaischajonsak (2012).

Figure 8 – Vertical rail deflection due to the pass-by HST Inter-city 125 with a speed of 199 km/h at Steventon site: (a) Time history; and (b) deflection spectrum. Red solid line (—), one wheelset; blue dashed line (— —), one bogie; and black dotted line (· ·), one passenger coach.

(a)   (b)
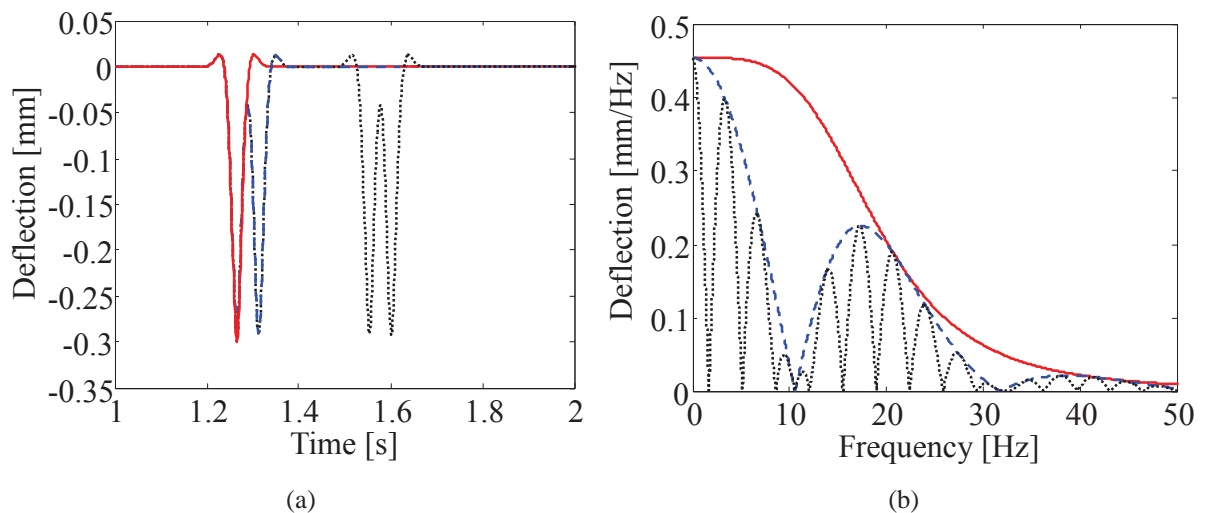
Source: Author.

Figure 9 shows the solution of Eq. (29) due the passage of a DMU class 220 Voyager with a speed of 118 km/h at Grazeley Green. In particular, in Fig. 9a, the red solid line shows the passage of a single wheelset, the red solid and blue dashed line shows the passage of a single bogie and the red solid, blue dashed and black dotted lines show the passage of an entire passenger car. Despite the geometry of the passing train at Grazeley Green being different from Steventon, the time histories of the quasi-static deflections are similar. It is observed that it only takes more time for the carriage pass through Grazeley Green than through Steventon, due the difference in train speed. A lower train speed results in a higher contact time between wheel and rail. This leads to a small deflection at Grazeley Green, but a larger contact time than at Steventon. Comparing both spectra shown in Fig. 8b and Fig. 9b, the effect of the train speed on the frequency range where the trainload energy is contained is clear. For the Grazeley Green site the frequency range is up to 30 Hz.

Figure 9 – Vertical rail deflection due to the pass-by DMU class 220 Voyager with a speed of 118 km/h at Grazeley Green site: (a) Time history; and (b) deflection spectrum. Red solid line (—), one wheelset; blue dashed line (— —), one bogie; and black dotted line (··), one passenger coach.

(a)   (b)
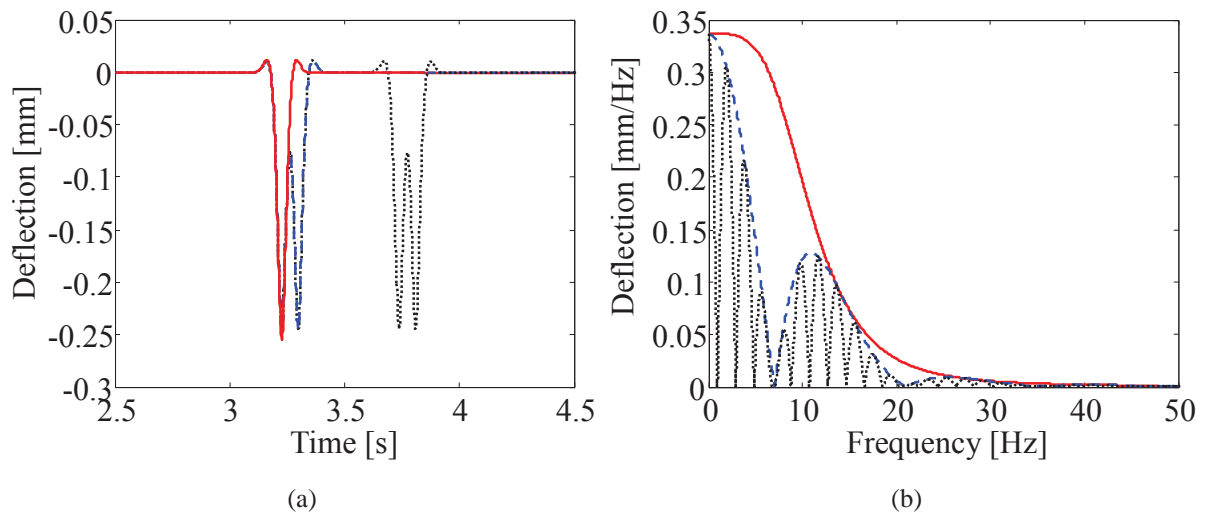
Source: Author.

When more than one wheelset is considered, the effect of the bogie spacing L_b or the carriage length L_c interferes in the excitation mechanism. This can be observed in the spectrum of the rail deflection. In the time histories shown in Fig. 8a and Fig. 9a, it can be seen that the passage of another wheelset introduces another load, similar to the passage of a single wheelset. In Fig. 8b and Fig. 9b, for a passage of a single bogie, it can be seen that the deflection spectrum

is modulated and its amplitude is limited by the deflection spectrum due the passage of a single wheelset. Similar behaviour is observed for the passage of an entire train carriage. The spectrum is modulated too, but, in this case, the envelope is the deflection spectrum due the passage of a single bogie.

Figure 10 – Vertical rail deflection due to the pass-by HST Inter-city 125 class 43, disregarding the power car, with 8 passenger car and a speed of 199 km/h in Steventon site: (a) Time history; and (b) Fourier coefficients.

(a)   (b)
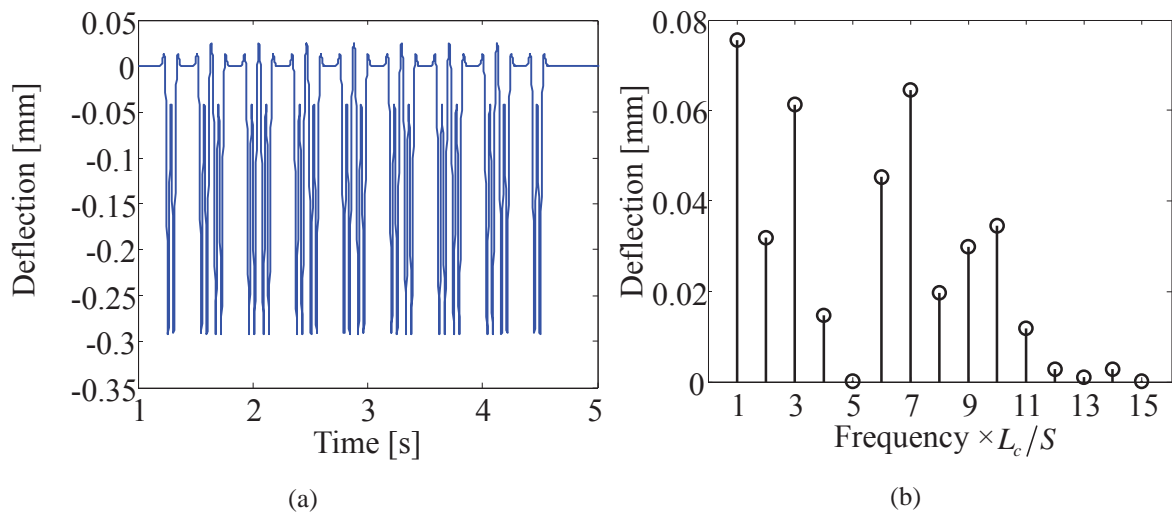
Source: Author.

Figure 10 shows the time history and the corresponding Fourier coefficients of the deflection for the passage of 8 passenger cars of an Inter-city 125 HST. It is noted that the Fourier coefficients in Fig. 10b have frequencies, which are related to the ratio between the train speed and the carriage length. This is similar to those observed in the influence factor (Fig. 7a), induced due the train loads (JU; LIN; HUANG, 2009).

The analysis for the passage of a train at Steventon can be carried out for a DMU train at Grazeley Green. The results are shown in Fig. 11. It can be seen that the amplitudes of the Fourier coefficients are different to the Steventon case, and the largest peaks appear at different frequencies. Also, it is observed that, as for the Inter-city 125 HST, from the 12th harmonic the amplitude is very low. However, it is clear from Fig. 11b that the dominant peaks appears at integer number of the frequency normalized by the ratio between train speed and the car length. As already observed by Ju et al. (2009) and Kouroussis. G et al. (2014), a small number of carriages induces less pronounced dominant peaks.

Figure 11 – Vertical rail deflection due to the pass-by HST class 220 with 4 passenger car, all driven, and a speed of 114 km/h in Grazeley Green site: (a) Time history; and (b) deflection spectrum.

(a)   (b)
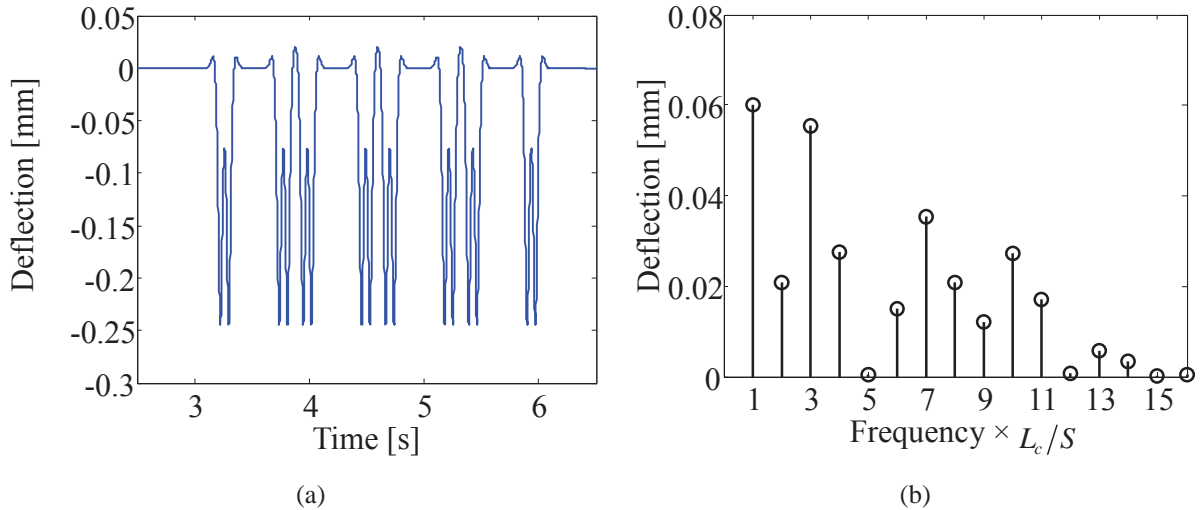
Source: Author.

To further examine the physical mechanism of excitation, the time history of an Inter-city 125 with 199 km/h velocity deflection at Steventon is shown in Fig. 12. In particular, Fig. 12a shows the velocity measurement[2] of the sleeper vibration, while Fig. 12b shows the velocity of the track deflection determined by the differentiation of Eq. (29). Comparing both figures, it can be seen that they are both similar. The effect of the rail deflection due the passage of a wheelset, and the effects of the passage of the bogies and entire train are clear. The small differences are due the presence of the power cars in the measured data and the vibration induced by the roughness due the contact between the wheel and the rail.

---

[2] The use of the measurement of the sleeper vibration, here is just to emphasise the effects of the rail track deflection. The measurements are better described in Chapter 4.

Figure 12 – Time history of (a) sleeper velocity; and (b) deflection velocity.

<div align="center">(a)</div>

<div align="center">(b)</div>
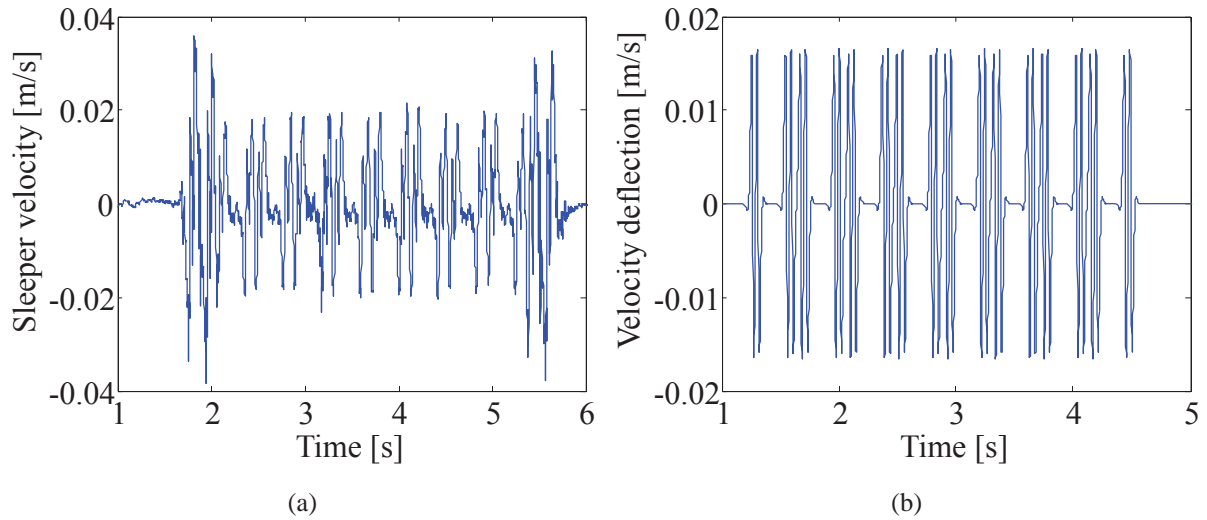
Source: Author.

3.5   Conclusions

The study in this chapter presented a basic railway track structure and some components that may affect the vibrations levels. A model for the influence factor of a trainload was introduced. It showed that the dominant frequencies due a quasi-static excitation are integer multiples of the ratio between the vehicle length and train speed. It also showed that an increase or decrease of the train speed does not change the amplitudes, it only shifts the dominant frequencies. A simple railway track was modelled considering an Euler-Bernoulli beam lying on a Winkler foundation as function of the ballast and rail stiffness and the rail bending stiffness. Numerical calculations for two geometrically different trains with different speeds showed that the passage of each wheelset produces a deflection curve similar to an impulse, which is very clear when the spectrum of a single wheelset is observed. Moreover, the dominant frequencies of the rail deflection are similar to those found from the influence factors and, as the number of carriages increases, the amplitude of the dominant frequency peaks also increases.

4   ENERGY HARVESTING FROM RAILWAY VIBRATION: MEASURED DATA

4.1   Introduction

One concern with railways is related to the mitigation of noise and vibration induced by passing trains. For decades, researchers have investigated railway and train interaction to increase the performance of this type of transport. Recently, mechanical energy from vibrations induced by passing trains has been converted into electrical energy and used to power microelectromechanical systems (MEMS), such as a wireless sensor network to transmit data for structural health monitoring, for example.

This chapter investigates the amount of energy that can be harvested by a single linear harvester from the vertical acceleration measured in the middle of a sleeper due the passage of a train. Four Inter-city 125 high speed trains (HST) are considered with different speeds at the Steventon site in the United Kingdom, and two Diesel multiple unit (DMU) Voyager trains, at Grazeley Green, also in the United Kingdom. Numerical analysis to investigate the optimum parameters for a linear energy harvester is performed and the maximum available mechanical energy that the device could potentially scavenge from these vibrating sources is calculated.

The complete set of results for the numerical analysis of an Inter-city 125 HST passing at Steventon site for different train speeds is presented in Appendix A. For a DMU Voyager train passing at Grazeley Green, the complete set of results is presented in Appendix B.

4.2   Measurements

In order to investigate the optimum parameters necessary for an energy harvesting device to maximize its performance, the vibrations induced by passing trains should be first evaluated. The measurements of ground vibration presented here has been carried out at two sites in Southern England during September 2008 (TRIEPAISCHAJONSAK, 2012)[3].

The two sites were located at Steventon, on the Didcot to Swindon line and Grazeley Green on the Basingstoke to Reading line, as shown in Fig. 13 and Fig. 14. The soil in both cases consists of deep layers of clay, which at the time of the measurements, was saturated.

---

[3] The measurements were carried out by Dr Triepaischajonsak as part of her thesis *The influence of various excitation mechanisms on ground vibration from trains* and by Dr Jones and Dr Ryue as part of RRUK project work. Professor Dr Thompson, from ISVR, gave to the author of this dissertation the measurement data for this research project.

Figure 13 – Location of Steventon test site, map view (grey solid line - railway track).

Source: Google maps – adapted from Triepaischajonsak (2012).

Figure 14 – Location of Grazeley Green site, map view of (grey solid line - railway track) (a) Basingstoke to Reading line; (b) region of measurement.

| (a) | (b) |

Source: Google maps – adapted from Triepaischajonsak (2012).

The following equipment was used to collect the vibration data: piezoelectric ICP accelerometers PCB type 353B03 with a frequency range of up to 7 kHz and mass of 10.5 g; a signal conditioner ICP type 480E09; a PROSIG analyser with 8 channels. The experiment at each site involved measuring vibration due to various passing trains. In these experiments, the vibration was measured at the centre of a railway sleeper as shown in Fig. 15. The results from various types of trains are used to investigate the optimum system parameters to harvest the maximum energy.

Figure 15 – The accelerometer measurement position on a railway sleeper.

Source: Adapted from Triepaischajonsak (2012).

In order to calculate the speed of the trains, a digital video camera was used to record the time taken for the train to pass over the site. One type of train was measured on the Didcot to Swindon line at Steventon and another type of train on the Basingstoke to Reading line at Grazeley Green. These are indicated, with the corresponding lengths, in Table 3. The speeds of trains were calculated from their lengths and the time taken for them to pass through the site. They are shown in Table 3. In Triepaischajonsak's thesis (2012) many train measurements were presented for both sites. However, for the research project described in this dissertation, Professor Dr Thompson from the Institute of Sound and Vibration Research in Southampton (ISVR) give four train measurements from the Steventon site and two from the Grazeley Green site. At the first site, the measurement was carried out for a Class 43 (HST) train, as known as an Inter-city 125. It consists of two power cars, one in each end, and eight passenger carriages. At the second site, the measurement was carried out for a Diesel Multiple Unit (DMU) class 220 Voyager train that consists of four passenger carriages, all of which are driven. Fig. 16 shows an example of each train model.

Figure 16 – Passenger trains: (a) Inter-city 125 HST class 43; and (b) DMU Voyager class 220.

| (a) | (b) |

Source: (a)Tehrani et al. (2013); (b) Llewelyn (2010)

Table 3 – The lengths, time taken and speed for each type of trains passing by Steventon and Grazeley Green sites.

Location / Type of the train		Length [m] / car		Time taken [s]	Speed [km/h]
		Power	Passenger		
Steventon	Class 43 HST	17.79	22.86	5.10	162
				4.62	178
				4.22	195
				4.15	199
Grazeley Green	DMU class 220	-	22.82	3.54	114
				3.51	118

Source: Author.

For each train measurement, acceleration time-histories were recorded. The times taken were chosen to ensure that all useful data were kept. Fig. 17a shows the acceleration time-histories for a Class 43 (HST) at Steventon site and Fig. 17b shows the acceleration time-histories for a Class 220 train at Grazeley Green. The acceleration time-histories were acquired at a sample rate of 1 kHz for 32.7 seconds, but only 7 seconds of data are shown.

Figure 17 – Acceleration time-histories of the vertical sleeper vibration for two different passing trains: (a) Steventon site with 199 km/h; (b) Grazeley Green site with 118 km/h.

(a)   (b)
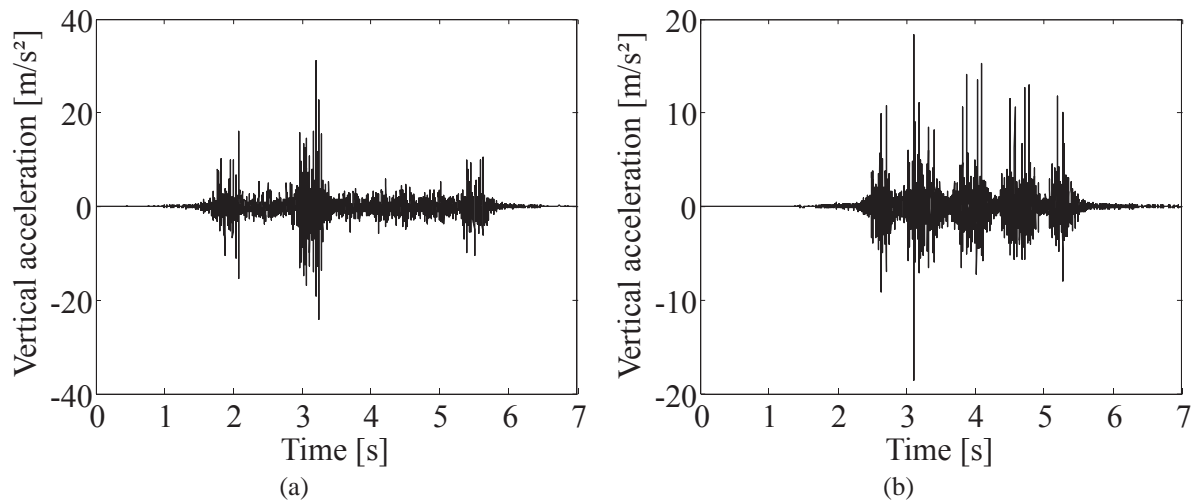
Source: Author.

4.3   Train induced vibration

The mechanisms of vibration induced by a passing train were discussed in chapter 3. The vibration induced due the passage of a train is caused by two mechanisms. One is due the quasi-static excitation, where the trainloads cause a very small deflection of the rail, known as quasi-static deflection, which in general, occurs at low frequencies. The other mechanism is due the train dynamics, principally due the roughness and the interaction between the train wheels and the rail. Since the operational frequency range of the harvester is below 35 Hz, as observed by Tehrani et al. (2013), the dynamics of the railway track can be disregarded as shown by Thompson (2008) in a comparison of excitation mechanisms for low frequencies.

The power spectral density (PSD) of the vertical acceleration of a sleeper for an Inter-city 125 HST with a velocity of 199 km/h and 162 km/h are shown in Fig. 18. For the other trains passing at Steventon site with a speed of 178 km/h and 195 km/h, the PSD of the vertical acceleration of these trains are shown in Appendix A, which contains the complete set of results for the Stevenson site. For the sleeper vertical acceleration of a DMU class 220 at Grazeley Green site, the PSD is shown in Fig. 19, and the PSD of DMU Voyager with a speed of 114 km/h is shown in Appendix B, which contains a complete set of data for the Grazeley Green site. At the top of each figure showing the PSD, another frequency axis is shown, which is the frequency normalized by the ratio between the train speed and the length of the passenger carriage (S/L_c). For the PSD of the passing trains at Steventon and Grazeley Green site, it can be noted that the peaks in the spectrum appears to be an integer multiple of the ratio between the train speed and the carriage length. This ratio was referred to as the trainload dominant frequencies in (JU; LIN; HUANG, 2009).

In particular, from Fig. 18, for a passing train at Steventon, the effect of the train speed is cleared observed when comparing Fig. 18a and Fig. 18b. As the velocity of a passing train, with the same geometry, increases (decreases), the trainload dominant frequencies shift to higher (lower) frequencies. As the amplitude of the acceleration spectrum is proportional to the amplitude of the displacement spectrum multiplied by frequency squared ($Y\omega^2$), the dominant frequencies change with the train speed; the acceleration spectrum also changes. In addition, it is also observed that the maximum acceleration occurs when the harmonic frequency corresponds to the 7th order.

Figure 18 – PSD of the sleeper vertical acceleration at Steventon site for an Inter-city 125 HST class 43 pass-by train: (a) 199 km/h; and (b) 162 km/h.

(a)

(b)
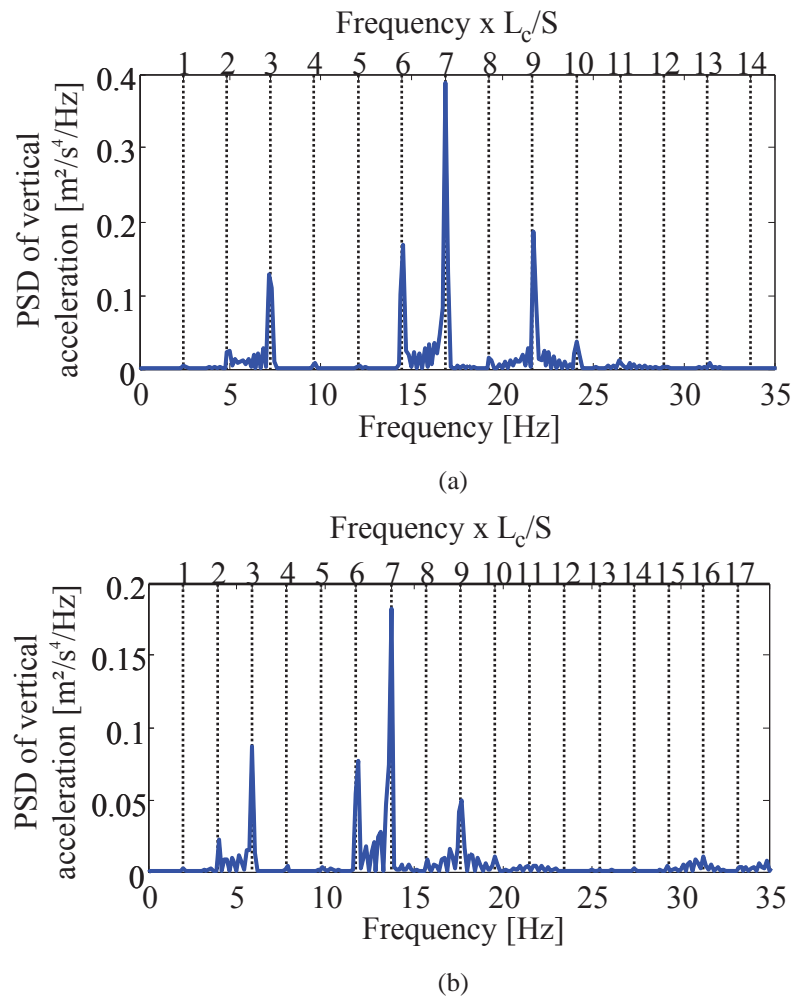
Source: Author.

Examining the PSD of the vertical acceleration of a sleeper at Grazeley Green site shown in Fig. 19, it can be seen that the trainload dominant frequencies are different from those observed from the passing trains at the Steventon site. As the geometry of both trains differ, as observed in the influence factors from an Inter-city 125 HST and a DMU Voyager, shown in Fig. 7, it is expected that the amplitudes at the trainload dominant frequencies will differ.

For the DMU Voyager passing through Grazeley Green with a velocity of 118 km/h, it can be seen that there are two frequencies with very close acceleration amplitude, with the amplitude corresponding to the 3rd harmonic order being slightly higher. Comparing this with the PSD of the DMU Voyager passing train with a speed of 114 km/h shown in Fig. B.2, the effect of the train speed can be observed. It can also be noted that the acceleration peak corresponding to the 10th harmonic order is slightly higher.

Figure 19 – PSD of the sleeper vertical acceleration at Grazeley Green Site for a DMU class 220 Voyage pass-by train with 118 km/h.
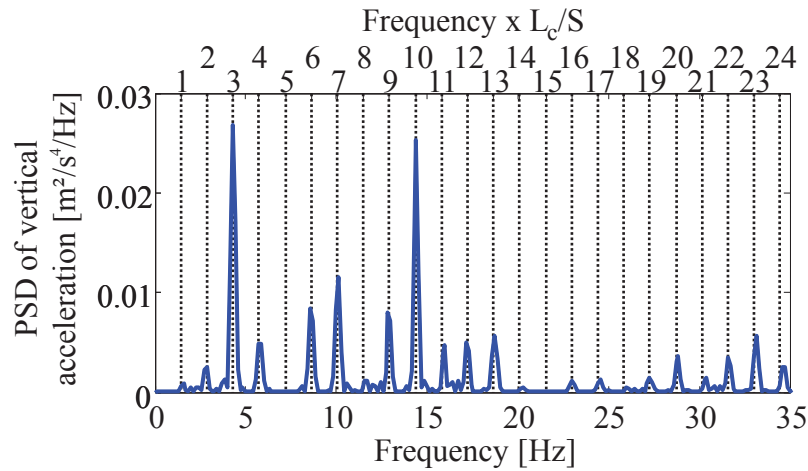
Source: Author.

4.4 Optimization of a harvester for a single passing train

In this section, an investigation into the maximum energy that can be potentially harvested from a vibrating source is considered for the two railway sites. As discussed in chapter 2, one of the conditions for a linear oscillator to achieve a high performance is that it operates at resonance. From the equation of motion for a single-degree-of-freedom (SDOF) mass-spring-damper system subjected to base excitation given by Eq. 2, shown here for convenience as

$$m\ddot{z}(t) + c\dot{z}(t) + kz(t) = -m\ddot{y}(t), \tag{30}$$

the best natural frequency and damping ratio are determined by carrying out a numerical simulation for the base acceleration time history shown in Fig. 17. The numerical integration is performed in *Matlab* using *Newmark* method. The mass is set to 1 kg and the natural frequency varied from 0.1 Hz up to 35 Hz with an increment of 0.1429 Hz. For each natural frequency, the optimum damping ratio is determined. The range of damping considered was from 0.0001 up to 0.05 with an increment of 0.0001.

The numerical integration of the equation of motion gives the oscillator behaviour for different parameters. In a second step, the maximum relative displacement amplitude is

extracted to determine the device size restriction, while the relative velocity is substituted into Eq. 7, also showed here for convenience as

$$E = \int_0^{t_e} c\dot{z}(t)^2 \, dt. \tag{31}$$

and integrated for the period of excitation to calculate the energy harvested.

The analysis here considers only the time where the train was passing through the measurement point and was inducing vibration into the mechanical system. That is, the analysis is only performed during the time the energy harvester is subjected to forced vibration.

4.4.1   Pass-by train at Steventon

The results from the passage of an Inter-city 125 HST with a speed of 199 km/h are shown in Fig. 20. In particular, Fig. 20a shows the maximum energy harvested for each natural frequency. Fig. 20b shows the damping ratio necessary for the oscillator achieve its maximum performance for each natural frequency. Fig. 20c shows the maximum relative displacement amplitude that the seismic mass oscillates in relation to the harvester base for a mechanical system subjected to vibration induced by a passing train. From Fig. 20a it can be observed that the frequency at which the highest energy is harvested coincides with the dominant trainload frequencies observed in the PSD of the vertical acceleration in Fig. 18a. The harvester scavenges the maximum energy when the acceleration is maximum, corresponding to 16.86 Hz, which is the 7th harmonic. In Fig. 20b it is possible to see, that for the natural frequencies where the oscillator harvests more energy, the oscillator requires very light damping. This is because it is more advantageous for the oscillator have large relative motion, which can be seen in Fig. 20c.

A linear energy harvester at the Steventon railway site being excited by a HST with 199 km/h has an optimum natural frequency of 16.86 Hz and damping ratio of 0.0044. This results in 0.2713 J of energy harvested for 1 kg of mass with a relative displacement of about 5 mm.

Figure 20 – Results for an energy harvester for each natural frequency from sleeper vibration due the passage of an Inter-city 125 HST class 43 with 199 km/h: (a) energy harvested; (b) optimum damping ratio; and (c) maximum relative displacement amplitude

(a)

(b)

(c)
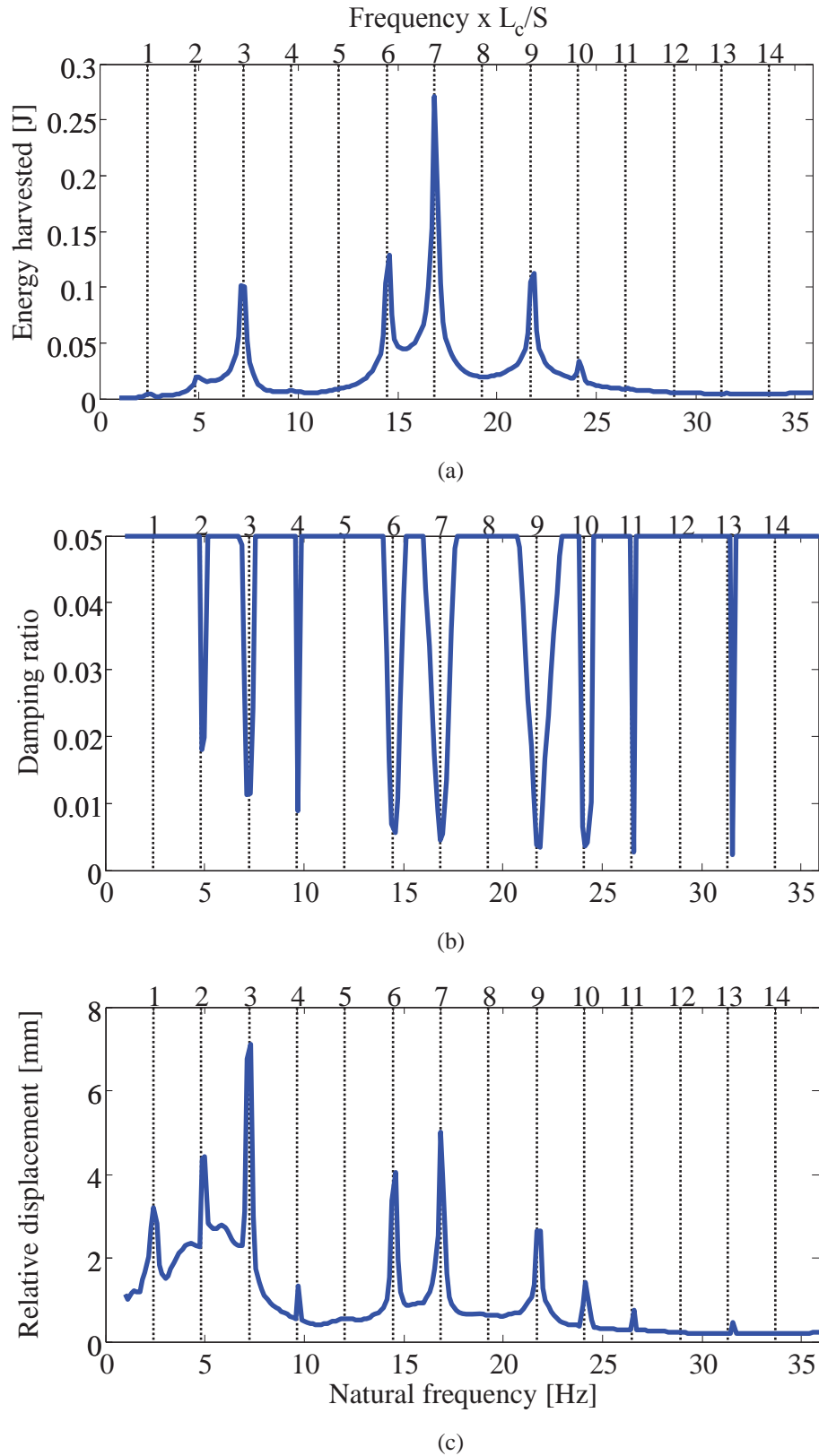
Source: Author.

The same analysis is carried out for the other passing trains at Steventon. The results of a single linear oscillator for the maximum energy harvested, the optimum damping ratio and the maximum relative displacement of an Inter-city 125 HST with speeds of 162 km/h; 178 km/h; and 195 km/h are shown in Appendix A, in Fig. A.7, Fig. A.8 and Fig. A.9, respectively, indicated by the black solid line. The optimum mechanical system parameters for an Inter-city 125 HST with different speeds are summarized in Table 4.

Table 4 – Comparative between energy harvester design for passing trains with different speed at Steventon.

Oscillator parameters	Train speed [km/h]			
	199	195	178	162
Maximum energy harvested [J]	0.2713	0.2595	0.1802	0.1388
Natural frequency [Hz]	16.86	16.57	15.14	13.72
Damping ratio (ζ)	0.0044	0.0043	0.0046	0.0045
Relative displacement [mm]	5.018	5.056	4.541	4.522

Source: Author.

As can be seen, the optimum design for an energy harvester applied at Steventon to scavenge mechanical energy from an Inter-city 125 HST with different speeds shows a large difference in performance. This is because the acceleration amplitude is proportional to the base displacement multiplied by the square of the dominant trainload frequencies. This, in turn, it shifts to higher (lower) frequencies with increase (decrease) in train speed. For trains with the lowest speed (162 km/h) the oscillator was able to harvest only 50% of energy compared to that for the highest train speed (199 km/h). The maximum relative displacement amplitude showed a considerable difference too, as did the undamped natural frequency. However, the major observation in these analyses is the fact that for this particular train the harvester scavenges its maximum energy always from the frequency corresponding to the 7th harmonic, independent of the train speed.

4.4.2   Pass-by train at Grazeley Green

The results from the passage of a DMU Voyager class 220 with a speed of 118 km/h are shown in Fig. 21. In particular, Fig. 21a shows the maximum energy harvested for each

natural frequency. Fig. 21b shows the damping ratio necessary for the oscillator to achieve its maximum performance for each natural frequency. Fig. 21c shows the maximum relative displacement, i.e. the device size for each natural frequency. From Fig. 21a it is observed that as well as an Inter-city 125 HST at Steventon site, for the passage of a DMU Voyager, the frequency at which the largest amount of energy is harvested coincides with the dominant trainload frequencies observed in the PSD of the vertical acceleration in Fig. 19. Although the harvester has two frequencies where there is the capacity to scavenge a similar amount of energy (the 3rd and 10th harmonics), the device with a natural frequency of 4.28 Hz, corresponding to the 3rd harmonic has a marginally better performance.

In Fig. 21b it is possible to see that for the natural frequency where the oscillator harvests more energy, the oscillator requires a light damping. This was also the case for a passing train at the Steventon site and is because it is more advantageous for the oscillator have large relative motion, which can be seen in Fig. 21c.

A linear energy harvester at the Grazeley Green railway site being excited by a DMU Voyager train with 118 km/h has an optimum natural frequency of 4.28 Hz and damping ratio of 0.0218. This results in 0.0214 J of energy harvested for 1 kg of mass with a relative displacement of about 5.5 mm.

The same analysis is carried out for the other passing train at Grazeley Green with a speed of 114 km/h. The results are shown in Appendix B, in Fig B.4, indicated by the blue solid line. The optimum mechanical system parameters for a DMU Voyager with two different speeds are summarized in Table 5.

Table 5 – Optimum parameters of an energy harvester comparative between the passing trains at Grazeley Green.

Oscillator parameters	Train speed [km/h]	
	118	114
Maximum energy harvested [J]	0.0214	0.0208
Natural frequency [Hz]	4.28	13.86
Damping ratio (ζ)	0.0218	0.0065
Relative displacement [mm]	5.449	1.718

Source: Author.

Figure 21 – Results of an energy harvester for each natural frequency from sleeper vibration due the passage of a DMU class 220 with 118 km/h: (a) energy harvested; (b) optimum damping ratio; and (c) maximum relative displacement amplitude.

(a)

(b)

(c)
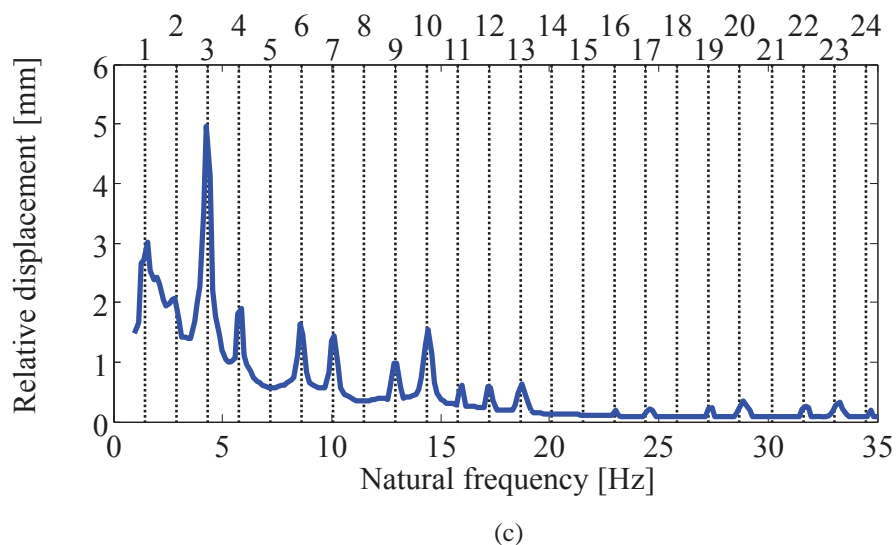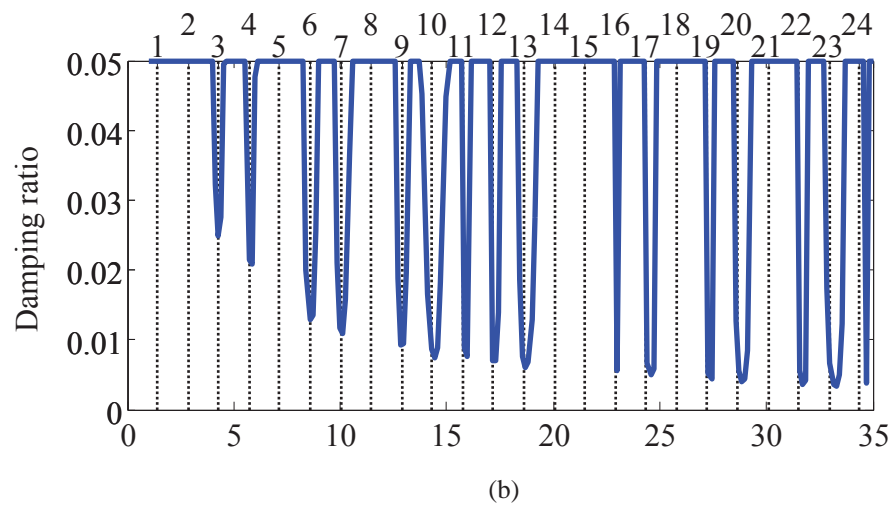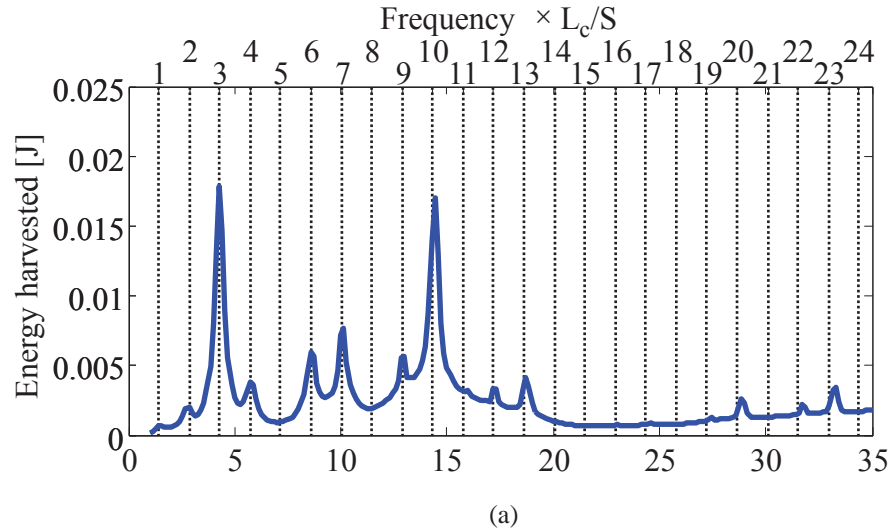
Source: Author.

As can be observed, the optimum design for an energy harvester at the Grazeley Green site to scavenge mechanical energy from a DMU Voyager shows a slightly higher performance for the fastest train. A large difference is observed in the natural frequency even though both train speeds are close. This is because for the fastest train the optimum natural frequency corresponds to the 3rd harmonic, while for the other passing train the optimum natural frequency corresponds to the 10th harmonic. This is why there is a large difference in the relative displacement for the two devices.

4.5   Single energy harvesting device at Steventon

The energy harvesting device applied in a real environment is subject to vibrations from different sources. In a railway line, despite each line have a specific train type and range of train speeds, due the many factors, such as the length of the railway line, the number of people that uses this transport system for example, the speed that a train passes through a point on the railway line is not always the same. In addition, for some lines, more than one train type passes through it.

At the Steventon site, from the measurement data, the Inter-city 125 HST passes with a range of speeds from 162 km/h up to 199 km/h, all with the excitation frequency of the 7th harmonic that generates the most energy. The corresponding natural frequencies of the optimum devices range from 13.72 Hz to 16.86 Hz. The amount of energy harvested by a single harvester tuned to particular speed (natural frequency), when excited by all the four trains on the Steventon site is shown in Fig. 22. Each set of four columns represents the results obtained by a single oscillator with the parameters set to match the optimum mechanical system parameters for a particular train. In particular, from Fig. 22a, it can be clearly seen that the harvester can only scavenge a significant amount of energy for the passing train that excites the natural frequency of the device for which it is tuned to, or for a train that has a speed very close to this. For trains with a large difference in speed from this, the amount of energy harvested is so small that can be disregarded. For passing trains that excite a frequency different to the harvester natural frequency, the relative motion is also very small as can be seen in Fig. 22b.

Figure 22 – Performance of a linear oscillator with optimum parameters design of each passing trains subjected to vibrations of different train speeds: ⊞ 199 km/h, ◺ 195 km/h, ⦀ 178 km/h and ▨ 162 km/h. (a) Energy harvested; and (b) Maximum relative displacement.

(a)   (b)
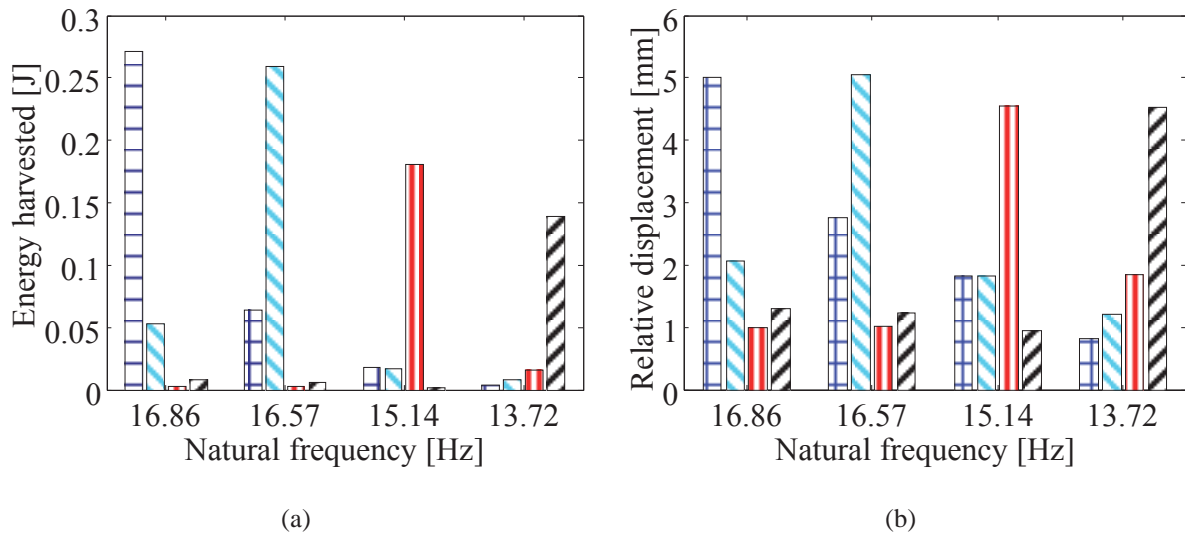
Source: Author.

4.6   Conclusions

This chapter has investigated the optimum parameters of an energy harvester to scavenge energy from sleeper vibrations at the Steventon and Grazeley Green railway sites. It was shown that in general, the harvester has a high performance when the oscillator natural frequency is set to match one of the dominant trainload frequencies. For the Steventon site this corresponded to the 7th harmonic, and at the Grazeley Green site this corresponded to either the 3rd or 10th harmonic depending on the train speed A single passing train can generate an amount of energy around 0.14 J to 0.27 J at Steventon site and around 0.02 J at Grazeley Green site. The optimum damping ratio required to harvest the maximum energy was found to be very light so that the oscillator had relatively large motion of around 4.5 to 5.5 mm. It was also found that a harvester designed for on particular train speed was not very effective for similar trains running at different speed. This is further examined in the next chapter.

5 ENERGY HARVESTING FROM RAILWAY VIBRATION: ANALYTICAL

5.1 Introduction

In chapter 4, an investigation into the amount of energy that can be scavenged from linear energy harvesters subject to vibrations induced by passing trains in two different sites was carried out numerically. In this chapter, an investigation is carried out into the energy that can be harvested using the approximate analytical expression derived by Gatti et al. (2014), discussed in chapter 2. In addition, the total energy harvested by a linear oscillator due to the passing of trains with different speeds is analysed using the analytical model.

The complete set of results considering the analytical expression for an Inter-city 125 HST passing at Steventon site for different train speeds are presented in Appendix A. For a DMU Voyager train passing at Grazeley Green, the complete set of results are presented in Appendix B.

5.2 Frequency content of the measurement input

To see more clearly the features of the input vibration to the energy harvester, the velocities are calculated from the vertical accelerations measured at Steventon and Grazeley Green for trains passing at different speeds by computing the cumulative integral via the trapezoidal method.

5.2.1 Steventon

The time history of the vertical velocity and the corresponding Fourier coefficients measured at the Steventon site induced by an Inter-city 125 HST with speed of 199 km/h are shown in Fig. 23. For the other train speeds, 162 km/h, 178 km/h and 195 km/h, they are shown in Appendix A, specifically in Fig. A.5, Fig. A.6, respectively.

The time period highlighted as a red solid line, corresponding to the time period of a passage of a single passenger carriage, is used to calculate the Fourier coefficients of the input velocity. From Fig. 23a, it is possible to note that, different from the acceleration time history, the velocity appears to be predominantly time-periodic, except at the start and end of the train. The larger vibration at each end of the time history is due the heavier power cars This configuration of the train is known as the pull and push mode (LOMBAERT; DEGRANDE,

2009). The amplitudes of the first fifteen Fourier coefficients from the time-periodic velocity, corresponding to the passage of a single passenger carriage, are shown in Fig. 23b for the frequency axis normalized by the ratio between train speed and the carriage length (S/L_c). It can be seen that the vertical velocity has peaks at the 3rd and 7th harmonics. The single frequency vibration corresponding to each of these coefficients can be used as a base input into the energy harvester.

Figure 23 – Vertical velocity of an Inter-city 125 HST with 199 km/h: (a) Time history (· · ·) blue dotted line and time period (—) red solid line; and (b) Fourier coefficients.

(a)   (b)
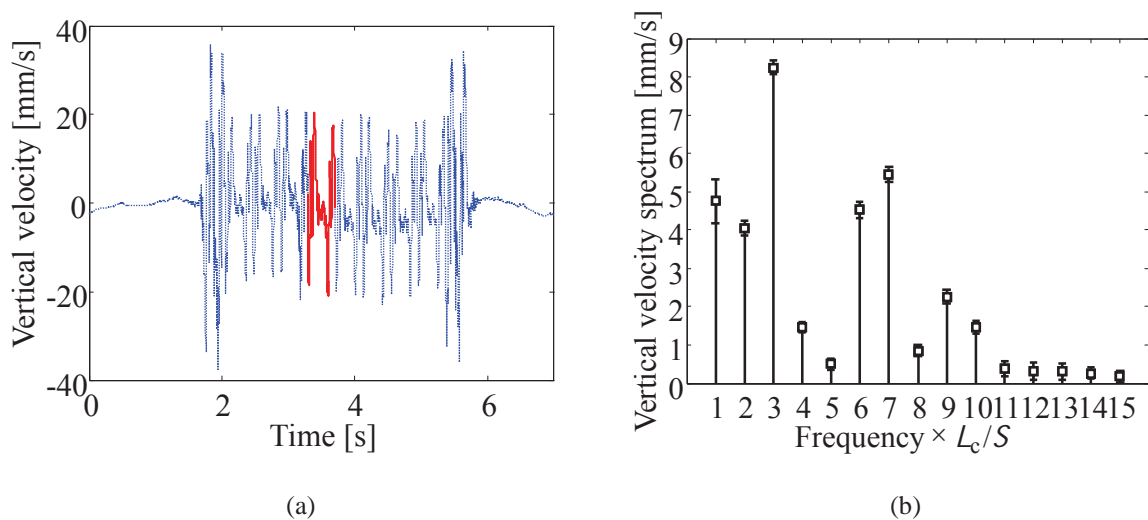
Source: Author.

5.2.2   Grazeley Green

Similar to the vibrations induced by passing trains at Steventon, the time history of DMU class 220 Voyager train the vertical velocity and the amplitude of the Fourier coefficients of a passing train with speed of 118 km/h are shown in Fig. 24. The time period highlighted as a red solid line, corresponding to the time period of a passage of a single passenger carriage, is used to calculate the Fourier coefficients of the input velocity. From Fig. 24a, it is possible to note that it has different vibration characteristics from the Inter-city 125 due the presence of power cars at its ends. For a DMU Voyager train, that has 4 driven passenger cars, the velocity appears to be time-periodic. The amplitudes of the first fifteen Fourier coefficients from the time-periodic velocity, corresponding to the passage of a single passenger carriage, are shown in Fig. 24b for the frequency axis normalized by the ratio between train speed and the carriage length (S/L_c). It can be seen that the peak in the vertical velocity occurs at the 3rd harmonic.

Again, the single frequency vibration corresponding to these coefficients can be used as a base input into the energy harvester.

Figure 24 – Vertical velocity of a DMU Voyager with 118 km/h: (a) Time history (· · ·) blue dotted line and time period (—) red solid line; and (b) Fourier coefficients.

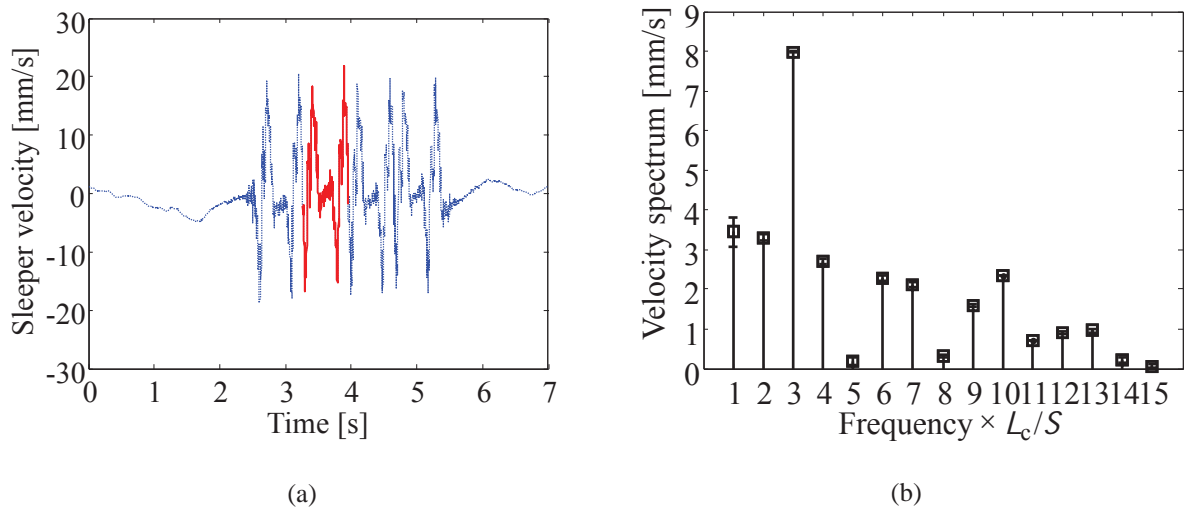(a)   (b)

Source: Author.

The analysis for vibrations induced by a DMU class 220 Voyager with a speed of 114 km/h is similar for the train speed of 118 km/h. The vertical velocity time history and the amplitude of the Fourier coefficients are presented in the Appendix B, specifically in Fig. B.3.

5.3 Optimum parameters and energy harvested for each harmonic component – approximate energy harvester equation

The determination of the maximum energy harvested and its respective optimum parameters are obtained by the mathematical model of a linear resonator energy harvester for each harmonic. The measured data from vibrations induced by passing trains described in section 5.2 are applied to the simple approximate expression given in Eq. (22), shown here for convenience as

$$E_{max} \approx \frac{1}{2} m V^2 \left(\frac{\pi n}{2} \right)^2 \left(1 - e^{-4} + 4e^{-2} \right). \tag{32}$$

To determine the maximum amount of energy that the oscillator scavenges, the square of the velocity Fourier coefficients are multiplied by a mass of 1 kg and by the number of

excitation cycles corresponding to each natural frequency. The optimum damping ratios are determined by Eq. (21). The maximum relative displacement amplitudes for the optimum damping ratios are calculated using Eq. (23). The equations are shown here for convenience and are respectively given by

$$\zeta_{opt} \approx \frac{1}{\pi n} \text{ and} \tag{33}$$

$$Z_{max} = \frac{Y \pi n}{2}\left(1 - e^{-2}\right). \tag{34}$$

5.3.1 Steventon site

An investigation of the optimum parameters of an energy harvester and evaluation of its performance are carried out for the four passing trains at Steventon with different speeds. The Fourier coefficients of the vertical velocity for each Inter-city 125 HST passenger coach passing with a speed of 199 km/h, shown in Fig. 23b, are used as a base input velocity to Eq. (32) and Eq. (34). From the total excitation time of 4.15 s shown in Table 3, the number of cycles are determined by the multiplication of the frequency corresponding to each harmonic by the excitation time. The results are shown in Fig. 25 presented with two horizontal axes. The bottom axis represents the natural frequency and the upper axis the harmonic order. The analytical results are plotted for 8 coaches with the black square (□) representing the mean value and a black dash (─) for the standard deviation, while the numerical ones as a blue solid line (─). In particular, the energy harvested for each single harmonic of a passing HST with 199 km/h is shown in Fig. 25a comparing it with the numerical solution of the total energy harvested for each natural frequency. For the others passing trains with speeds of 162 km/h, 178 km/h and 195 km/h, the same analysis is performed and is shown in Appendix A, Fig. A.7, Fig. A.8, and Fig. A.9, respectively. From Fig. 25a-b-c, it can be noted that the results obtained using the approximate expression for the energy harvester for a limited time-periodic vibration have good agreement with the numerical solution. Additionally, it can be seen that excitation by the 7th harmonic frequency alone can be used to describe the behaviour of the optimised energy harvester subject to vibration induced by the passage of an Inter-city 125 HST. Table 6 shows the summarized results for the numerical results compared with the analytical results for each passing train.

Figure 25 – Results of numerical analysis (—) blue solid line and contribution of each harmonic, (□) black square for the mean value and (—) black dash for the standard deviation, for an energy harvester due the passage of an Inter-city 125 HST with a speed of 199 km/h: (a) Energy harvested; (b) damping ratio; and (c) maximum relative displacement.

(a)

(b)

(c)
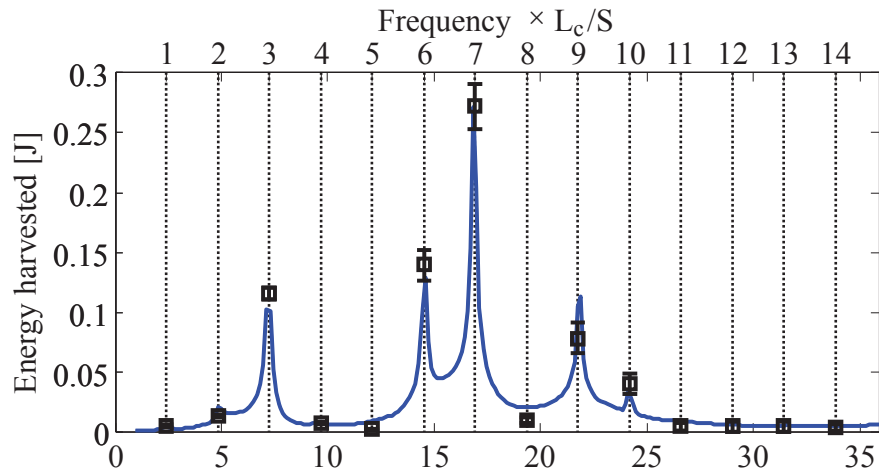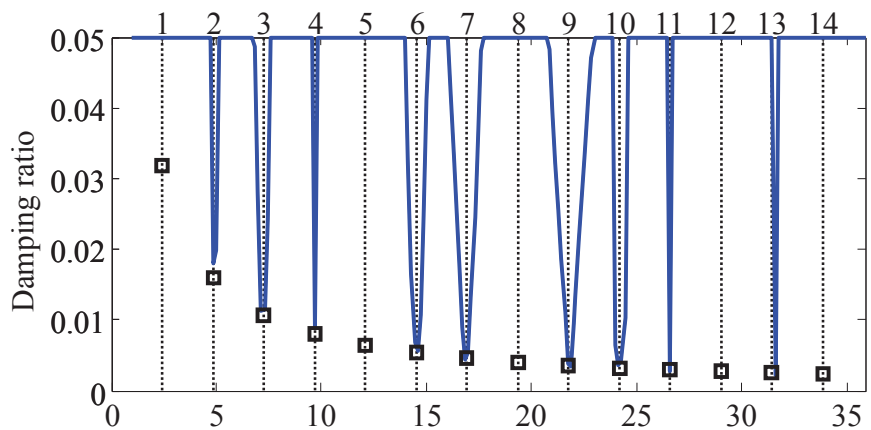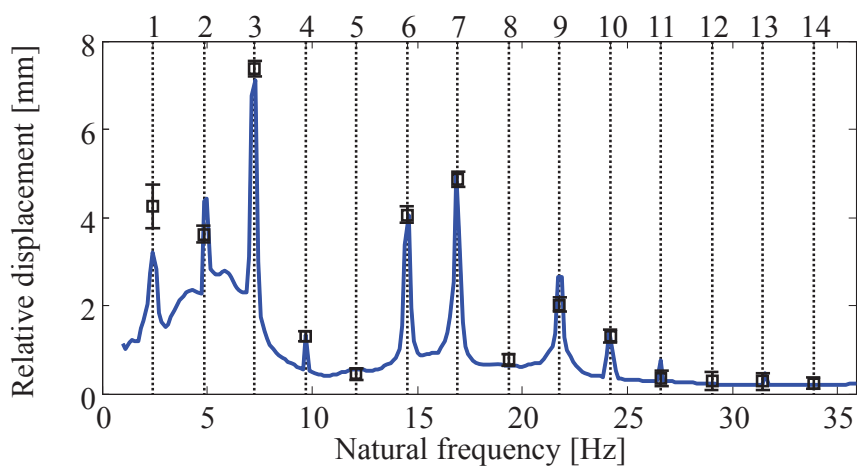
Source: Author.

Table 6 – Comparison between numerical and analytical results of an energy harvester design for an Inter-city 125 HST passing with different speeds at Steventon.

| Oscillator parameters | Train speed [km/h] | | | | | | | |
| | Numerical | | | | Analytical | | | |
	199	195	178	162	199	195	178	162
Maximum energy harvested [J]	0.2633	0.2595	0.1800	0.1360	0.2722	0.2604	0.1750	0.1338
Nat. Freq. [Hz]	16.86	16.57	15.14	13.72	16.86	16.57	15.14	13.72
Damping ratio	0.0044	0.0045	0.0046	0.0045	0.0045			
Rel. displacement [mm]	5.018	5.046	4.544	4.522	4.858	4.852	4.356	4.201

Source: Author.

5.3.2 Grazeley Green site

Similar to a passing train in Steventon, at Grazeley Green, the optimum parameters of an energy harvester using the approximate expression for a linear resonator considering a limited time-periodic excitation are carried out. From vibrations induced by the passage of a DMU Voyager train with a speed of 118 km/h, the Fourier coefficients of the vertical velocity extracted due the passage of each passenger coach, shown in Fig. 24b, are used as the base velocity input. From the total excitation time of 3.5 s shown in Table 2, the number of cycles are determined by the multiplication of the frequency corresponding to each harmonic and the excitation time. Results from the analytical study of the mechanical device are shown in Fig. 26 with two horizontal axes. The bottom axis represents the natural frequency and the upper axis the harmonic order. The analytical results are plotted for four coaches with the black square (□) representing the mean value and a black dash (─) for the standard deviation, while the numerical one as a blue solid line (─). A comparison between the analytical and numerical solutions again shows good agreement. In particular, from vibrations induced by a passing train with a speed of 118 km/h, Fig. 26a shows that the single exciting frequency, corresponding to the 3rd harmonic order can be used to determine the behaviour of an energy harvester operating at its best performance. From the passing train with a speed of 114 km/h, shown in Appendix B, Fig. B.4, a comparison between the analytical and numerical results also shows good agreement. The summarized results for the numerical and the analytical studies of each passing train are shown in Table 7.
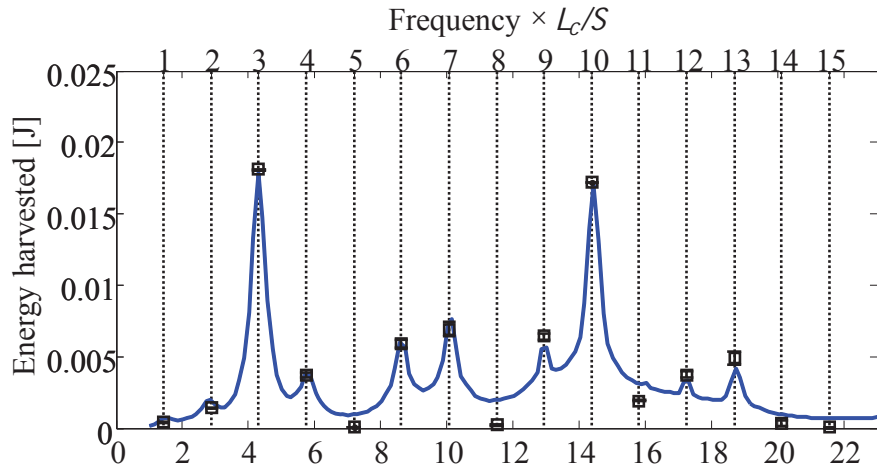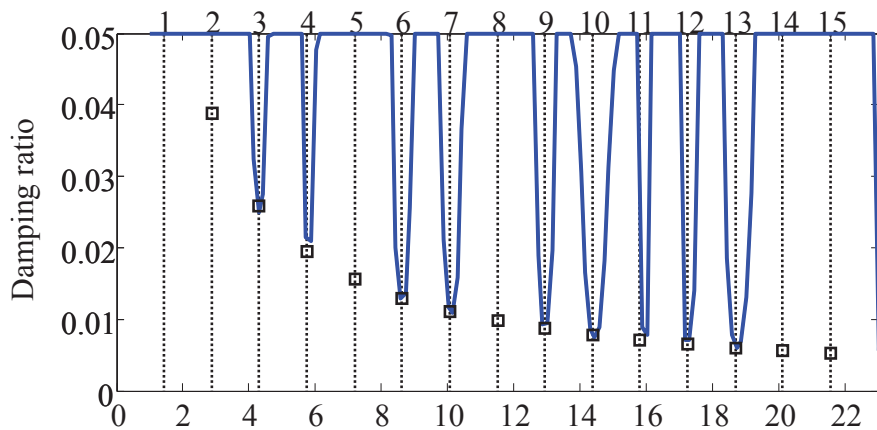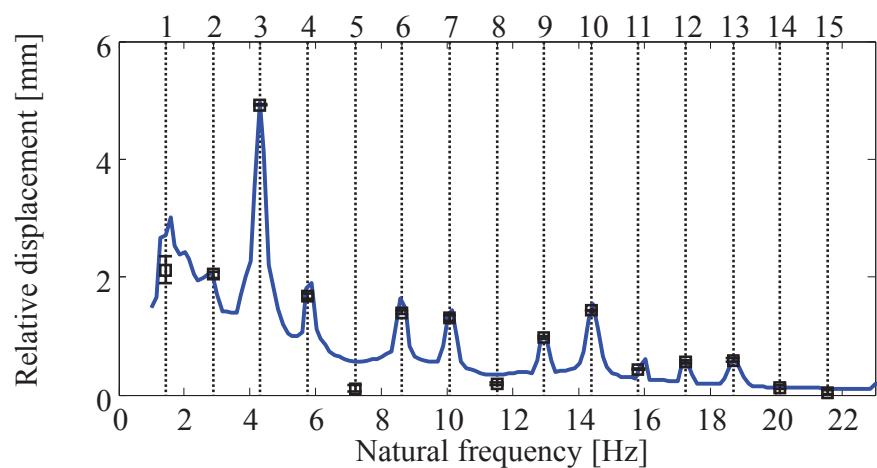
Figure 26 – Results of numerical analysis (—) blue solid line and contribution of each harmonic, (□) black square for the mean value and (—) black dash for the standard deviation, for an energy harvester due the passage of a DMU Voyager with a speed of 118 km/h: (a) Energy harvested; (b) damping ratio; and (c) maximum relative displacement.

(a)

(b)

(c)

Source: Author.

Table 7 – Comparison between numerical and analytical results of an energy harvester design for a DMU Voyager train passing with different speeds at Grazeley Green.

Oscillator parameters	Train speed [km/h]			
	Numerical		Analytical	
	118	114	118	114
Maximum energy harvested [J]	0.0214	0.0208	0.0220	0.0205
Natural frequency [Hz]	4.28	13.86	4.28	13.86
Damping ratio (ζ)	0.0218	0.0065	0.0024	0.0066
Relative displacement [mm]	5.449	1.718	5.425	1.847

Source: Author.

5.4 Energy harvested from vibration induced by passing trains – analytical study

In the last section, the approximate equation for energy harvested derived in Chapter 2 was used to investigate the contribution of the harmonics of the sleeper vibration due the passage of High Speed Trains to the total energy scavenged by a linear oscillator. Here, the analysis is carried out considering the relative displacement response of a linear mass-spring-damper mechanical system, Eq. 15, shown again for convenience as

$$z(\tau) = \frac{Y\Omega^2}{\sqrt{\left(1-\Omega^2\right)^2 + 4\zeta^2\Omega^2}}\left(\cos\left(\Omega\tau - \varphi\right) - \frac{e^{-\zeta\tau}}{\sqrt{1-\zeta^2}}\cos\left(\sqrt{1-\zeta^2}\tau - \alpha\right)\right), \tag{35}$$

where the phase angles are $\varphi = \arctan\left(\dfrac{2\Omega\zeta}{1-\Omega^2}\right)$ and $\alpha = \arctan\left(\dfrac{\left(1+\Omega^2\right)\zeta}{\left(1-\Omega^2\right)\sqrt{1-\zeta^2}}\right)$ and $\tau = \omega_n t$.

The relative displacement is differentiated to obtain the relative velocity and is integrated over n excitation cycles to estimate the energy harvested by

$$E = 2m\zeta\omega_n^2\int_0^{\frac{2\pi n}{\Omega}}\left(\frac{\partial z(\tau)}{\partial \tau}\right)^2 d\tau. \tag{36}$$

5.4.1   Vertical displacement of the sleeper

In chapter 3 it was observed that the vibration of interest for energy harvesting is caused by the quasi-static deflection of the rail due to the passage of a train. In addition, if the train geometry is unchanged from train to train, the amplitude of the rail deflection is the same independent of the train speed. Moreover it was seen in the last section that at the Steventon site the total energy harvested by a linear oscillator could be calculated considering only the 7th harmonic of the vibration induced by a passing train.

From four vertical acceleration data sets measured in the centre of the sleeper at the Steventon site due the passage of trains with different speeds, the vertical displacements of the sleeper vibration are obtained by integrating twice using the cumulative trapezoidal function in *Matlab*. This is shown in Fig. 27 with the horizontal axis corresponding to the frequency normalized by the ratio between the train speed and the carriage length.

Figure 27 – Spectrum of the vertical displacement due the passage of an Inter-city 125 HST with different speeds: (—) blue solid line is 199 km/h; (— —) red dashed line is 195 km/h; (— · —) magenta dash-dotted line is 178 km/h; and (· ·) black dotted line is 162 km/h.


(a)

(b)
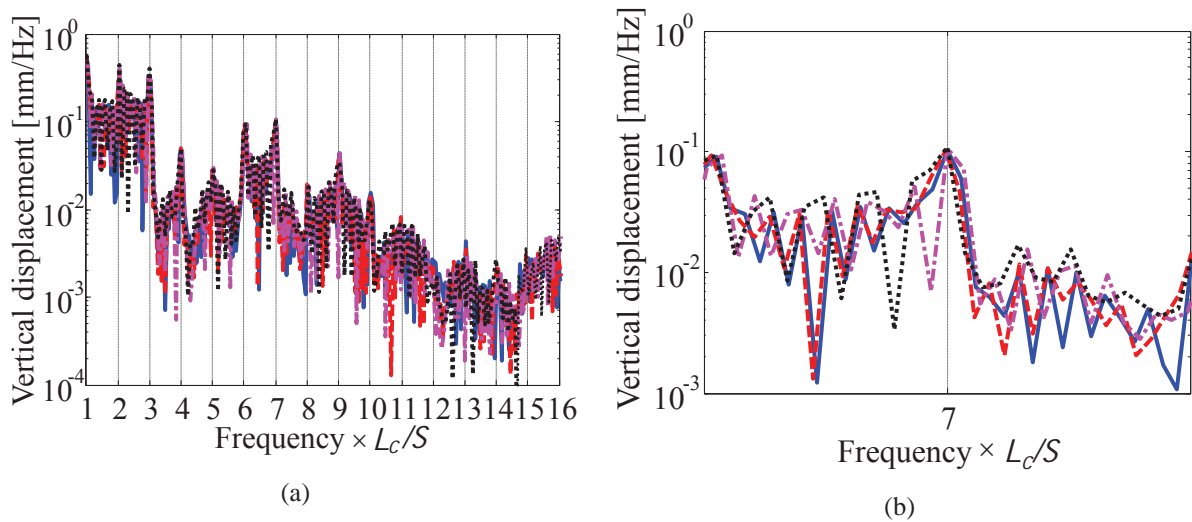
Source: Author.

The spectrum of the vertical displacement due the passage of an Inter-city 125 HST with different speeds shown in Fig. 27a shows that, when the horizontal axis is an integer number, the amplitude for the four passing trains appears to be the same independent of the train speed. This is clear in the close-up of the 7th harmonic shown in Fig. 27b. This indicates

that the main source of vibration induced by the passing trains are due the static loads of the train that cause a quasi-static deflection of the rail.

In order, to investigate the behaviour of an energy harvester oscillator subject to vibrations induced by the passage of an Inter-city 125 composed of 2 power cars and 8 passenger coach, the Fourier coefficients for the four measured data sets at Steventon are extracted. For each passing train, the Fourier coefficients are extracted from 8 periodic samples that correspond to the passage of the passenger carriages. An example of the passage of a single carriage can be seen in Fig. 23 as a red line. The amplitude of the vertical velocity for each harmonic is divided by its respective frequency to obtain the amplitude of the vertical displacement for each harmonic. This is shown in Fig. 28 for the harmonics from 5 to 15.

Figure 28 – Mean value, ($\square$) black square, and standard deviation, ($-$) black dash, of the amplitude of the vertical displacement coefficients for each harmonic.
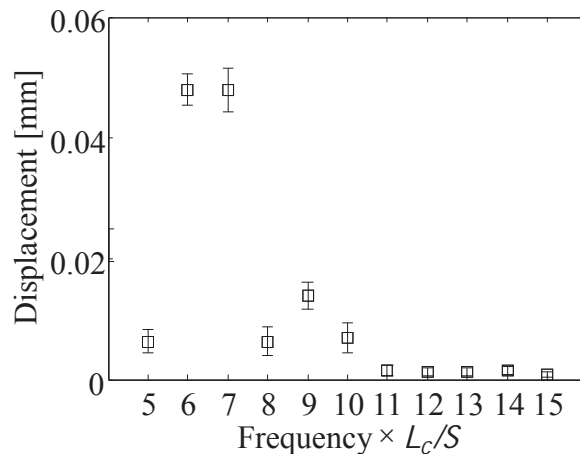
Source: Author.

As can be seen in Fig. 28, the difference in amplitude for each harmonic, indicated by the standard deviation, is very small. Therefore, for this range of frequencies, the main source of excitation is the quasi-static excitation.

In the following sections, the amplitudes of the vertical displacement of the 7th harmonic, extracted from each carriage of all passing trains in the measurement set, is used to evaluate the energy harvested for passing trains with different speeds.
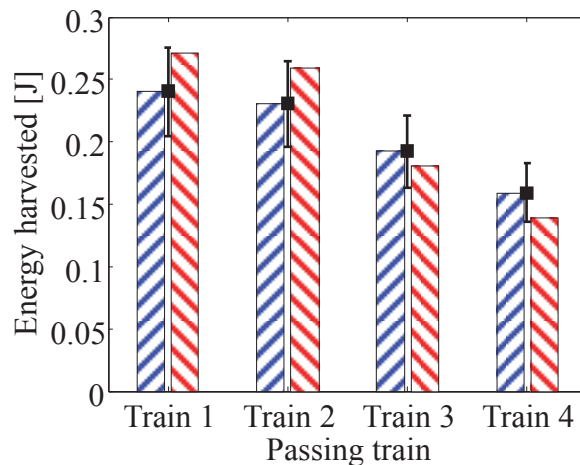
5.4.2   Energy harvested

Using each amplitude of the 7th harmonic of the vertical displacement, extracted from the passage of each passenger coach from all train data set, a damping ratio of 0.004547, corresponding to the optimum damping ratio estimated in Section 5.3.1, and assuming the oscillator is at resonance, the energy harvested by a linear oscillator is calculated for 70 cycles of excitation. For train speeds equal to those measured at Steventon, the average and the standard deviation of the energies harvested calculated analytically is showed with a comparison with the numerical results in Fig. 29 and Table 8.

Table 8 – Comparative between the energy harvested obtained numerically and analytically.

Train		1	2	3	4
Speed [km/h]		199	195	178	162
Natural frequency [Hz]		16.86	16.57	15.14	13.72
Damping ratio		0.004547			
Cycles		70			
Energy harvested [J]	Numerical	0.271	0.260	0.180	0.139
	Analytical — Average	0.240	0.230	0.192	0.159
	Analytical — Standard deviation	0.035	0.034	0.028	0.023

Source: Author.

Figure 29 – Comparative between numerical and analytical energy harvested. ▨ Average energy harvested – analytical; and ▨ numerical; (─) black dash is the standard deviation.
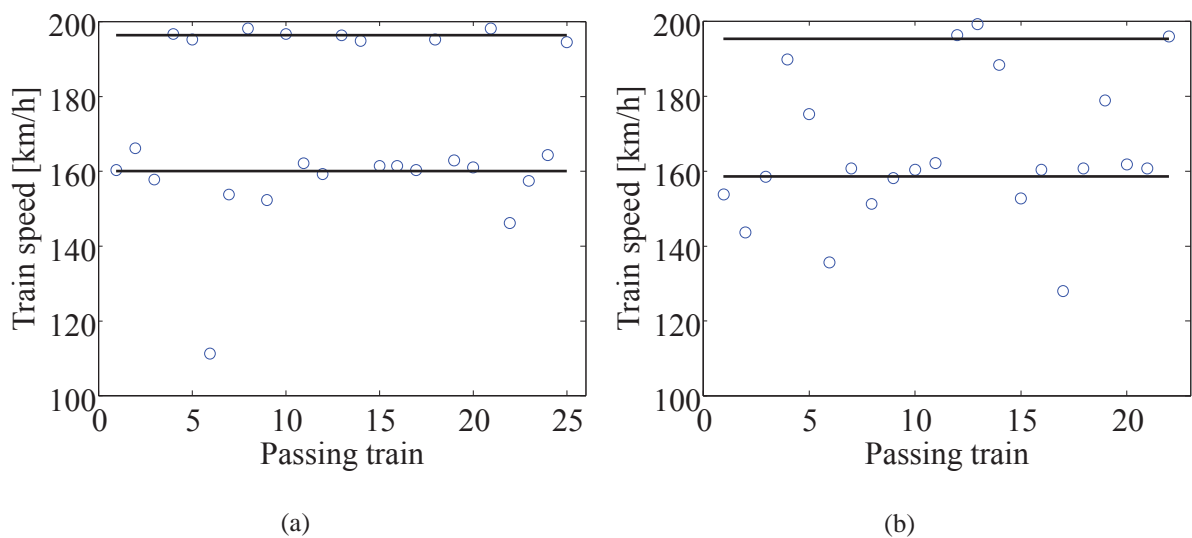

Source: Author.

The results from the analytical analysis shows that this method to evaluate the energy harvested, considering only the contribution of the 7th harmonic from vibrations induced by passing trains, showed a good agreement with the numerical results. Therefore, it is considered that this method can be used to describe the behaviour of an oscillator subject to vibrations from a passing train with a speed different from those measured at Steventon.

5.5   Train speeds at the Steventon site

In a railway environment, usually, the speed of a train is restricted due to the route the type of train and operational considerations. Although they operate with high speeds, this does not means that the vehicle speed is constant throughout their journey, and it is not the same for all passing trains.

From the experiment about ground vibration in railway environment, carried out by Triepaischajonsak in her PhD thesis (TRIEPAISCHAJONSAK, 2012) and the data given by Professor David Thompson from the Institute of Sound and Vibration Research – University of Southampton, the train speeds measured at Steventon during 2 days of experiments is shown in Fig. 30.

Figure 30 – Speed of an Inter-city 125 passing trains at Steventon in 2 measurement days: (a) first day; and (b) second day. (—) black solid line is the average; and (○) blue circle is the train speed.

(a)   (b)

Source: Author.

In Figure 30 it is very clear that the repeatability of passing trains with the same speed is very low. However, despite the paucity of data about the speeds of the passing trains, it can be seen in Fig. 30a and Fig. 30b that there are two average speed lines which the trains tends to pass more frequently. The most likely explanation for this route, which links Swindon to Didcot, is probably due the presence of a rail station close to the measurement site. Sometimes the train stops at this station and at other times it does not. For the first day of experiments these two average lines occur at around 160 and 196 km/h, and for the second day at about 158 and 195 km/h.

5.6 Optimum parameters and total energy harvested by a single oscillator at Steventon site

The study of an energy harvesting device is essential to understand the behaviour of a linear oscillator subject to vibrations induced by many passing trains with different speeds and under different operational conditions.

5.6.1 For a large range of train speed – 160 to 200 km/h

As shown in Fig. 30, the speed of passing train is not the same for every train, furthermore. It is seen that, particularly at Steventon site, there are 2 speeds which the passing trains tend towards. From this, using the average of the amplitudes of the 7th harmonic of the vertical displacement, extracted from the measurement data set, and the number of excitation cycles equal to 70, the energy harvested is calculated considering a range of speed from 160 up to 200 km/h with an increment of 5 km/h. The investigation of the oscillator behaviour subject to these passing trains is evaluated considering the natural frequency equal to the 7th harmonic frequency of each passing train and a damping ratio equal to 0.004547. The energy harvested for each oscillator due the passage of each train and the sums of energies harvested by a single oscillator due the passage of all trains is shown in Fig. 31.

Figure 31 show the energy harvested by 9 oscillators due the passage of 9 trains with different speeds. The natural frequency of each oscillator is set to be equal to the frequency corresponding to the 7th harmonic of one of the passing trains and each bar represent the total energy harvested by the oscillator due the passage of a single train. The total energy harvested by a single oscillator, represented as a black square (□).

Figure 31 – Energy harvested for a single oscillator scavenging energy from vibrations induced by passing trains with a range of speed of 160 to 200 km/h. (□) black square is the sum of energies harvested for each oscillator.
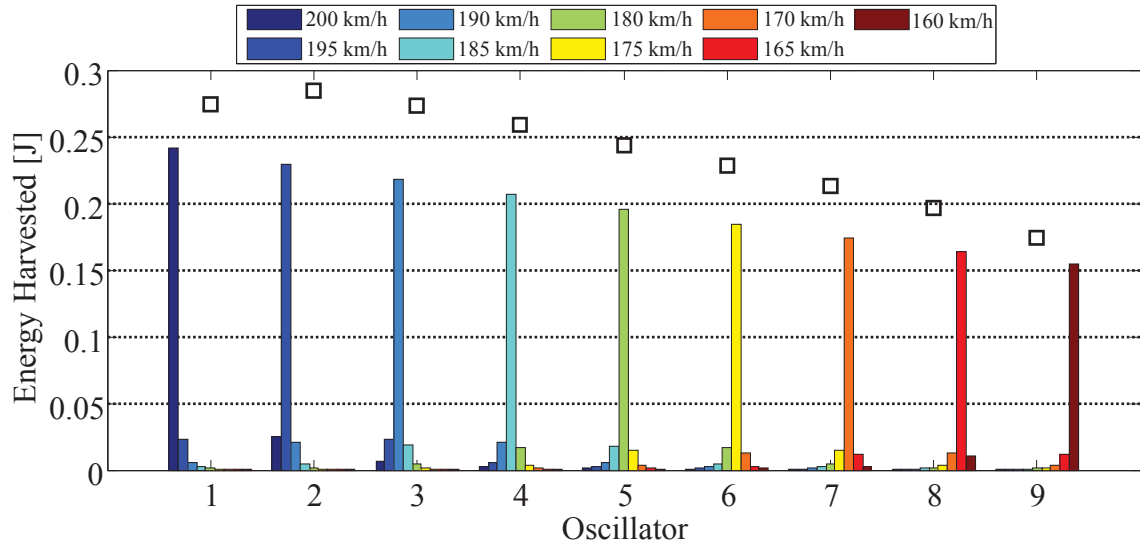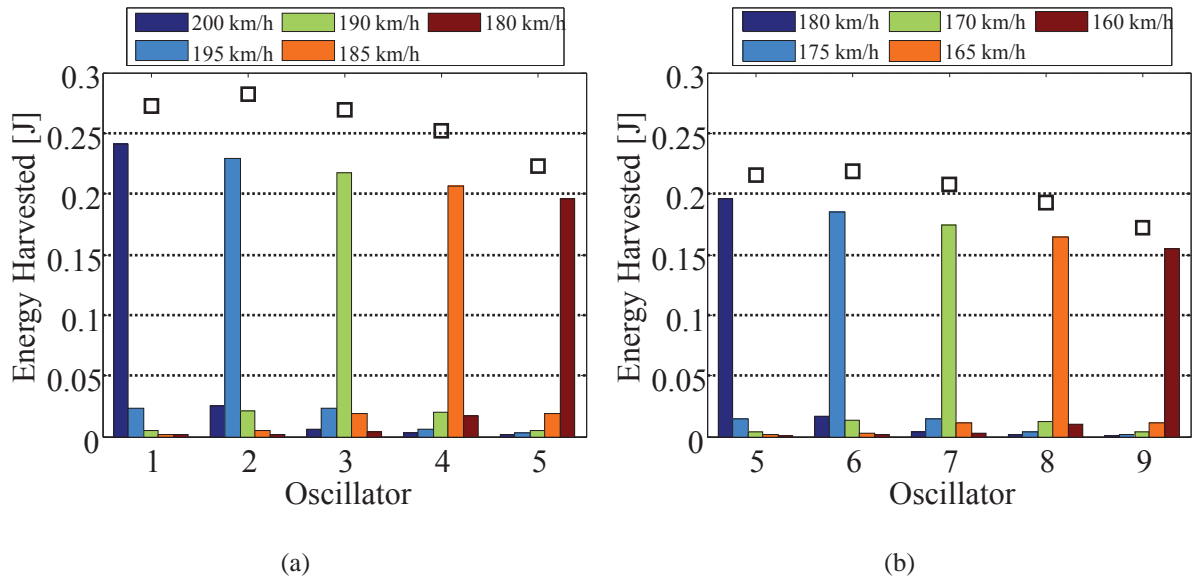

Source: Author.

As already seen, as fast is the train, higher is the sleeper vertical acceleration and, consequently, higher is the energy harvested. The results in Fig. 31 show that when the oscillator is at resonance, the device tuned for the particular train has its highest performance and the energy harvested increases linearly with the train speed. When a train passes with a speed of 160 km/h the oscillator is able to scavenge $0.154\,J$, while for a speed of 200 km/h, $0.241\,J$ can be harvested. However, in Fig. 31 it is clear that bandwidth is an important limitation for a linear energy harvesting device. It is clear that a harvester only has a significant performance when it is in resonance with the passing train, otherwise, for other train speeds (the difference in excitation frequency is 0.425 Hz), the performance is far lower. For passing trains with a speed difference greater than 5 km/h from the optimised oscillator, the energy harvested is almost zero. The sum of the energies harvested by each oscillator is predominantly due the energy induced by the passing train for which the oscillator is tuned. Only the trains with higher and lower speed of 5 km/h of the targeted train contribute realistically to the total energy harvested. Although, at resonance, the oscillator 2 harvest less energy than the oscillator 1, note that, due the presence of a passing train with a speed higher than the target train's natural frequency, when subject from vibration induced by passing trains with these train speed range, the performance of the oscillator 2 is higher than the oscillator 1. That is, the sum of energies

harvested by the oscillator 2 is greater than the oscillator 1. This is clearer in Fig. 32, which shows half the speed range of Fig. 31.

Figure 32 – Energy harvested for a single oscillator scavenging energy from vibrations induced by passing trains with a range of speed of: (a) 180 to 200 km/h; and (b) 160 to 180 km/h. (□) black square is the sum of energies harvested for each oscillator.

(a)   (b)

Source: Author.

In particular, Fig 32a show the energy harvested by a single oscillator from vibrations induced by passing trains with speeds from 180 to 200 km/h and Fig. 32b shows for a range of speeds from 160 to 180 km/h. The sum of energies for each oscillator is almost the same as observed in Fig. 31. The only significant difference is observed at oscillator 5. This occurs for this oscillator because, for Fig. 32a, there is not any passing train with a speed lower than the target train, while for Fig. 32b, there is not any passing train with a higher speed. In addition, despite in Fig. 32 the oscillator is subject to the same number of passing trains, the difference between the sums of the energies harvested is due the fact that, the oscillator harvests more energy from fastest trains.

5.6.2   For a small range of train speed – 155 to 165 km/h and 190 to 200 km/h

From the analysis conducted up to now, the results have shown that the linear energy harvester is limited by its narrow bandwidth, and a single oscillator cannot cover all the train speeds observed at Steventon. However, as already seen, there are two average speeds that the

oscillator could have a better performance if its parameters are set to cover only a range of passing train speeds close to these speeds.

Therefore, an investigation is carried out to determine the optimum oscillator parameters necessary for a single linear energy harvester scavenge the maximum amount of energy from vibration induced by passing trains with a range of speed from 155 to 165 km/h and from 190 to 200 km/h with an increment of 1 km/h. The oscillator natural frequency is set to match the excitation frequency correspond to the 7th harmonic of each passing train and the damping ratio is evaluated for a range of 0.004 up to 0.009 with a increment of 10^{-6}. The average of the amplitudes of the 7th harmonic of the vertical displacement, extracted from the measurement data, and 70 excitation cycles are used to simulate the sleeper vibration induced by passing trains with these range of speeds. The energy harvested from each passing train and the sum of the energies harvested by each oscillator are shown in Fig. 33 and Table 9, and Fig. 34 and Table 10, for a range of train speed of 155 to 165 km/h and 190 to 200 km/h, respectively. The sums of energies harvested by each oscillator, shown as (□) black square, are plotted normalized by a factor of 3 only for the scaling purpose.

Figure 33 – Energy harvested by a single oscillator from vibrations induced by a passing train with a range of speed of 155 to 165 km/h. (□) black square is the sum of energies harvested normalized by a factor of 3.
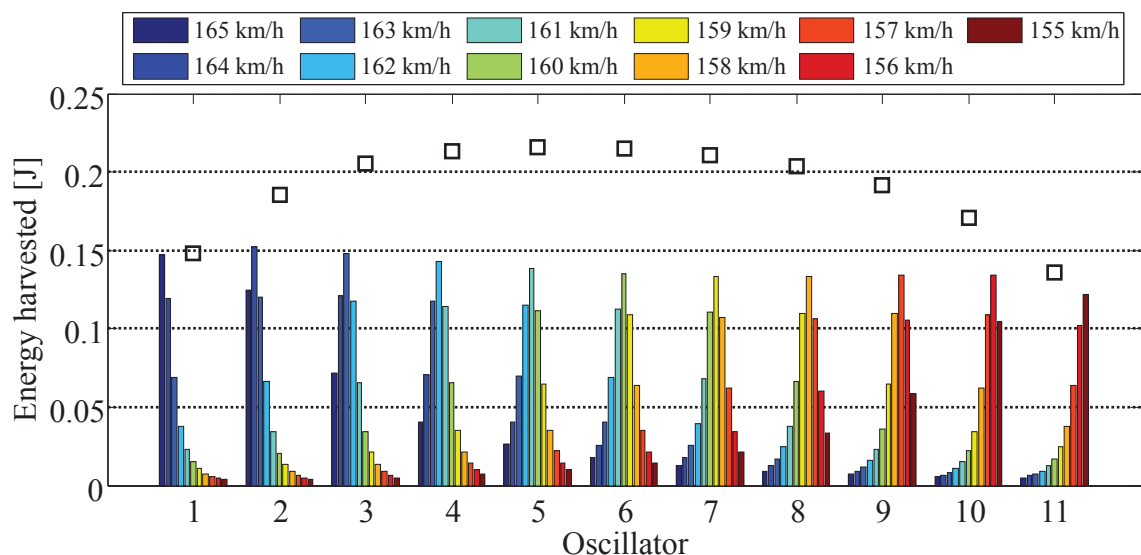
Source: Author.

Table 9 – Optimum parameters and total energy harvested from a single oscillator for a range of passing train speeds of 155 to 165 km/h.
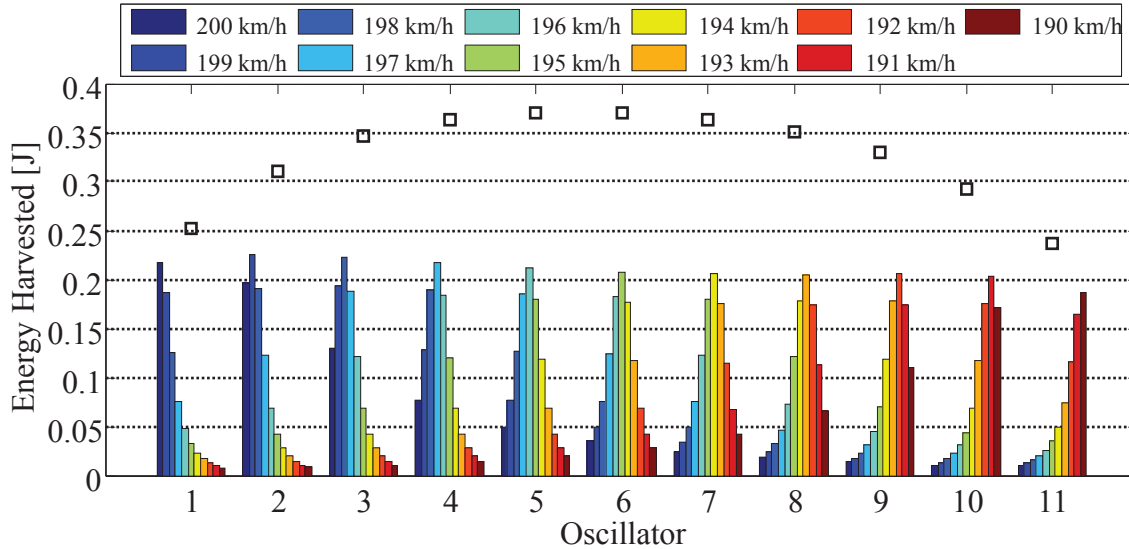
Oscillator										
1	2	3	4	5	6	7	8	9	10	11
Natural frequency [Hz] / Corresponding train speed [km/h]										
14.03	13.95	13.86	13.78	13.69	13.61	13.52	13.44	13.35	13.27	13.18
(165)	(164)	(163)	(162)	(161)	(160)	(159)	(158)	(157)	(156)	(155)
Damping ratio (10^{-3})										
7.655	6.635	7.028	7.570	7.931	8.138	8.152	7.979	7.583	7.244	8.856
Total energy harvested [J]										
0.444	0.557	0.615	0.639	0.647	0.643	0.631	0.610	0.574	0.512	0.407

Source: Author.

The results in Fig. 33 and Table 9, considering a small range of speeds, showed that in fact, the optimal operational condition for the linear oscillator is when it is at resonance. However, it is seen that for passing trains, which excites frequencies close to the energy harvester natural frequency, the oscillator performance is slightly worse. Moreover, it seemingly, only for a difference of 2 km/h in speed from the target train speed, the energy harvesters have a reasonable performance. From Table 9 is seen that the damping ratio, different from the optimized oscillator to a single passing train ($\zeta = 0.004547$), is slightly higher when there are more than one passing train inducing vibration. This increase in damping leads to a detrimental effect on the performance at resonance, on the other hand, has beneficial effect on the harvester performance when it is not at resonance.

Also, as observed in Fig. 31, the oscillator natural frequency is not set to match the frequency excited by the faster train. Therefore, it can be state that the vibrations induced by these passing trains, with an excitation frequency different from the oscillator natural frequency, also have a significant contribution to the total energy harvested. The same behaviour is observed in Fig. 34. From the sleeper vibrations induced by 11 passing trains with a range of speed from 155 to 165 km/h, is the oscillator 5, whose natural frequency is 13.69 Hz and damping ratio is 0.007931, the oscillator parameters that present the higher performance. In total, this oscillator can harvest 0.647 J after the passage of all these high speed trains.

Figure 34 – Energy harvested by a single oscillator from vibrations induced by a passing train with a range of speed of 190 to 200 km/h. (□) black square is the sum of energies harvested normalized by a factor of 3.

Source: Author.

Table 10 – Optimum parameters and total energy harvested from a single oscillator for a range of passing train speeds of 190 to 200 km/h.

					Oscillator					
1	2	3	4	5	6	7	8	9	10	11
Natural frequency [Hz] / Corresponding train speed [km/h]										
17.01	16.92	16.84	16.75	16.67	16.58	16.50	16.41	16.33	16.24	16.16
(200)	(199)	(198)	(197)	(196)	(195)	(194)	(193)	(192)	(191)	(190)
Damping ratio (10^{-3})										
7.593	6.494	6.582	6.969	7.276	7.418	7.430	7.276	6.984	6.974	8.554
Total energy harvested [J]										
0.755	0.931	1.040	1.091	1.110	1.109	1.091	1.053	0.990	0.877	0.710

Source: Author.

The same analysis performed above, can be applied for the range of speed from 190 to 200 km/h, shown in Fig. 34. The same limitation due its narrow bandwidth is observed here. Also, for these range of train speeds, it seemingly, the oscillator has a reasonable performance for passing trains with a difference of 2 km/h in speed from the target train speed. Moreover, from Table 10, also is shown that the damping ratio, different from the optimized oscillator to

a single passing train, is slightly. From the sleeper vibrations induced by 11 passing trains with a range of speed from 190 to 200 km/h, is the oscillator 5, whose natural frequency is 16.67 Hz and damping ratio is 0.007276, the oscillator parameters that present the higher performance. In total, this oscillator can harvest 0.110 J after the passage of all these high speed trains.

5.7   Conclusions

In this chapter, an investigation about the contribution of the harmonics of the sleeper vibration due the passage of a single train to the total energy harvested by single tuned harvester was carried out using the expressions derived in Chapter 2. The results for this analysis in Steventon and Grazeley Green sites, have shown good agreement when compared with the numerical results. In particular, from vibrations at Steventon site, it was shown that the response of the device tuned to the 7th harmonic and excited by only the 7th harmonic is similar to that when the same device is excited by all the harmonics in the excitation time history. From vibrations at Grazeley Green site, it was shown that a tuned device excited by the 3rd or the 10th harmonics is representative of the device being excited by all the harmonics in the excitation time history, depending on the train speed.

In addition, in this chapter, an investigation into the performance of a single linear oscillator at the Steventon site subject to vibration induced by passing trains with different speeds was also carried out. At first, the investigation considered all the train speeds observed at Steventon. Then, investigations were carried out to determine the optimum parameters and to evaluate the performance of a single linear oscillator to cover a small range of speeds close to one of the average speeds at Steventon. The results showed that the energy harvester has a high performance when it is operating at resonance and is able to harvest a reasonable amount of energy for passing trains with a difference of 2 km/h in speed from the target train speed. However, for a difference greater than 2 km/h from the target speed, the harvester performance decays rapidly.

For the number of passing trains considered in this investigation, the analysis showed that, for the slowest train speed range (155 to 165 km/h), the harvester with a natural frequency of 13.69 Hz (161km/h) was able to scavenge 0.65 J for a damping ratio of 0.007931. For the highest train speed range (190 to 200 km/h), the harvester with a natural frequency of 16.67 Hz (196 km/h), was able to scavenge about 1.1 J for a damping ratio of 0.007276.

6 FINAL REMARKS

In this chapter the general conclusions drawn from the work described in this dissertation are presented. In addition, proposals and suggestions for future work are also presented.

6.1 Conclusions

This dissertation has described an investigation into how much energy can be potentially scavenged from a linear single-degree-of-freedom energy harvesting device subject to vibrations at the centre of the sleeper induced by passing trains. It was found that the harvester must be tuned to a frequency at which the acceleration amplitude is the greatest, and this corresponds to one of the trainload harmonics.

The investigation showed that the energy harvested from vibrations induced by passing trains at Steventon and Grazeley Green in the UK are of small order but, potentially, more energy can be harvested from vibrations induced by faster trains. For the Inter-city 125 HST, an energy harvesting device has a high performance when its natural frequency is set to match the frequency corresponding to the 7th harmonic independent of the train speed. The harvester for this specific train was able to scavenge 0.1360 J to 0.2633 J for passing trains with speeds of 162 km/h to 199 km/h. For the DMU Voyager, it was shown that the natural frequency must be set to match frequencies corresponding to the 3rd and 10th harmonics as both have almost the same capacity to generate energy. The numerical analysis showed that, for this train, the harvester is able to scavenge 0.0208 J from a passing train with a speed of 114 km/h and 0.0214 J for a speed of 118 km/h. The analysis showed that in all cases the energy harvesters should have light damping to enable a large relative motion.

The approximate analytical expressions, derived by Gatti et al. (2014) for the optimum damping and the corresponding maximum energy harvested, used to investigate the optimum parameters and the contribution of each harmonic for the total energy harvested by a linear resonator subjected to sleeper vibrations induced by passing trains, showed a good agreement with the numerical analysis. The differences observed in this comparison are due the approximations implemented in the mathematical model. Moreover the excitation frequency of the model was a single harmonic while in the numerical analysis the investigation was carried out considering all harmonics.

The investigation for a single energy harvester subject to vibrations induced by passing trains with different speeds showed that, for a linear oscillator, the device has a good performance for a difference in speed of up to 2 km/h in relation to the optimum speed for the device. For a slightly higher difference in speed from this, the performance of the oscillator drastically decay up to a point, which for a large difference in speed, the energy harvested by the oscillator can be disregarded.

6.2   Future works

From this work, the following future work may be suggested:

In this work, it was clear that the greatest concern in the application of a linear SDOF mass-spring-damper system to harvest energy from vibrations induced by passing trains with different speed is due to the limitation due to its narrow bandwidth. For future work, with the aim to overcome this limitation, suggestions are made to increase the performance of the oscillator, for example

- Investigate the performance of an energy harvester considering a multi-degree-of-freedom mass-spring-damper mechanical system;
- Investigate the performance of an energy harvester considering a nonlinear mass-spring-damper system;

In addition, in this work only the mechanical energy harvested from vibrations induced by a passing train was evaluated. Future work can investigate the optimum parameters for an energy harvesting device considering the transducer effects and the total electrical energy generate for an energy harvester can be evaluated for applicability in railway vibrations.

REFERENCES

ALI, S. F.; FRISWELL, M. I.; ADHIKARI, S. Analysis of energy harvesters for highway bridges. **Journal of Intelligent Material Systems and Structures**, London, v. 22, n. 16, p. 1929-1938, 2011. Available: <http://jim.sagepub.com/content/22/16/1929.abstract>. Access: 12 jan. 2014.

AMIN KARAMI, M.; INMAN, D. J. Powering pacemakers from heartbeat vibrations using linear and nonlinear energy harvesters. **Applied Physics Letters**, Melville, v. 100, n. 4, 2012. Available: <http://scitation.aip.org/content/aip/journal/apl/100/4/10.1063/1.3679102>. Access: 15 mar. 2015.

AMIRTHARAJAH, R.; CHANDRAKASAN, A. P. Self-powered signal processing using vibration-based power generation. **Journal of IEEE Solid-State Circuits,** Piscataway, v. 33, n. 5, p. 687-695, 1998.

ANTON, S. R.; SODANO, H. A. A review of power harvesting using piezoelectric materials (2003-2006). **Smart Materials and Structures**, Bristol, v. 16, n. 3, p. R1, 2007. Available: <http://stacks.iop.org/0964-1726/16/i=3/a=R01>. Access: 12 jun. 2014.

AUERSCH, L. The excitation of ground vibration by rail traffic: theory of vehicles track and soil interaction and measurements on high-speed lines. **Journal of Sound and Vibration**, London, v. 284, n. 1-2, p. 103-132, 2005. Available: <http://www.sciencedirect.com/science/article/-pii/S0022460X04005620>. Access: 25 jun. 2014.

CASSIDY, I. L.; SCRUGGS, J. T.; BEHRENS, S.; GAVIN, H. P. Design and experimental characterization of an electromagnetic transducer for large-scale vibratory energy harvesting applications. **Journal of Intelligent Material Systems and Structures**, London, v. 22, n. 17, p. 2009-2024, 2011. Available: <http://ji-m.sagepub.com/content/22/17/2009.abstract>. Access: 12 abr. 2015.

CHOW, T. T.; HE, W.; JI, J. An experimental study of façade-integrated photovoltaic/water-heating system. **Applied Thermal Engineering**, Kidlington, v. 27, n. 1, p. 37-45, 2007. Available: <http://www.sciencedirect.com/science/article/pii/S1359431106001797>. Access: 14 abr. 2015

COONDOO, I. PANWAR, N.; MAIWA, H.; KHOLKIN, A. L. Improved piezoelectric and energy harvesting characteristics in lead-free Fe2O3 modified KNN ceramics. **Journal of Electroceramics**, New York, p. 1-7, 2015. Available: <http://dx.doi.org/10.1007/s10832-015-9983-z>. Access: 25 set. 2014.

DAGDEVIREN, C.; YANG, B. D.; SYM Y.; TRAN, P. L.; JOW, P.; ANDERSON, E.; XIA, J.; DORAISWAMY, V.; DEHDASHTI, B.; FENG, X.; LU, B.; POSTON, R.; KHALPEY, Z.; GHAFFARI, R.; HUANG, Y. SLEPIAN, M. J.; ROGERS, J. A. Conformal piezoelectric energy harvesting and storage from motions of the heart, lung, and diaphragm. **Proceedings of the National Academy of Sciences**, Kiskville, v. 111, n. 5, p. 1927-1932, 2014. Available: <http://www.pnas.org/content/111/5/1927.abstract>. Access: 27 dez. 2014.

DWIVEDY, S. K.; REDDY, A.; GARG, A. Dynamic analysis of parametrically excited piezoelectric bimorph beam for energy harvesting. In: SINHA, J. K. (Ed.). **Vibration engineering and technology of machinery**. New York: Springer International Publishing, 2015. p. 363-371. (Mechanisms and Machine Science, 23).

ESVELD, C. **Modern railway track**. 2. ed. Zaltbommel: MRT-productions Zaltbommel, 2001. Available: <http://www.esveld.com/MRT_Selection.pdf>. Access: 15 jun. 2015.

GATTI, G.; BRENNAN, M. J.; TEHRANI, M. G.; THOMPSON, D. J. On energy harvesting from time-limited excitation: simulation and case study. In: BIENNIAL ISMA CONFERENCE ON NOISE AND VIBRATION ENGINEERING, 21, 2014, Leuven. **Proceedings of the…** Leuven: ISMA, 2014.

GRASSIE, S. L.; GREGORY, R. W.; HARRISON, D.; JOHSON, K. L. The dynamic response of railway track to high frequency vertical excitation. **Journal of Mechanical Engineering Science**, Pahang Darul Makmur, v. 24, n. 2, p. 77-90, 1982. Available: <http://jms.sagepub.com/con-tent/24/2/77.abstract>. Access: 15 mar. 2015.

GUYOMAR, D.; JAYET, Y.; PETIT, L.; LEFEUVRE, E.; MONNIER, T.; RICHARD, C.; LALLART, M. Synchronized switch harvesting applied to selfpowered smart systems: Piezoactive microgenerators for autonomous wireless transmitters. **Sensors and Actuators A: Physical**, Amsterdam, v. 138, n. 1, p. 151-160, 2007. Available: <http://www.sciencedirect.com/scien-ce/article/pii/S0924424707002944>. Access: 12 abr. 2015.

HANSEN, S. E.; POURGHODRAT, A.; NELSON, C. A.; FATEH, M. On-track testing of a power harvesting device for railroad track health monitoring. In: SPIE, HEALTH MONITORING OF STRUCTURAL AND BIOLOGICAL SYSTEMS, 2010. **Proceedings of the…** 2010. Available <http://dx.doi.org/10.1117/12.848831>. Access: 25 jun. 2015.

HIROKANE, J.; SAGA, T.; MURAMATSU, T.; SHIRAKAWA, I. History of contribution of photovoltaic cells to telecommunications. In: TELECOMMUNICATIONS CONFERENCE (HISTELCON), 2, REGION CONFERENCE ON THE HISTORY, 8, 2010, Madrid. **Proceedings of the…** Madrid: IEEE, 2010. 6 p. Available: <http://ieeexplore.ieee.org/stamp/stamp.jsp?arnumber=5735313>. Access: 12 jun. 2015.

HOFFMANN, D.; FOLKMER, B.; MANOLI, Y. Fabrication, characterization and modelling of electrostatic micro-generators. **Journal of Micromechanics and Microengineering**, Bristol, v. 19, n. 9, p. 094001, 2009. Available: <http://stacks.iop.org/0960-1317/19/i=9/a=094001>. Access: 12 jun. 2015.

HOWE, J. Look for wood in crossties. **Forest Products Journal**, 1976.

JU, S.-H.; LIN, H.-T.; HUANG, J.-Y. Dominant frequencies of train-induced vibrations. **Journal of Sound and Vibration**, London, v. 319, n. 1-2, p. 247-259, 2009. Available: <http://www.sciencedirect.com/science/article/pii/S0022460X08004860>. Access: 20 jun. 2015.

KOUROUSSIS, G.; CONNOLLY, D. P.; VERLINDEN, O. Railway-induced ground vibrations and a review of vehicle effects. **International Journal of Rail Transportation**, Abingdon, v. 2, n. 2, p. 69-110, 2014. Available: <http://dx.doi.org/10.1080/23248378.2014.897791>. Access: 10 jan. 2015.

KREMER, D.; LIU, K. A nonlinear energy sink with an energy harvester: transient responses. **Journal of Sound and Vibration**, London, v. 333, n. 20, p. 4859-4880, 2014. Available: <http://www.sciencedirect.com/science/article/pii/S0022460X14004003>. Access: 10 mar. 2015.

KRYLOV, V.; FERGUSON, C. Calculation of low-frequency ground vibrations from railway trains. **Applied Acoustics**, Kidlington, v. 42, n. 3, p. 199-213, 1994. Available: <http://www.science-direct.com/science/article/pii/0003682X94901090>. Access: 12 jan. 2015.

KULAH, H.; NAJAFI, K. Energy scavenging from low-frequency vibrations by using frequency Up-conversion for wireless sensor applications. **Sensors Journal, IEEE**, Piscataway, v. 8, n. 3, p. 261-268, 2008.

LALLART, M.; INMAN, D. J.; GUYOMAR, D. Transient performance of energy harvesting strategies under constant force magnitude excitation. **Journal of Intelligent Material Systems and Structures**, London, v. 21, n. 13, p. 1279-1291, 2010. Available: <http://jim.sagepub.com/content/21/13/1279.abstract>. Access: 14 maio 2014.

LEE, D. G.; CARMAN, G. P.; MURPHY, D.; SCHULENBURG, C. Theoretical comparison of the energy harvesting capability among various electrostatic mechanisms from structure aspect. **Sensors and Actuators A: Physical**, Amsterdam, v. 156, n. 1, p. 208-216, 2009. Available: <http://www.sciencedirect.com/science/article/pii/S09-24424709000533>. Access: 12 jan. 2015.

LLEWELYN, H. **Bombardier class 220 Voyager**, set. 2010. Available: <http://commons.wikimedia.org/wiki/File%3AHugh_llewelyn_220_002_(6701873995).jpg>. Access: 10 mar. 2015.

LOMBAERT, G.; DEGRANDE, G. Ground-borne vibration due to static and dynamic axle loads of InterCity and high-speed trains. **Journal of Sound and Vibration**, London, v. 319, n. 3-5, p. 1036-1066, 2009. Available: <http://www.sciencedirect.com/science/article/pii/S002246-0X0800624X>. Access: 12 dez. 2014.

LU, X.; FLINT, I.; NIYATO, D.; PRIVAULT, N.; WANG, P. Performance analysis of simultaneous wireless information and power transfer with ambient RF energy harvesting. In: IEEE WIRELESS COMMUNICATIONS AND NETWORKING CONFERENCE, 2015, New Orleans. **Proceedings of the…** New Orleans: IEEE, 2015. Available: <http://arxiv.org/pdf/1501.00683v1.pdf>. Acesso em: 15 abr. 2015. Access: 10 jun. 2015.

MIAO, P.; MITCHESON, P. D.; HOLMES, A. S.; YEATMAN, E. M.; GREEN, T. C.; STARK, B. H. Mems inertial power generators for biomedical applications. **Microsystem Technologies**, Heidelberg, v. 12, n. 10-11, p. 1079-1083, 2006. Available: <http://dx.doi.org/10.1007/-s00542-006-0152-9>. Access: 10 abr. 2014.

MITCHESON, P. D.; MIAO, P.; STARK, B. H.; YEATMAN, E. M.; HOLMES, A. S.; GREEN, T. C. MEMS electrostatic micropower generator for low frequency operation. **Sensors and Actuators A: Physical**, Amsterdam, v. 115, n. 2-3, p. 523-529, 2004. Available: <http://www.sciencedirect.com/science/article/pii/S0924424704002985>. Access: 12 jun. 2014.

MORAIS, R.; MATOS, S. G.; FERNANDES, M. A.; VALENTE, A. L. G.; SOARES, S. F. S. P; FERREIRA, P. J. S. G.; REIS, M. J. C. S. Sun, wind and water flow as energy supply for small stationary data acquisition platforms. **Computers and Electronics in Agriculture**, Amsterdam, v. 64, n. 2, p. 120-132, 2008. Available: <http://www.sciencedirect.com/science/article/pii/S01-68169908001257>. Access: 25 jun. 2014.

NELSON, C. A.; PLATT, S. R.; ALBRECHT, D.; KAMARAJUGADDA, V.; FATEH, M. Power harvesting for railroad track health monitoring using piezoelectric and inductive devices. In: SPIE, ACTIVE AND PASSIVE SMART STRUCTURES AND INTEGRATED SYSTEMS, 2008. **Proceedings of the…** Available: <http://dx.doi.org/10.1117/12.775884>. Access: 12 dez. 2014.

POBERING, S.; SCHWESINGER, N. A novel hydropower harvesting device MEMS, NANO and smart systems. ON INTERNATIONAL CONFERENCE, ICMENS 2004. **Proceedings of the…** [S.l]: IEEE, 2004. p. 480-485. Available: <http://ieeexplore.ieee.org/stamp/stamp.jsp?tp=&arnumber=1508997>. Access: 12 dez. 2014.

RAO, S. S. **Vibrações mecânicas**. 4. ed. São Paulo: Pearson Prentice Hall, 2008. 424 p.

RENAUD, M.; STERKEN, T.; FIORINI, P.; PUERS, R.; BAERT, K.; VAN HOOF, C. Scavenging energy from human body: design of a piezoelectric transducer solid-state sensors, actuators and microsystems, 2005. ON DIGEST OF TECHNICAL PAPERS. TRANSDUCERS '05. THE 13TH INTERNATIONAL CONFERENCE. **Proceedings of the…** [S.l.]: IEEE, 2005. p. 784-787. Available: <http://ieeexplore.ieee.org/stamp/stamp.jsp?tp=&arnumber=1496534>. Access: 12 nov. 2014

SABA, R.; ELLIOTT, S.; BAUMANN, O. **Vibration power harvesting from head motion**. Southampton, GB, University of Southampton, 2012. 18p. (ISVR Technical Memorandum, 998).

SAHA, C. R.; O'DONNELL, T.; WANG, N.; MC CLOSKEY, P. Electromagnetic generator for harvesting energy from human motion. **Sensors and Actuators A: Physical**, Amsterdam, v. 147, n. 1, p. 248-253, 2008. Available: <http://www.sciencedirect.com/science/article/pii/S092-4424708001398>. Access: 10 mar. 2014.

SARI, I.; BALKAN, T.; KULAH, H. A wideband electromagnetic micro power generator for wireless microsystems. INTERNATIONAL SOLID-STATE SENSORS, ACTUATORS AND MICROSYSTEMS CONFERENCE, TRANSDUCERS 2007, Lyon. **Proceedings of the…** Lyon: IEEE, 2007. p. 275-278. Available: <http://ieeexplore.ieee.org/stamp/stamp.jsp?tp=&arnumber=4300122>. Access: 12 jan. 2015.

SELIG, E. T.; WATERS, J. M. **Track geotechnology and substructure management**. London: Thomas Telford, 1994. 446 p.

SERRE, J. C.; PÉREZ-RODRÍGUEZ A.; FONDEVILLA N.; MARTINCIC E.; MORANTE J.R.; MONTSERRAT J.; ESTEVE. Linear and non-linear behavior of mechanical resonators for optimized inertial electromagnetic microgenerators. **Microsystem Technologies**, Heidelberg, v. 15, n. 8, p. 1217-1223, 2009. Available: <http://dx.doi.org/10.1007/s00542-009-0825-2>. Access: 12 jan. 2015.

SHENG, X.; JONES, C. J. C.; PETYT, M. Ground vibration generated by a load moving along a railway track. **Journal of Sound and Vibration**, London, v. 228, n. 1, p. 129-156, 1999. Available: <http://www.sciencedirect.com/science/article/pii/S0022460X99924069>. Access: 14 mar. 2015.

SHENG, X.; JONES, C. J. C.; THOMPSON, D. J. A theoretical study on the influence of the track on train-induced ground vibration. **Journal of Sound and Vibration**, London, v. 272, n. 3-5, p. 909-936, 2004. Available: <http://www.sciencedirect.com/science/article/pii/S0022460X-03007818>. Access: 10 fev. 2015.

SHU, Y. C.; LIEN, I. C. Analysis of power output for piezoelectric energy harvesting systems. **Smart Materials and Structures**, Bristol, v. 15, n. 6, p. 1499, 2006. Available: <http://stacks.iop.-org/0964-1726/15/i=6/a=001>. Access: 12 fev. 2015.

SODANO, H. A.; INMAN, D. J.; PARK, G. Comparison of piezoelectric energy harvesting devices for recharging batteries. **Journal of Intelligent Material and Structures**, London, v. 16, n. 10, p. 799-807, 2005.

STEPHEN, N. G. On energy harvesting from ambient vibration. **Journal of Sound and Vibration**, London, v. 293, n. 1-2, p. 409-425, 2006. Available: <http://www.sciencedirect.com/-science/article/pii/S0022460X05006784>. Access: 12 jan. 2014.

TAN, H.; LEE, P. W. Q.; SEAH, W. K. G.; ZHI, A. E. Impact of power control in wireless sensor networks powered by ambient energy harvesting (WSN-HEAP) for railroad health monitoring. INTERNATIONAL CONFERENCE ON ADVANCED INFORMATION NETWORKING AND APPLICATIONS WORKSHOPS, WAINA '09, 2009. **Proceedings of the...** Bradford: IEEE, 2009. p. 804-809. Available: <http://ieeexplore.ieee.org/stamp/stamp.jsp?tp=&arnumber=5136748>. Access: 12 jan 2015.

TEHRANI, M. G.; GATTI, G.; BRENNAN, M. J.; THOMPSON, D. J. Energy harvesting from train vibration. In: INTERNATIONAL CONFERENCE ON VIBRATION PROBLEMS, ICOVP, 11, 2013. **Proceedings of the...** Lisbon: [s.n.], 2013. Available: <http://www.icovp.com/components/com_breezing-forms/uploads/416_paper0.pdf>. Access: 15 mar. 2014.

THOMPSON, D. **Railway noise and vibration: mechanisms, modelling and means of control**. New York: Elsevier, 2008. 536 p.

TORRES, E. O.; RINCON-MORA, G. A. Electrostatic energy-harvesting and battery-charging CMOS system prototype. **Circuits and Systems I: Regular Papers, IEEE Transactions on**, Piscataway, v. 56, n. 9, p. 1938-1948, 2009.

TRIEPAISCHAJONSAK, N. **The influence of various excitation mechanisms on ground vibration from trains**. Southampton : University of Southampton, 2012.

WILLIAMS, C. B.; SHEARWOOD, C.; HARRADINE, M. A. MELLOR, P. H.; BIRCH, T. S.; YATES, R. B. Development of an electromagnetic micro-generator. **Circuits, Devices and Systems, IEE Proceedings**, Piscataway, v. 148, n. 6, p. 337-342, dez. 2001.

WILLIAMS, C. B.; YATES, R. B. Analysis of a micro-electric generator for microsystems. **Sensors and Actuators A: Physical**, Amsterdam, v. 52, n. 1-3, p. 8-11, 1996. Available: <http://www.-sciencedirect.com/science/article/pii/092442479680118X>. Access: 15 abr. 2015.

WISCHKE, M.; MASUR, M.; KRÖNER, M.; WOIAS, P. Vibration harvesting in traffic tunnels to power wireless sensor nodes. **Smart Materials and Structures**, Bristol, v. 20, n. 8, p. 085014, 2011. Available: <http://stacks.-iop.org/0964-1726/20/i=8/a=085014>. Access: 13 abr. 2015.

YLLI, K.; HOFFMANN, D.; FOLKMER, B.; MANOLI, Y. Design, fabrication and characterization of an inductive human motion energy harvester for application in shoes. **Journal of Physics: Conference Series**, Bristol, v. 476, n. 1, p. 012012, 2013. Available: <http://-stacks.iop.org/17426596/476/i=1/a=012012>. Access: 12 maio 2015.

YLLI, K.; HOFFMANN, D.; WILLMANN, A. BECKER, P.; FOLKMER, B.; MANOLI, Y. Energy harvesting from human motion: exploiting swing and shock excitations. **Smart Materials and Structures**, Bristol, v. 24, n. 2, p. 025029, 2015. Available: <http://stacks.iop.org/-09641726/24/i=2/a=025029>. Access: 13 fev. 2015.

APPENDIX A: COMPLETE SET OF ANALYSIS FOR AN ENERGY HARVESTER AT STEVENTON SITE

In this appendix is shown the complete set of results for a linear energy harvester subject to vibration induced by an Inter-city 125 high speed train (HST), composed of 2 locomotive and 8 passenger cars, passing with different train speeds at Steventon site.

Figure A.1 – Acceleration time-history of a vertical sleeper vibration for different passing train speeds at Steventon site: (a) 162 km/h; and (b) 178 km/h.

(a)

(b)
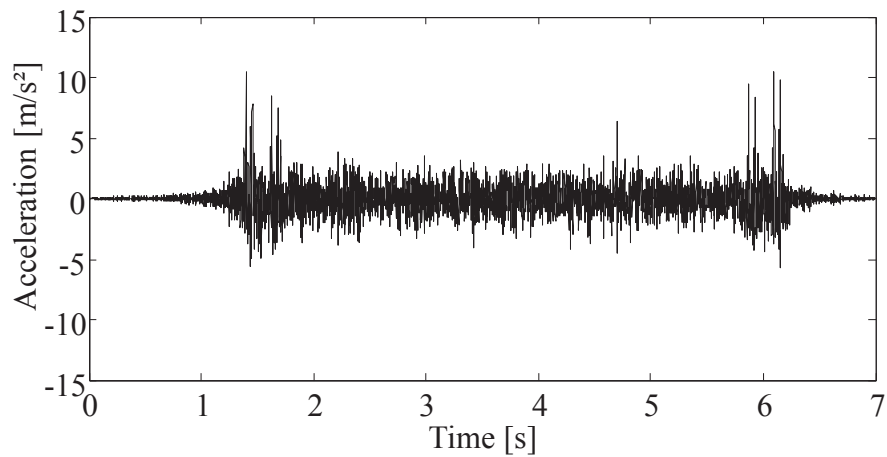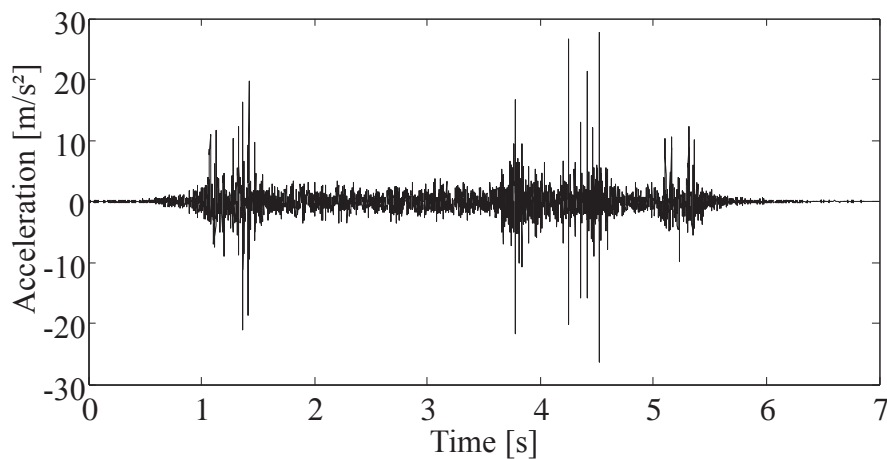
Source: Author

Figure A.2 – Acceleration time-history of a vertical sleeper vibration for different passing train speeds at Steventon site: (a) 195 km/h; and (b) 199 km/h.

(a)

(b)
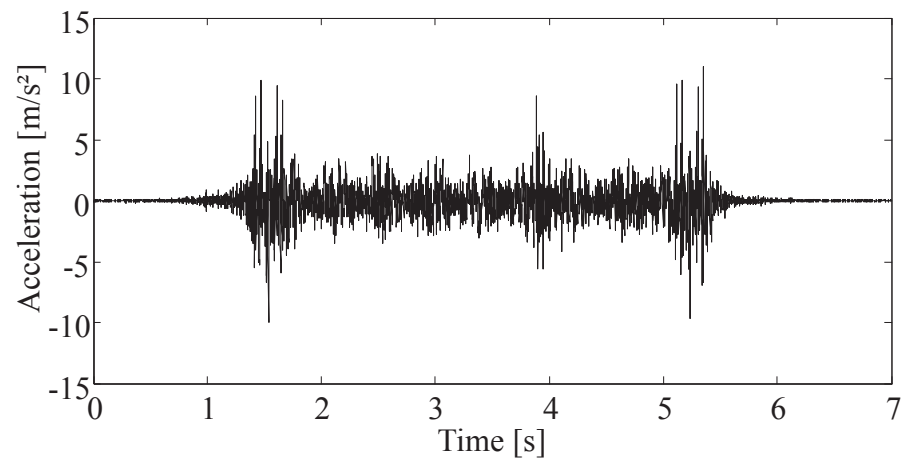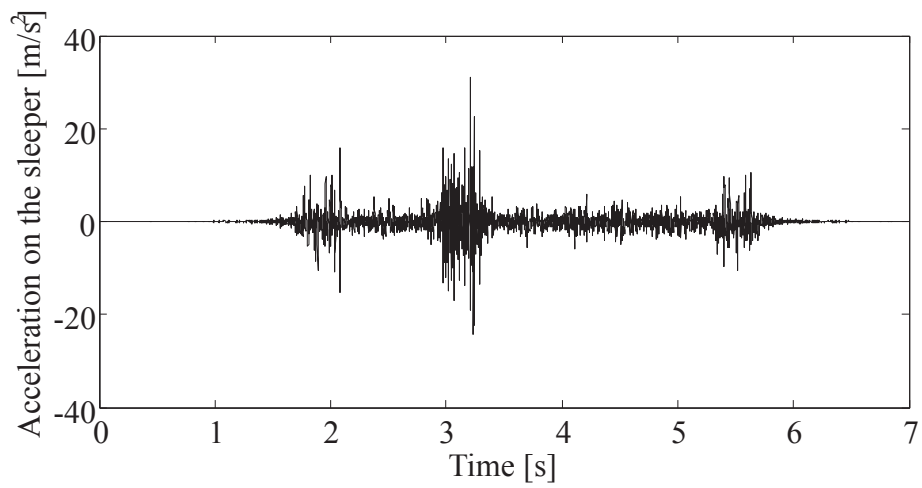
Source: Author

Figure A.3 – PSD of the sleeper vertical acceleration at Steventon site for an Inter-city 125 HST class 43 pass-by train: (a) 162 km/h; and (b) 178 km/h.

(a)

(b)
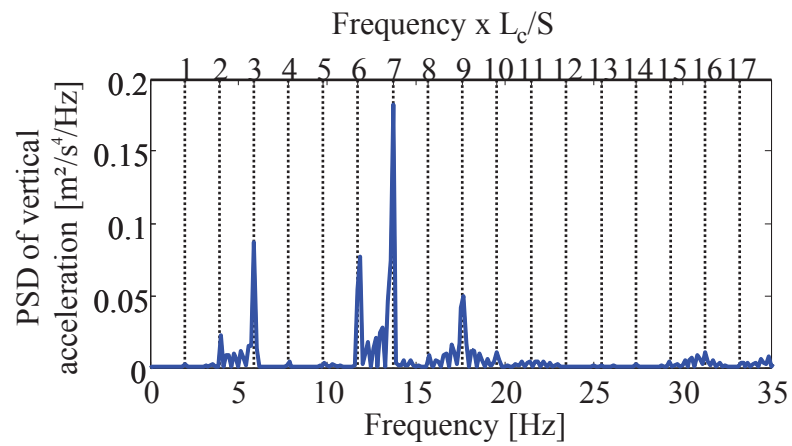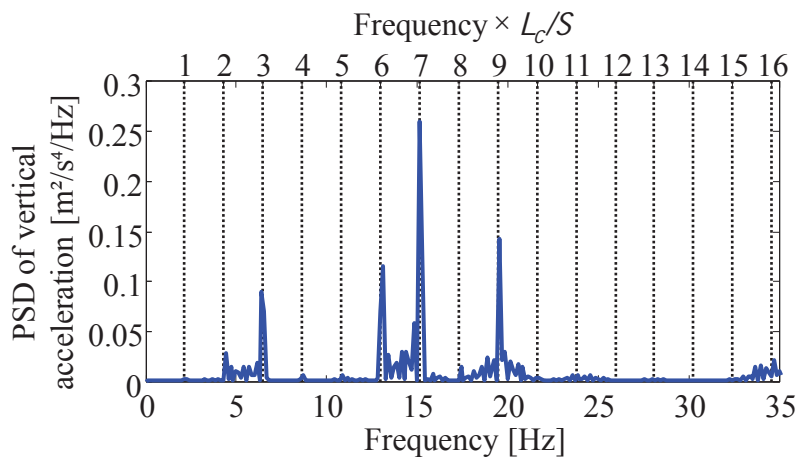
Source: Author.

Figure A.4 – PSD of the sleeper vertical accelertaion at Steventon induced by an Inter-city 125 HST with speed: (a) 195 km/h; and (b) 199 km/h.

(a)

(b)
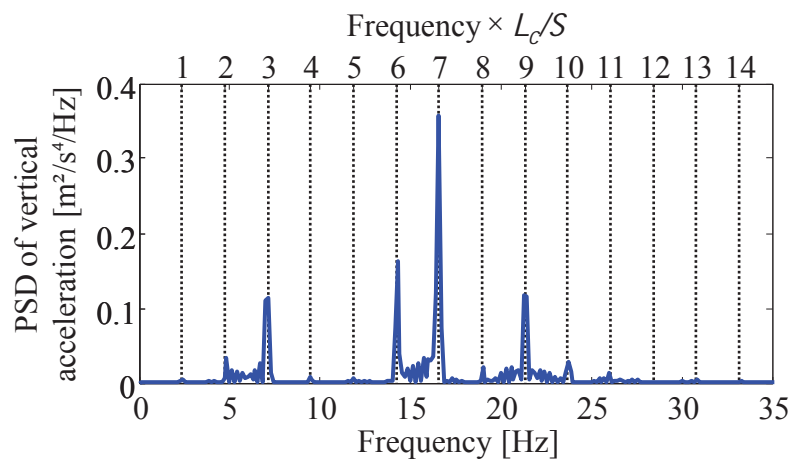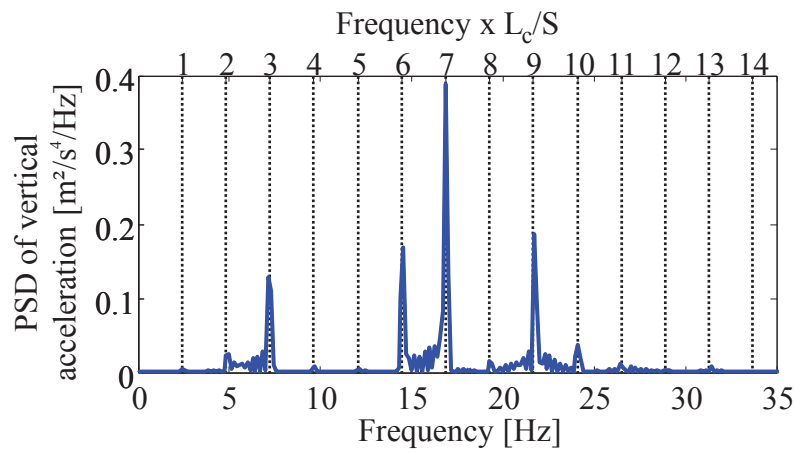
Source: Author.

Figure A.5 – Velocity time history: (a) and (c); and velocity Fourier coefficients: (b) and (d) due the passage of an Inter-city 125 HST with a speed of 162 km/h and 178 km/h.

(a)

(b)

(c)

(d)
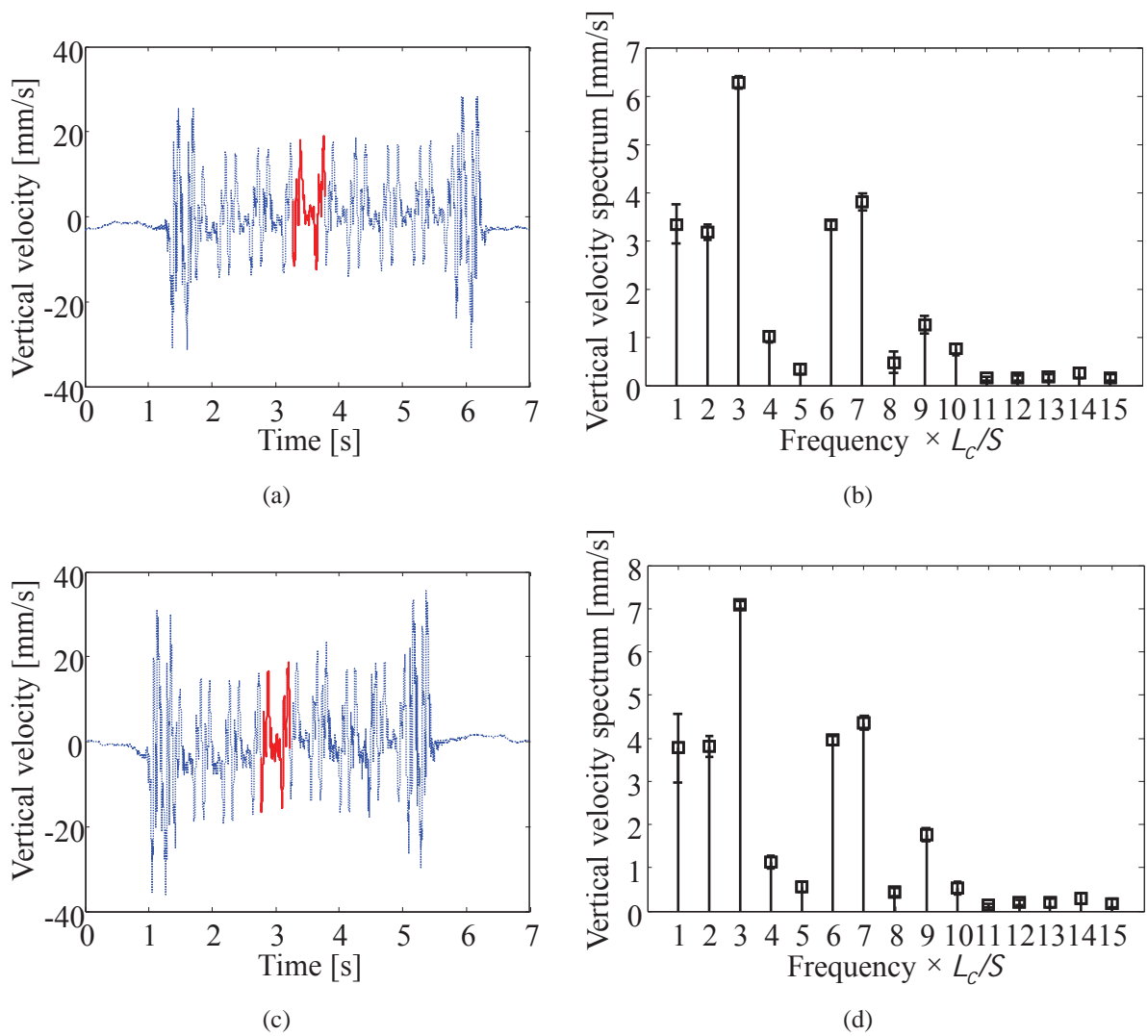
Source: Author.

Figure A.6 – Velocity time history: (a) and (c); and velocity Fourier coefficients: (b) and (d) due the passage of an Inter-city 125 HST with a speed of 195 km/h and 199 km/h.

(a)

(b)

(c)

(d)
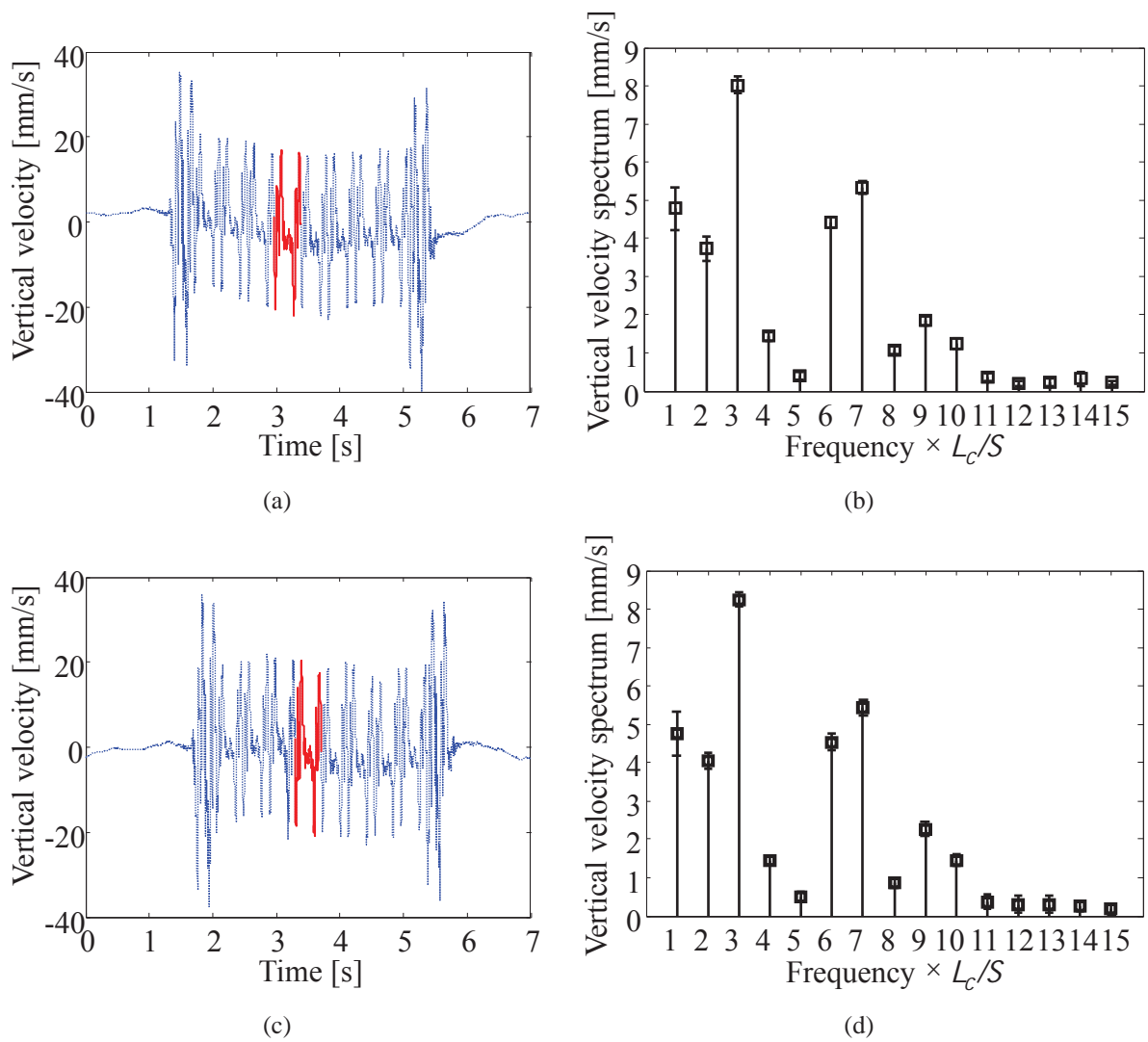
Source: Author.

Figure A.7 - Results of numerical analysis (—) blue solid line and contribution of each harmonic (□) black circle for an energy harvester due the passage of an Inter-city 125 HST with a speed of 162 km/h: (a) Energy harvested; (b) damping ratio; and (c) maximum relative displacement.
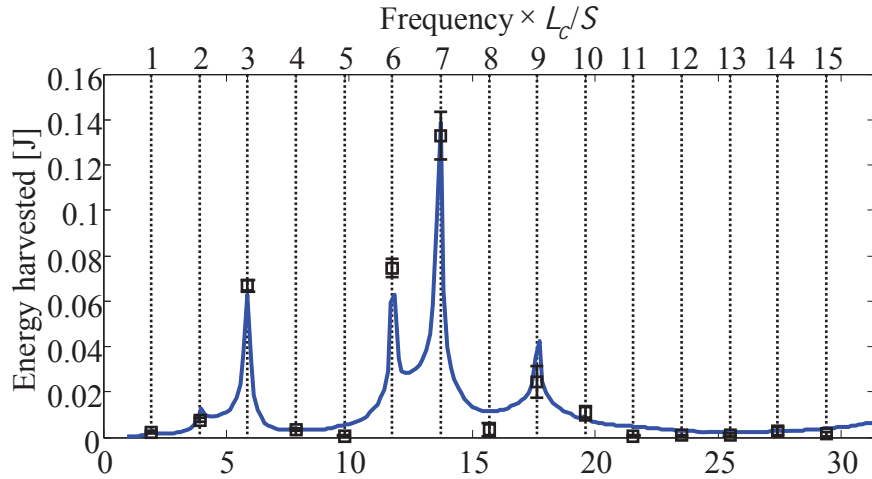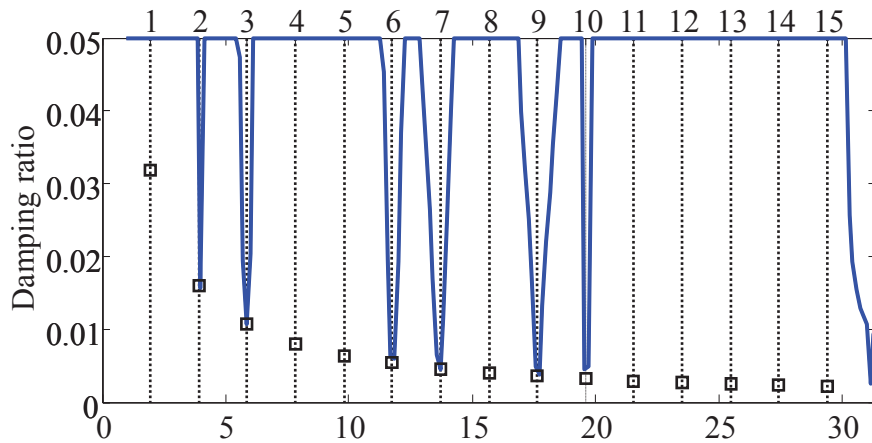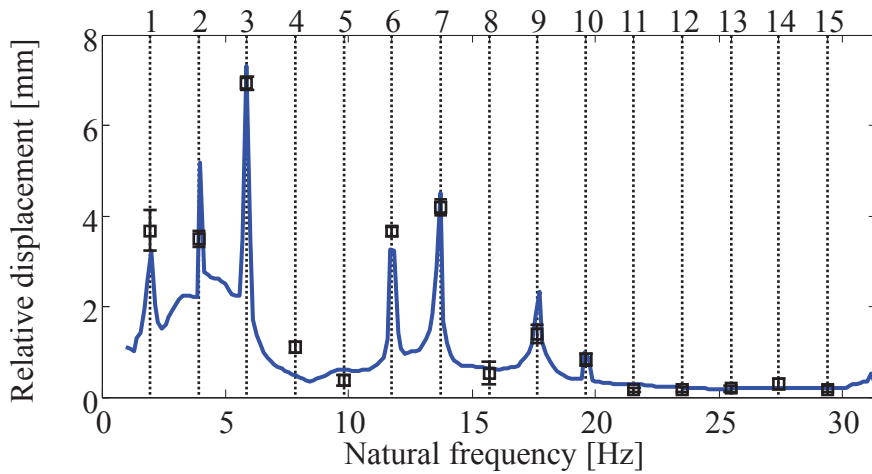
Source: Author.

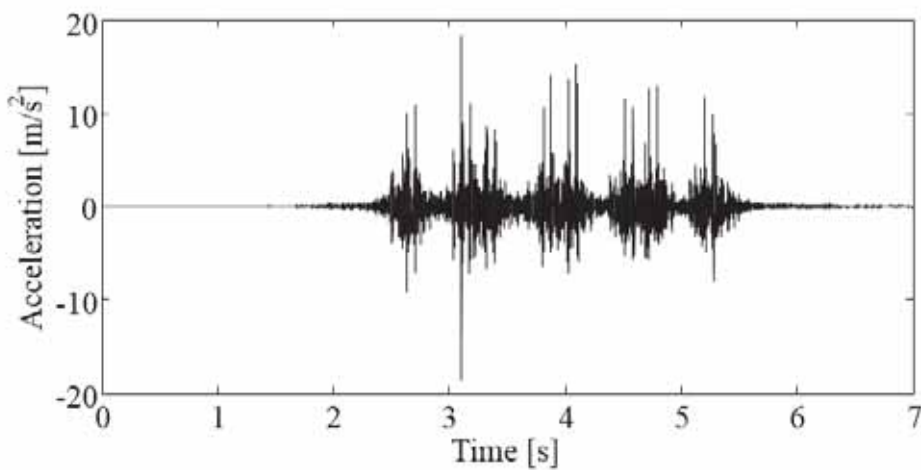Figure A.8 - Results of numerical analysis (—) blue solid line and contribution of each harmonic (□) black square for an energy harvester due the passage of an Inter-city 125 HST with a speed of 178 km/h: (a) Energy harvested; (b) damping ratio; and (c) maximum relative displacement.

(a)

(b)

(c)
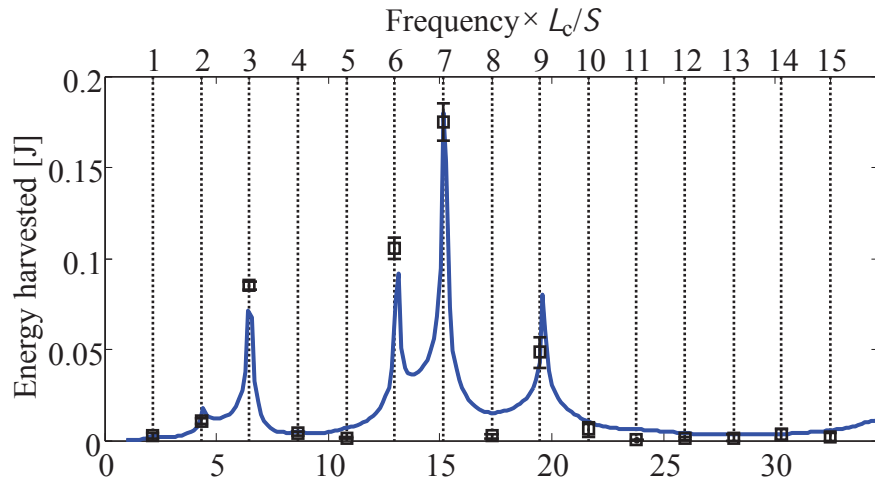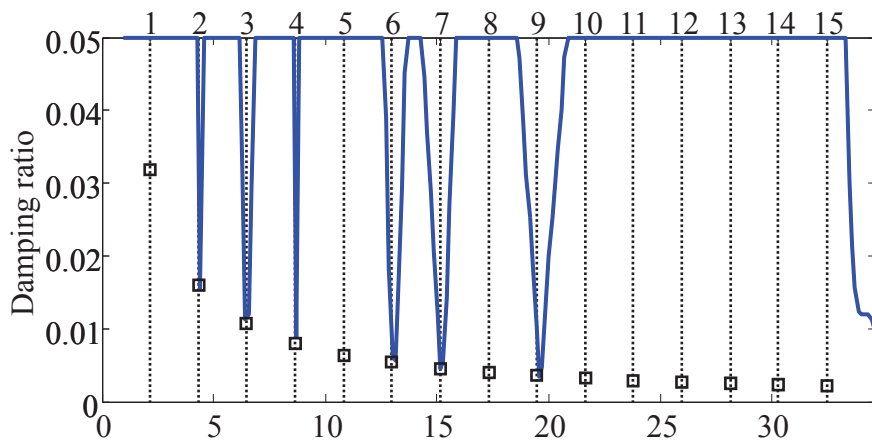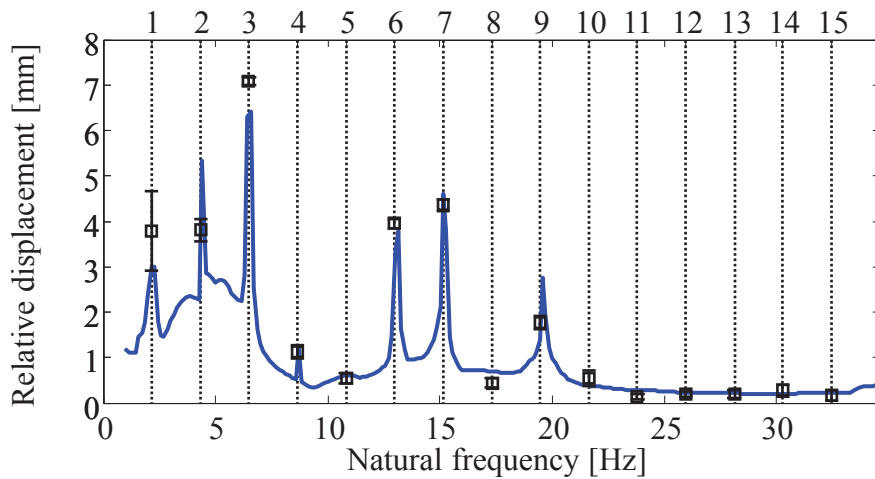
Source: Author.

Figure A.9 - Results of numerical analysis (—) blue solid line and contribution of each harmonic (□) black square for an energy harvester due the passage of an Inter-city 125 HST with a speed of 195 km/h: (a) Energy harvested; (b) damping ratio; and (c) maximum relative displacement.

(a)

(b)

(c)
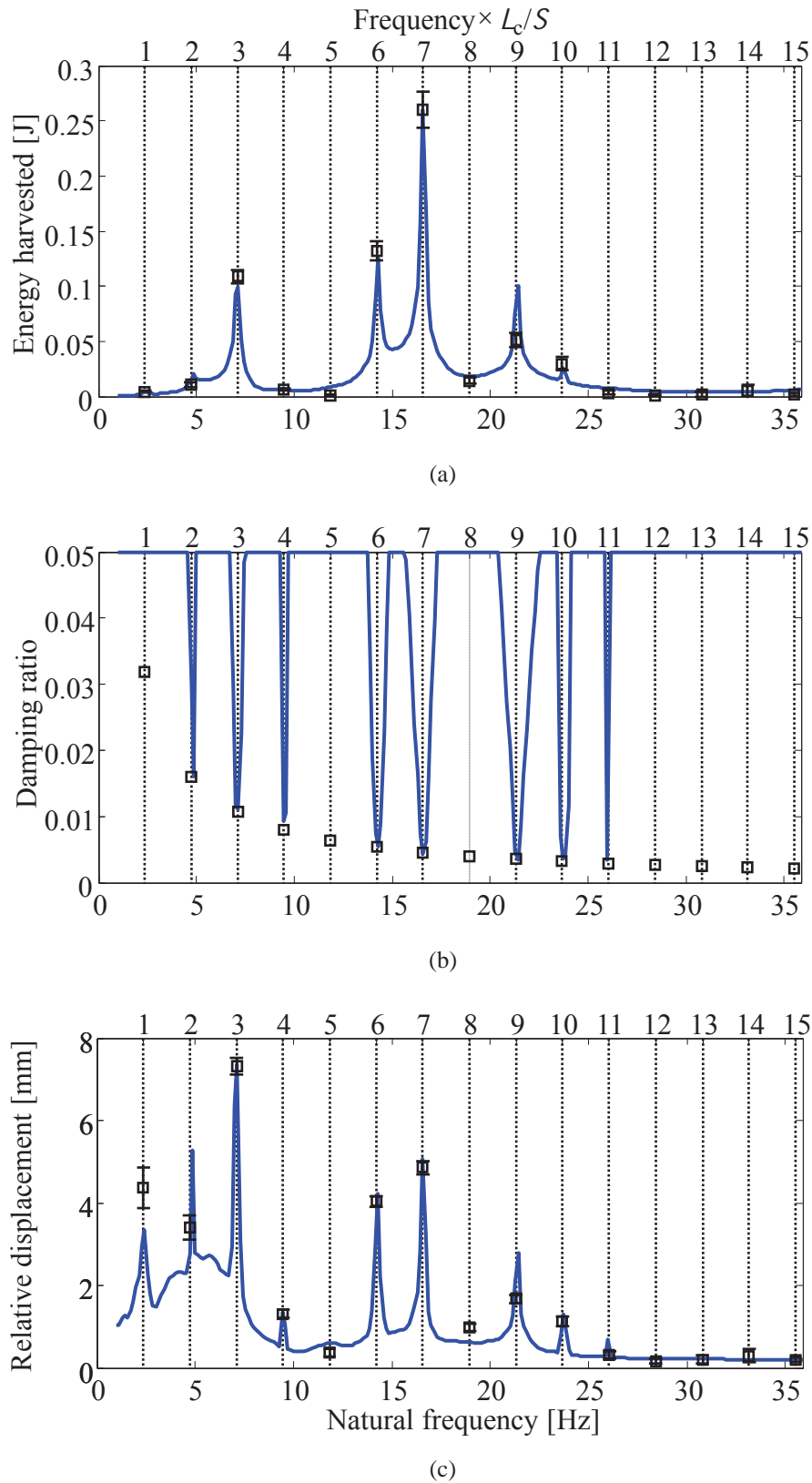
Source: Author.

Figure A.10 – Results of numerical analysis (—) blue solid line and contribution of each harmonic (□) black square for an energy harvester due the passage of an Inter-city 125 HST with a speed of 199 km/h: (a) Energy harvested; (b) damping ratio; and (c) maximum relative displacement.

(a)
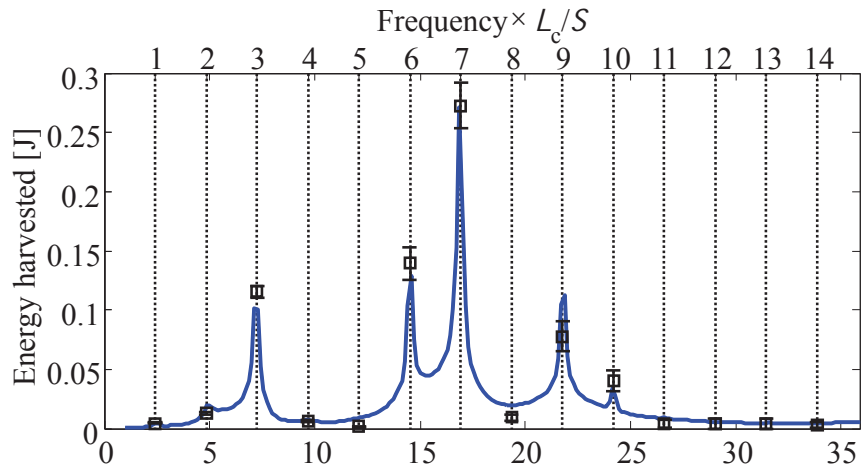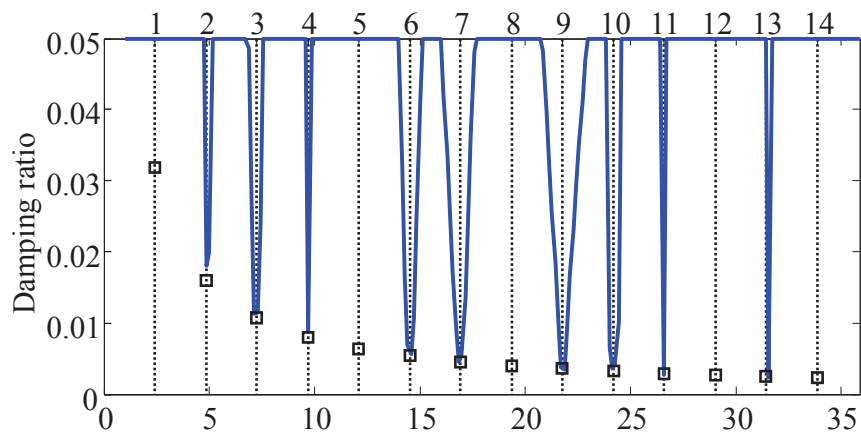
(b)
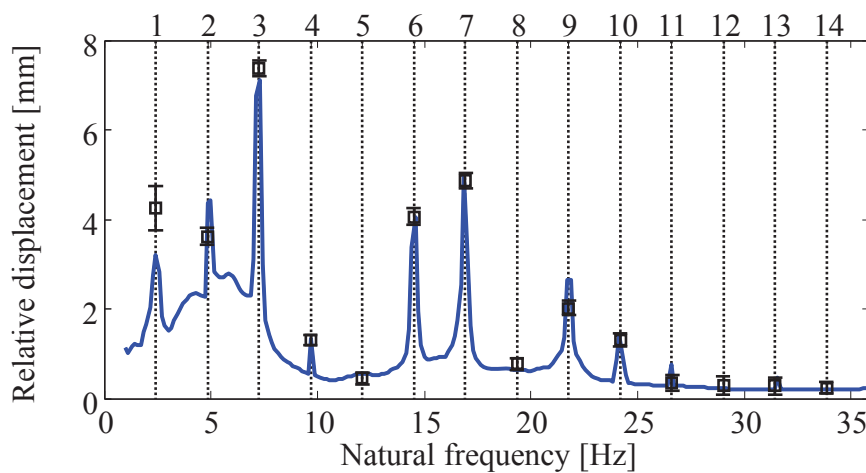
(c)

Source: Author.

APPENDIX B: COMPLETE SET OF ANALYSIS FOR AN ENERGY HARVESTER AT GRAZELEY GREEN SITE

In this appendix is shown a complete set of results for a linear energy harvester subject to vibration induced by a diesel multiple unit (DMU) Voyager, composed of 4 passenger cars all driven, passing with a speed of 114 km/h and 118 km/h at Grazeley Green site.

Figure B.1 – Acceleration time-history of a vertical sleeper vibration for two different passing trains speeds at Grazeley Green site of: (a) 114 km/h; and (b) 118 km/h.

(a)

(b)
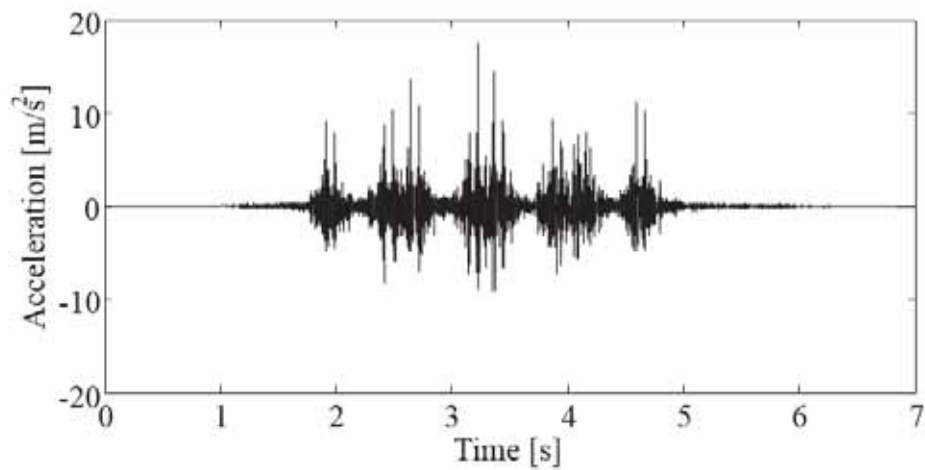
Source: Author.

Figure B.2 – PSD of the sleeper vertical accelertaion at Grazeley Green induced by a DMU Voyager with speed: (a) 114 km/h; and (b) 118 km/h.

(a)

(b)
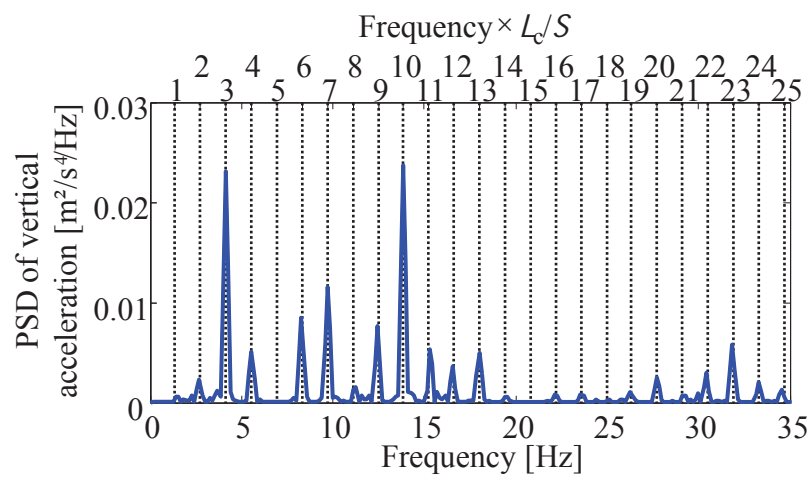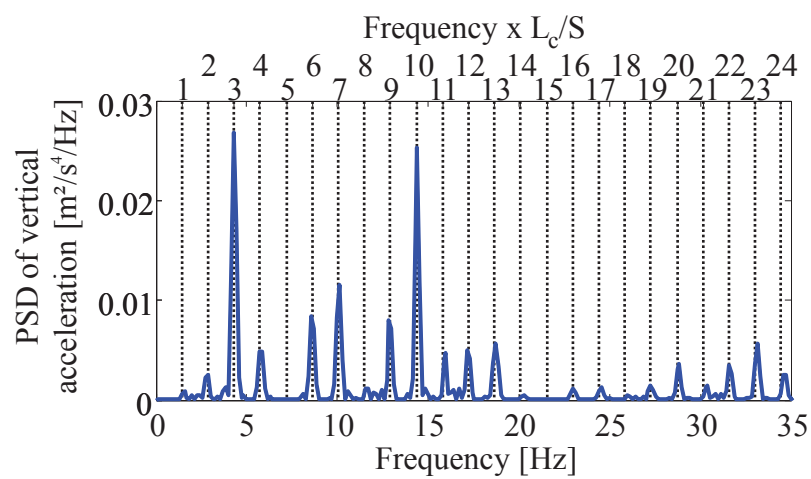
Source: Author.

Figure B.3 – Velocity time history: (a) and (c); and the velocity Fourier coefficients: (b) and (d) due the passage of a DMU Voyager with a speed of 114 km/h and 118 km/h..
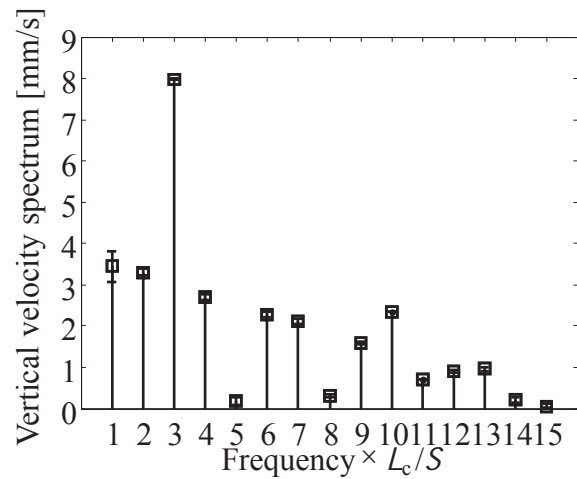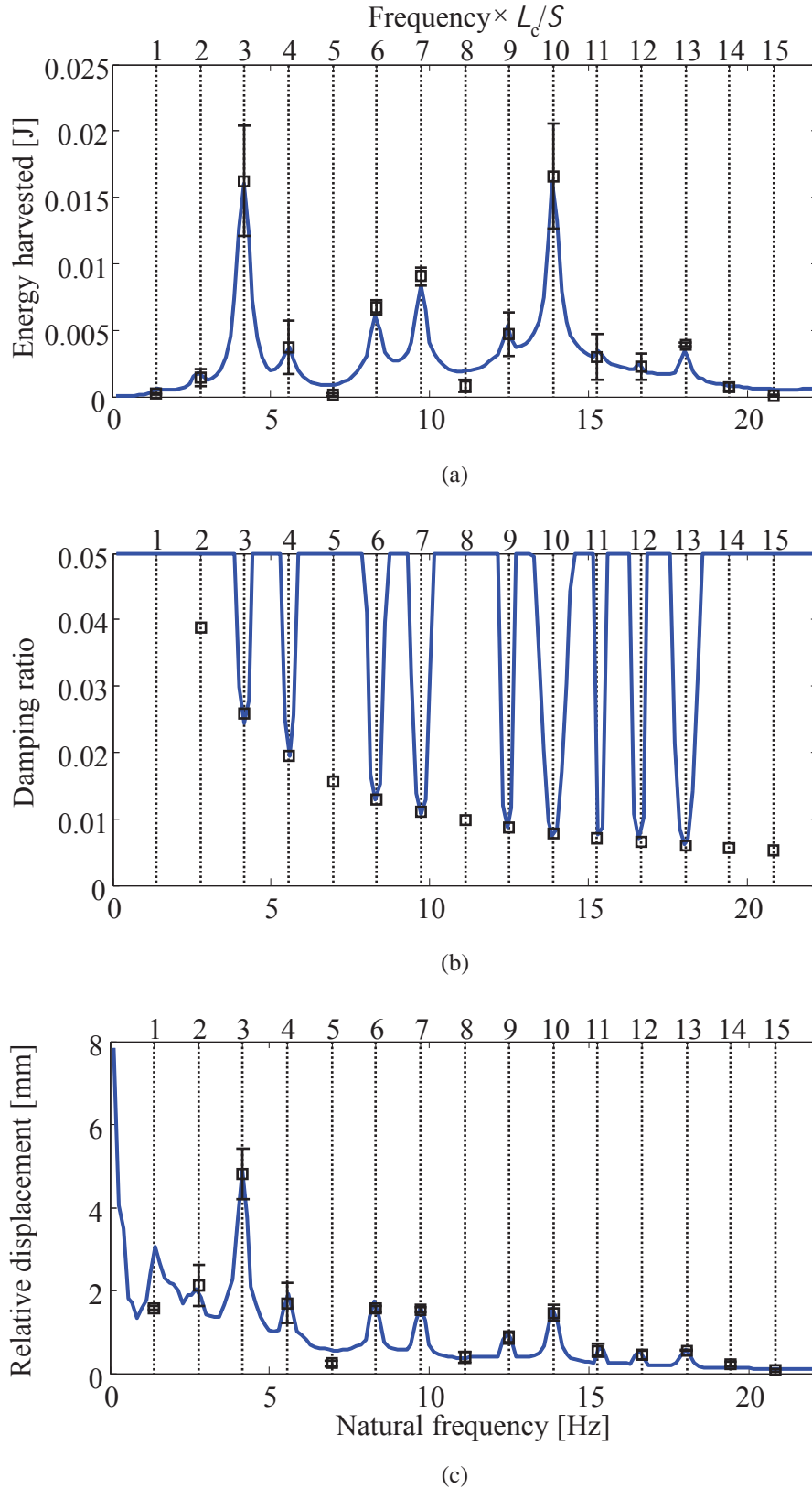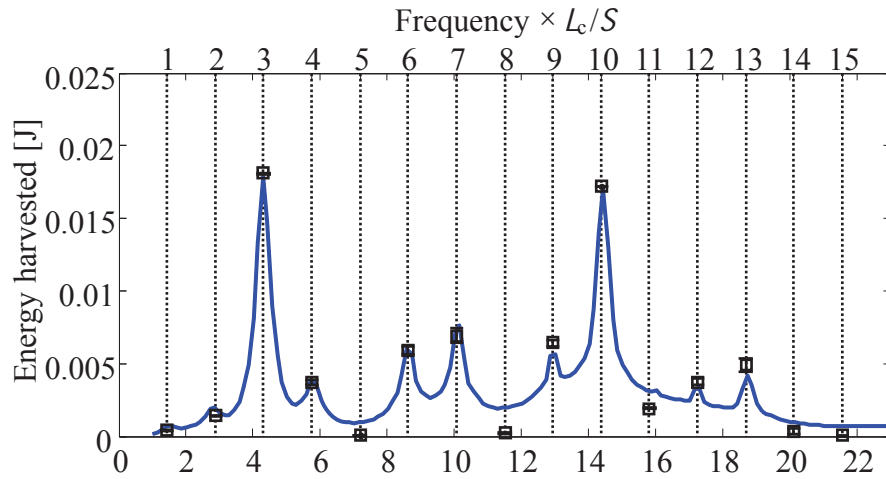

(a)

(b)

(c)

(d)
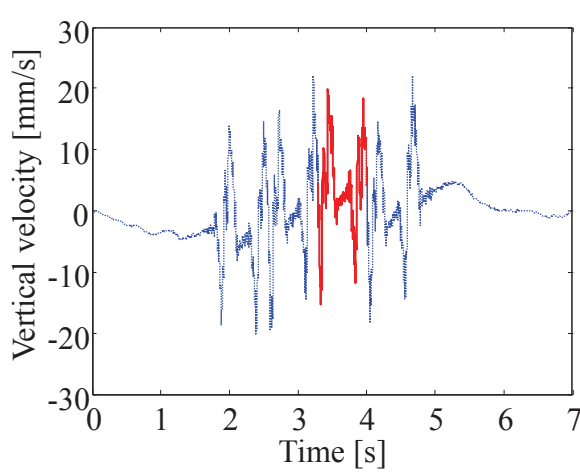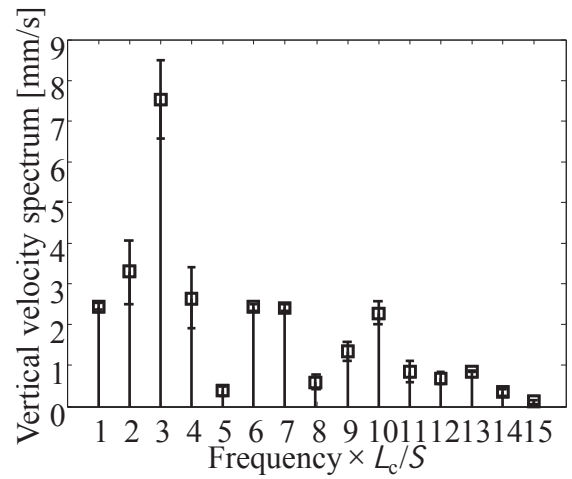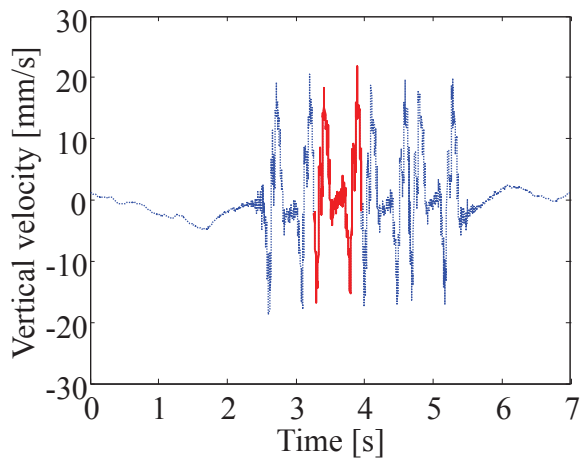
Source: Author.

Figure B.4 - Results of numerical analysis (—) blue solid line and contribution of each harmonic (□) black square for an energy harvester due the passage of a DMU Voyager with a speed of 114 km/h: (a) Energy harvested; (b) damping ratio; and (c) maximum relative displacement.
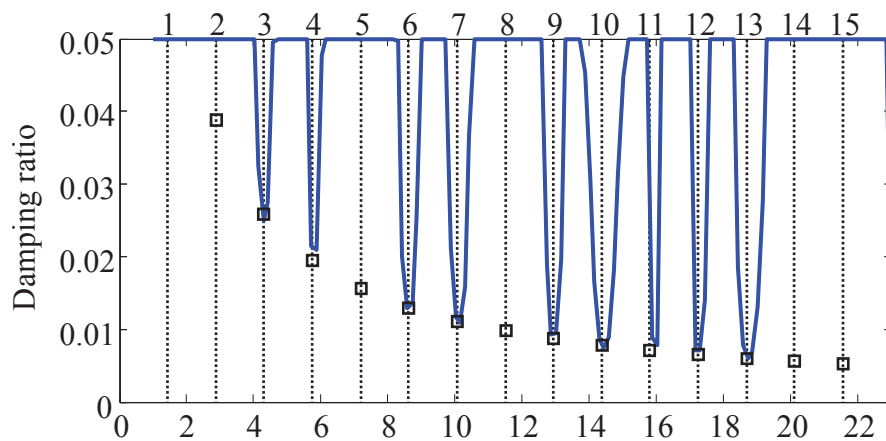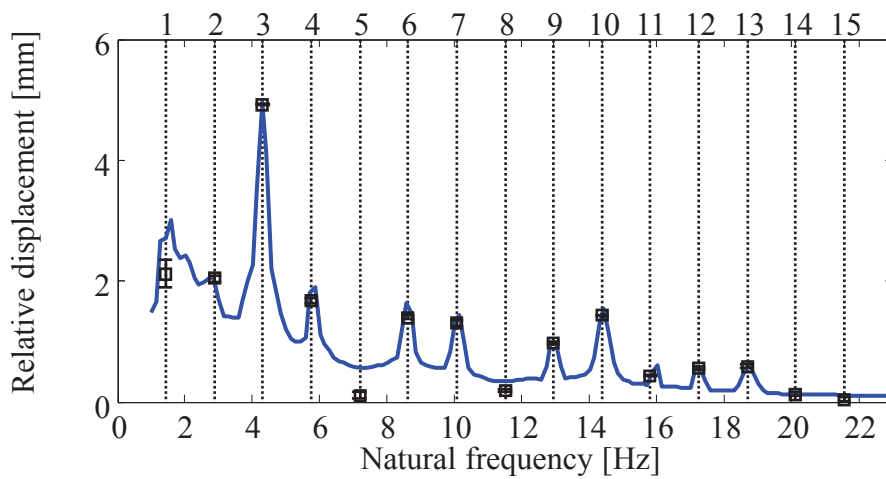

(a)

(b)

(c)

Source: Author.

Figure B.5 - Results of numerical analysis (—) blue solid line and contribution of each harmonic (□) black square for an energy harvester due the passage of a DMU Voyager with a speed of 118 km/h: (a) Energy harvested; (b) damping ratio; and (c) maximum relative displacement.

Source: Author.